Article

Cell

Inherited and *De Novo* Genetic Risk for Autism Impacts Shared Networks

Graphical Abstract

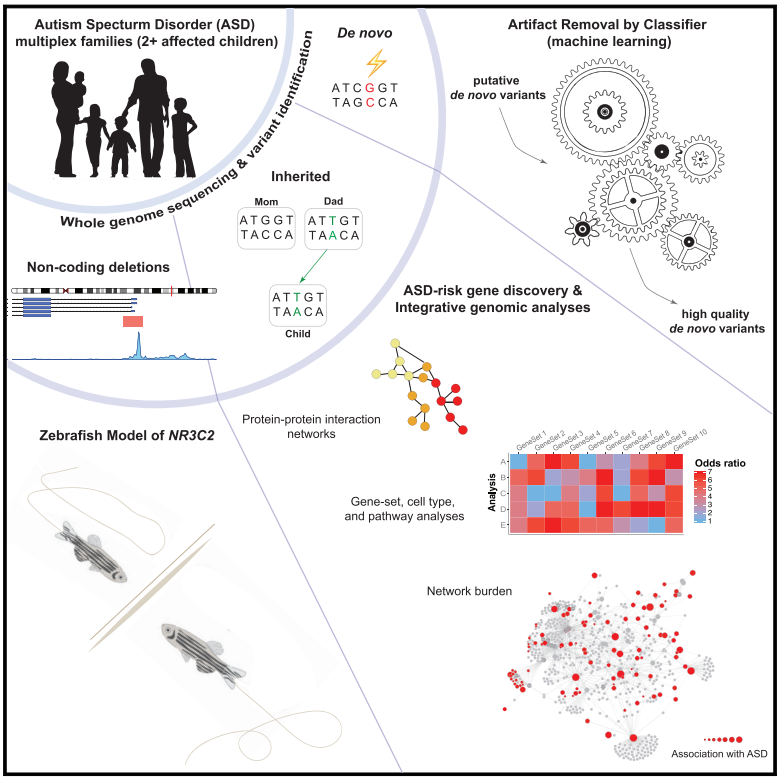

Highlights

- Identification of rare inherited variants associated with ASD and 16 new ASD risk genes
- Inherited risk reveals both new biological pathways and shared PPI with known genes
- We develop and validate a machine learning algorithm (ARC) to remove WGS artifacts
- NR3C2 mutations define a novel syndromic form of ASD, which we model in zebrafish

Authors

Elizabeth K. Ruzzo, Laura Pérez-Cano, Jae-Yoon Jung, ..., David A. Prober, Daniel H. Geschwind, Dennis P. Wall

Correspondence

dhg@mednet.ucla.edu (D.H.G.), dpwall@stanford.edu (D.P.W.)

In Brief

Whole-genome sequencing from families with multiple ASD-affected children allows identification of rare inherited variants associated with disease and definition of a syndromic form of disease caused by mutations in NR3C2.

Ruzzo et al., 2019, Cell *178*, 850–866
August 8, 2019
https://doi.org/10.1016/j.cell.2019.07.015

CellPress

Cell

Article

Inherited and *De Novo* Genetic Risk for Autism Impacts Shared Networks

Elizabeth K. Ruzzo,[1,2,11] Laura Pérez-Cano,[3,11] Jae-Yoon Jung,[4,5] Lee-kai Wang,[1,2] Dorna Kashef-Haghighi,[4,5,9] Chris Hartl,[6] Chanpreet Singh,[7] Jin Xu,[7] Jackson N. Hoekstra,[1,2] Olivia Leventhal,[1,2] Virpi M. Leppä,[3,10] Michael J. Gandal,[1,2] Kelley Paskov,[4,5] Nate Stockham,[4,5] Damon Polioudakis,[3] Jennifer K. Lowe,[1,2] David A. Prober,[7] Daniel H. Geschwind,[1,2,3,8,*] and Dennis P. Wall[4,5,12,*]

[1]Department of Psychiatry and Biobehavioral Sciences, Semel Institute, David Geffen School of Medicine, UCLA, Los Angeles, CA, USA
[2]Center for Autism Research and Treatment, Semel Institute, David Geffen School of Medicine, UCLA, Los Angeles, CA, USA
[3]Department of Neurology, David Geffen School of Medicine, UCLA, Los Angeles, CA, USA
[4]Department of Pediatrics, Division of Systems Medicine, Stanford University, Stanford, CA, USA
[5]Department of Biomedical Data Science, Stanford University, Stanford, CA, USA
[6]Bioinformatics IDP, University of California, Los Angeles, Los Angeles, CA, USA
[7]Division of Biology and Biological Engineering, California Institute of Technology, Pasadena, CA, USA
[8]Department of Human Genetics, David Geffen School of Medicine, UCLA, Los Angeles, CA, USA
[9]Present address: Illumina Artificial Intelligence Laboratory, Illumina, Inc., San Diego, CA, USA
[10]Present address: Department of Medical Epidemiology and Biostatistics, Karolinska Institutet, Stockholm, Sweden
[11]These authors contributed equally
[12]Lead Contact
*Correspondence: dhg@mednet.ucla.edu (D.H.G.), dpwall@stanford.edu (D.P.W.)
https://doi.org/10.1016/j.cell.2019.07.015

SUMMARY

We performed a comprehensive assessment of rare inherited variation in autism spectrum disorder (ASD) by analyzing whole-genome sequences of 2,308 individuals from families with multiple affected children. We implicate 69 genes in ASD risk, including 24 passing genome-wide Bonferroni correction and 16 new ASD risk genes, most supported by rare inherited variants, a substantial extension of previous findings. Biological pathways enriched for genes harboring inherited variants represent cytoskeletal organization and ion transport, which are distinct from pathways implicated in previous studies. Nevertheless, the *de novo* and inherited genes contribute to a common protein-protein interaction network. We also identified structural variants (SVs) affecting non-coding regions, implicating recurrent deletions in the promoters of *DLG2* and *NR3C2*. Loss of *nr3c2* function in zebrafish disrupts sleep and social function, overlapping with human ASD-related phenotypes. These data support the utility of studying multiplex families in ASD and are available through the Hartwell Autism Research and Technology portal.

INTRODUCTION

Autism spectrum disorder (ASD) is a neurodevelopmental disorder characterized by early deficits in social communication and interaction together with restricted and repetitive patterns of behavior, interest, or activity (American Psychiatric Association, 2013). Global prevalence is 1%–2% (Developmental Disabilities Monitoring Network Surveillance Year 2010 Principal Investigators and Centers for Disease Control and Prevention (CDC), 2014), with heritability estimated at 60%–90% (Colvert et al., 2015; Gaugler et al., 2014; Geschwind and Flint, 2015; Hoekstra et al., 2007; Klei et al., 2012; Sandin et al., 2014; Skuse et al., 2005).

Considerable progress in gene discovery has come from studies of families with one affected child (simplex families), identifying *de novo* copy number variants (CNVs) (Levy et al., 2011; Marshall et al., 2008; Sanders et al., 2011; Sebat et al., 2007), and *de novo* frameshift, splice acceptor, splice donor, or nonsense variants (collectively referred to as protein-truncating variants [PTVs]) (De Rubeis et al., 2014; Iossifov et al., 2012, 2014; O'Roak et al., 2012; Sanders et al., 2012) that increase ASD risk and account for an estimated 3%–5% of ASD cases (Constantino et al., 2010; Gaugler et al., 2014; Ozonoff et al., 2011; Sandin et al., 2014; Werling and Geschwind, 2015). Despite these remarkable advances in identifying *de novo* (germline) mutations in ASD, by definition, *de novo* mutations account for none of the substantial heritability of ASD.

To date, recurrent CNVs are the primary established form of inherited risk variation for ASD (Glessner et al., 2009; Leppa et al., 2016; Mefford et al., 2008). Exploration of other types of inherited risk variation (SNVs and indels) has been drawn primarily from families containing only one affected child (De Rubeis et al., 2014; Krumm et al., 2015), which are depleted for inherited risk compared with families with two or more affected children (multiplex families) (Ronemus et al., 2014; Sebat et al., 2007; Virkud et al., 2009). A recent study by the MSSNG consortium was limited to large rare CNVs and *de novo* protein-coding variation, despite drawing 40% of samples from multiplex ASD families (Yuen et al., 2017). Thus, a majority of ASD risk genes, especially those contributing to inherited risk, have yet to be identified. Moreover, without broader knowledge of individual genes contributing to heritable risk for ASD, whether rare *de novo*

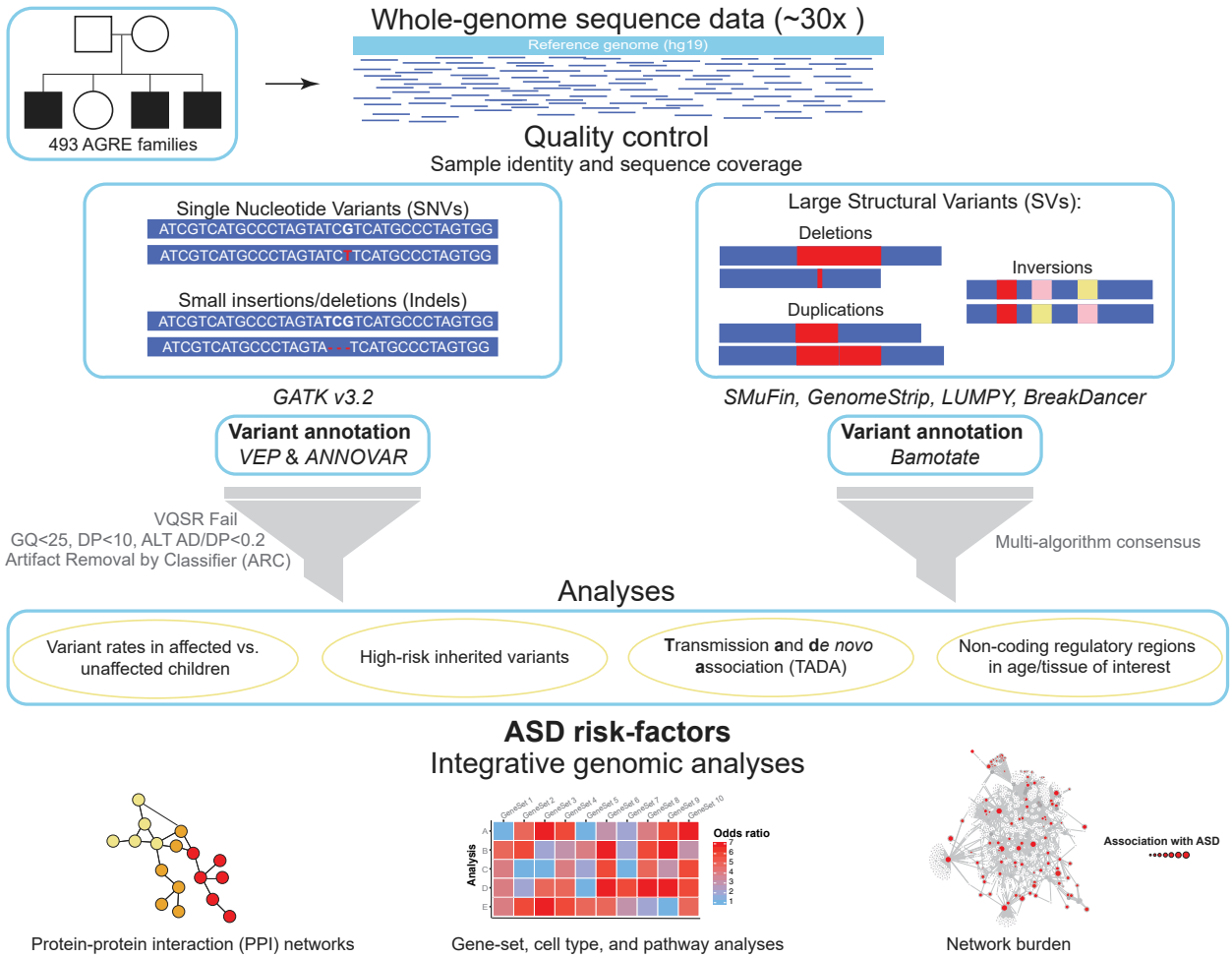

Figure 1. Overview of the Analysis Pipeline

High-coverage whole-genome sequence reads were aligned to the human reference genome (hg19) and quality control checks were applied to ensure both sample identity and sequencing coverage (Figure S1). SNVs and indels were called following GATK's best practices, annotated using both VEP and ANNOVAR, and then filtered for mildly stringent quality thresholds. All *de novo* variants were classified by ARC and high-confidence variants were retained (Figures 3, S3, and S4). Large SVs were identified by four different SV detection algorithms, three of which used aligned sequence reads and one that performed *de novo* alignment (SMuFin). Large SVs were annotated using Bamotate and then filtered for high-quality variants by using our multi-algorithm consensus pipeline. The resulting variants were then analyzed to identify ASD risk factors and perform integrative genomic analyses.

and inherited risk variants impact the same biological pathways remains an important but unanswered question. Here we used whole-genome sequencing (WGS) to identify both rare *de novo* and inherited genetic risk factors for ASD in both coding and non-coding regions of the genome in the largest cohort of multiplex families evaluated to date.

RESULTS

We analyzed high-coverage WGS data from 2,308 individuals in 493 multiplex ASD families from the Autism Genetic Resource Exchange (AGRE) (STAR Methods; Figure 1; Figure S1; Table S1). This cohort, the Hartwell Autism Research and Technology Initiative (iHART), includes 960 affected children and 217 unaffected children for whom both biological parents were sequenced.

Excess of High-Risk Inherited Variants in Affected Children

Previous studies have shown that siblings discordant for ASD exhibit similar overall mutation rates but differ in the rates of certain classes of deleterious mutations (e.g., *de novo* PTVs) and in the specific biological processes represented by genes hit with deleterious variants (e.g., chromatin modifiers) (Iossifov et al., 2012, 2014; O'Roak et al., 2012; Sanders et al., 2015). Because multiplex ASD families are expected to be enriched for inherited risk variants (Ronemus et al., 2014; Sebat et al., 2007; Virkud et al., 2009), we first assessed the rate of rare inherited variants in affected and unaffected children. We found no excess of rare (allele frequency [AF] $\leq$ 0.1%) inherited PTVs or missense variants in affected subjects (Figures 2A and S2A–S2E).

To investigate non-coding regions likely to have the largest association signal (An et al., 2018), we examined whether private

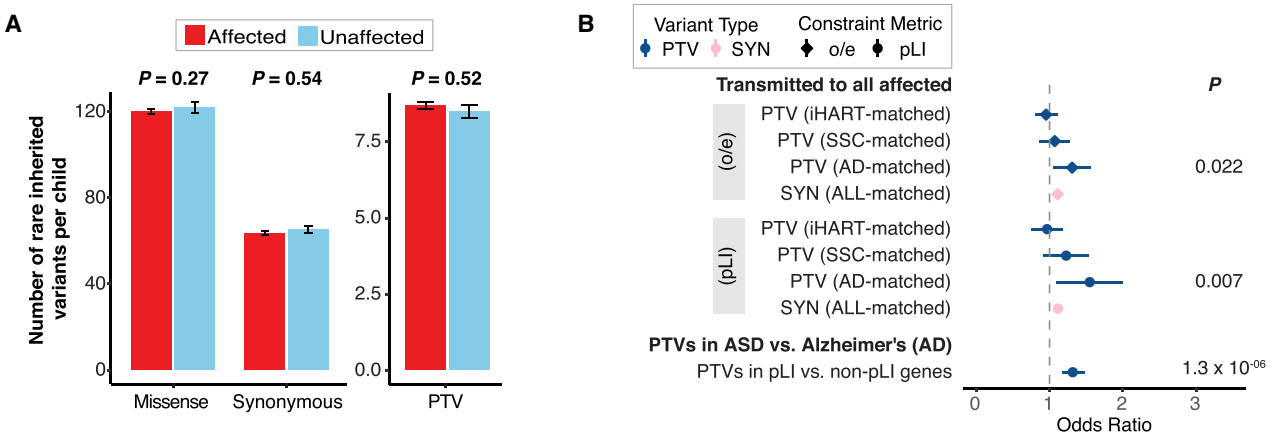

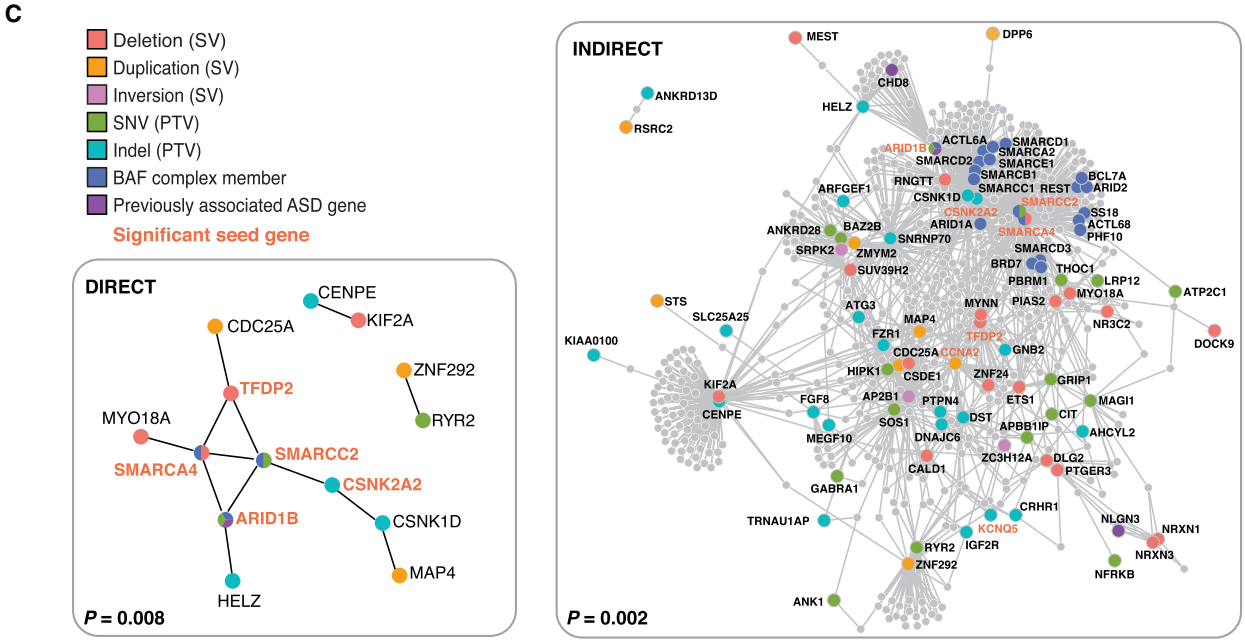

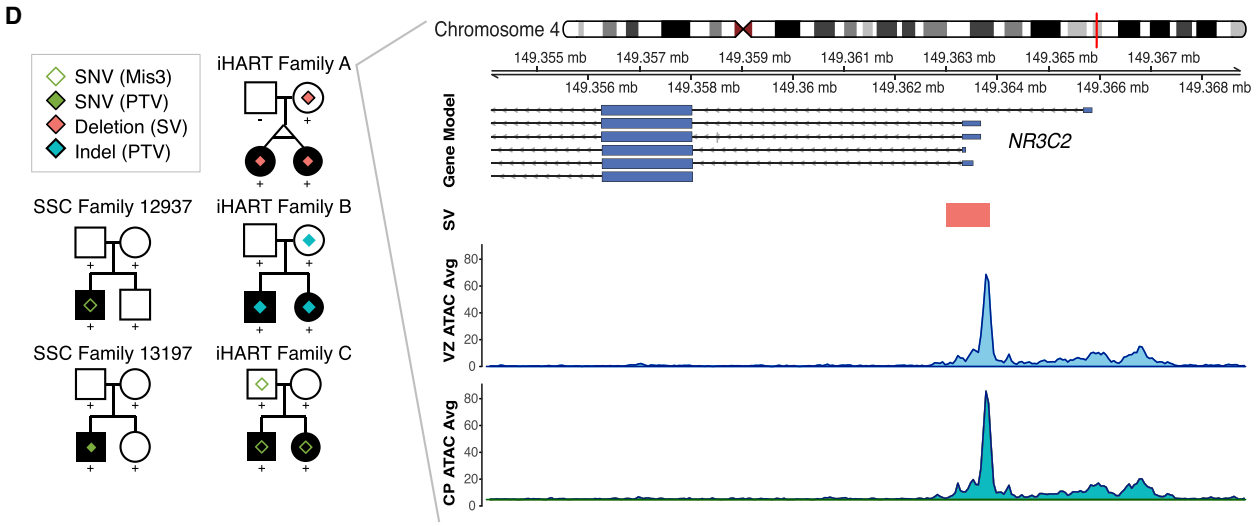

(legend on next page)

(observed in a single family) inherited variants were enriched in the promoter regions of affected versus unaffected iHART children (STAR Methods). We found no enrichment in affected subjects globally (STAR Methods; p = 0.07, quasi-Poisson linear regression), nor when restricting the analysis to promoters of known ASD risk genes (STAR Methods; p = 0.26, quasi-Poisson linear regression). We still found no significant excess of private inherited variants in the promoters of affected subjects when combined with 517 affected and 518 unaffected subjects from the Simons Simplex Cohort (SSC; STAR Methods; all genes, p = 0.14; ASD risk genes, p = 0.12).

Similarly, we observed no difference in the overall rate of rare inherited SVs nor gene-disrupting SVs between affected and unaffected individuals (Figures S2F–S2M). The absence of substantial rate differences for rare inherited variants is consistent with prior studies, which either found no global signal or only identified signals in selected candidates (Brandler et al., 2018; De Rubeis et al., 2014; Krumm et al., 2015; Leppa et al., 2016; Werling et al., 2018). Our findings are also consistent with the expected lower average effect size and reduced penetrance of inherited risk variation relative to *de novo* pathogenic mutations.

Given the low effect size of inherited risk variants, we further leveraged family structure to identify rare variants transmitted to all affected but no unaffected children under the hypothesis that such variants may confer a high disease risk. These high-risk inherited variants were further defined as variants disrupting highly constrained genes (those predicted to be the least tolerant to loss-of-function mutations in the human population; pLI $\geq$ 0.9; Lek et al., 2016; STAR Methods). We identified 98 unique genes harboring these high-risk inherited variants, including 62 PTVs and 40 SVs disrupting a coding exon or promoter. Three genes (*NR3C2*, *NRXN1*, and *ZMYM2*) were disrupted by a PTV in one family and a SV in a second family. To determine whether these findings were significant, we performed 1,000 permutations under the null, using the observed PTV counts and estimated gene mutation rates (Samocha et al., 2014; STAR Methods). We observed a striking depletion of PTVs in constrained genes in our cohort (observed = 57, expected = 255 by permutation; STAR Methods). Indeed, both iHART parents and SSC parents had five times fewer PTVs in constrained genes than expected from previously established *de novo* rates, whereas non-constrained genes follow the expected rate (Samocha et al., 2014; STAR Methods). This finding is consistent with natural selection acting rapidly to eliminate deleterious mutations.

We next updated our simulations to match the empirical ratio of PTVs in highly constrained genes (pLI $\geq$ 0.9) versus all genes in three cohorts: the SSC (Werling et al., 2018), this iHART cohort, or an Alzheimer's disease (AD) cohort (Bennett et al., 2018; STAR Methods), the latter selected for comparison because of the lack of ASD comorbidity. We observed a significant enrichment ($p < 0.05$ by permutation; STAR Methods) for high-risk inherited variants disrupting constrained genes in iHART when the PTV ratio was matched to AD (p = 0.007), trending enrichment when matched to SSC ($p < 0.16$), and no enrichment when matched to iHART (Figure 2B; STAR Methods). We draw two conclusions from these observations. First, the rare variant burden within constrained genes differs across the iHART, SSC, and AD cohorts; we observed significantly more PTVs in constrained genes in the parents within the ASD cohorts (iHART and SSC) than in the AD cohort (Fisher's exact test, $p = 1.3 \times 10^{-6}$; OR = 1.3; 95% confidence interval, 1.2–1.5; Figure 2B). Second, we validated the high-risk inherited approach (which identified 98 genes harboring high-risk inherited variants) by observing an excess of PTVs transmitted to all affected but not to unaffected children (transmission disequilibrium) in constrained genes (Figure 2B; p = 0.007; STAR Methods). Furthermore, genome-wide PTVs show a trend toward increased PTV transmission to all affected but no unaffected children (p = 0.08), suggesting that inherited PTVs, even in not highly constrained genes, increase ASD liability. Thus, although we find a significant signal for inherited variants in highly constrained genes, larger samples will be needed to reach significance for inherited, lower-penetrant variants more broadly.

High-Risk Inherited Coding and Non-coding Variants Form a Significant PPI Network

Because genes harboring *de novo* PTVs are enriched in gene networks representing specific biological pathways (Hormozdiari et al., 2015; Krishnan et al., 2016; Parikshak et al., 2013), we reasoned that similar enrichment among genes harboring inherited risk variants would provide orthogonal support for the

Figure 2. Inherited ASD Risk Genes

(A) The number of rare inherited coding variants per fully phase-able child is displayed for 960 affected (red) and 217 unaffected (blue) children by variant consequence. Mean ± standard error (SE) rates are shown.

(B) Odds ratios from simulations of high-risk inherited PTV or synonymous (SYN) variants. Results are shown for constrained genes (gnomAD pLI score or gnomAD o/e score) and the cohort used for calculation of the null PTV or SYN rate is displayed (cohort-matched class rate). The odds ratio resulting from a Fisher's exact test comparing the rate of PTVs in constrained versus non-constrained genes in the iHART and SSC cohorts with that observed in the AD cohort is also shown. Significant p values are displayed. Whiskers represent 95% confidence intervals.

(C) Direct and indirect PPI networks formed by constrained genes harboring PTVs or SVs (promoter- or exon-disrupting) transmitted to all affected but no unaffected children in a family. Proteins are colored according to the variant category of the variant identified in the high-risk inherited analysis, and previously known ASD risk genes (Sanders et al., 2015) are shown in purple. Significant seed genes are shown in bold and orange font. The p values are from 1,000 permutations.

(D) Pedigrees for five ASD families with coding or regulatory *NR3C2* variants. Squares: male; circles: female; filled shapes: individual with ASD; +: sequenced individual. Both SSC families harbor *de novo* variants in the proband (a PTV in SSC13197 and a probably damaging missense [Mis3, a "probably damaging" prediction by PolyPhen-2; Adzhubei et al., 2010] in SSC12937). iHART families A–C harbor rare inherited variants transmitted to both affected children, including an ~850-bp deletion in family A, a PTV in family B, and a Mis3 variant in family C. The *NR3C2* promoter-disrupting deletion (orange rectangle, chr4:149363005-149363852) overlaps a functional non-coding regulatory region in the developing human brain (chr4:149362706-149367485) (de la Torre-Ubieta et al., 2018). The average ATAC-seq peak read depth from the cortical plate (CP) and ventricular zone (VZ) of developing human brain samples (n = 3) are shown below the *NR3C2* deletion.

role of these genes in ASD biology. Indeed, the protein products of the 98 genes harboring high-risk inherited variation form a significant direct protein-protein interaction (PPI) network ($p < 0.008$; STAR Methods; Figure 2C) as well as a significant indirect PPI network ($p < 0.002$) that highlights seven risk genes as significantly connected hubs (corrected seed score $p < 0.05$) (Figure 2C). This PPI network is enriched for members of the BAF (SWI/SNF) complex (two-sided Fisher's exact test; $p = 0.02$; OR = 5.9; 95% confidence interval, 1.1–20.7), including *ARID1B*, *SMARCC2*, and *SMARCA4,* which are involved in chromatin remodeling during cortical neurogenesis and have previously been associated with *de novo* variation in ASD (Parikshak et al., 2013; Vandeweyer et al., 2014). These data show, for the first time, that rare inherited and *de novo* variations impact potentially overlapping molecular processes based on their convergence within a PPI network.

Inherited Regulatory Deletions Disrupt *NR3C2* and *DLG2*

Among the 98 genes harboring high-risk inherited variation, we focused on *NR3C2*, which had not been consistently associated with ASD in previous studies (transmitted and *de novo* association [TADA] false discovery rate [FDR] = 0.079 [De Rubeis et al., 2014], TADA FDR = 0.136 [Sanders et al., 2015]). Our analysis of high-risk inherited variation provides the first evidence of inherited risk in *NR3C2*, including non-coding structural variation, and further supports *NR3C2* as an ASD risk gene (Figure 2D). The three families with *NR3C2* risk variants share striking phenotypic similarities, defining a new syndromic form of ASD characterized by metacarpal hypoplasia, a high arched palate, sensory hypersensitivity, and abnormal prosody (Table S1).

A second gene identified by the analysis of high-risk inherited variation was *DLG2*, which is associated with cognition and learning in mice and humans (Belgard and Geschwind, 2013; Nithianantharajah et al., 2013) but was not previously implicated in ASD. We identified three families with the same 2.5-kb deletion in the *DLG2* promoter (Figure S2N), which falls in a recently defined, functional, non-coding regulatory region in the developing human brain (de la Torre-Ubieta et al., 2018; Figure S2N) and likely arose independently because the deletion is found on a different haplotype in each family (STAR Methods; Table S1). No deletions overlap the *DLG2* promoter deletion in controls (n = 26,565 controls; STAR Methods), suggesting that this region is highly constrained. This rare regulatory mutation is significantly associated with ASD (3 of 484 unrelated affected children versus 0 of 2,889 WGS controls, two-sided Fisher's exact test, $p = 0.003$, OR = Inf, 95% CI = 2.47-Inf).

Identification of High-Quality *De Novo* Variants by Machine Learning

De novo missense variants and PTVs have been identified as significant risk factors for ASD in simplex families (De Rubeis et al., 2014; Iossifov et al., 2014; Samocha et al., 2014). However, true *de novo* mutations may be indistinguishable from data artifacts, especially in WGS data derived from lymphoblastoid cell line (LCL) DNA, which, despite widespread use in the genetics community, may contain mutations introduced and propagated during cell line transformation that are unrelated to disease biology (Conrad et al., 2011; Abecasis et al., 2010). We reasoned that removal of LCL-derived artifacts from samples whose biomaterials were limited to LCL DNA (Table S1) would be critical for *de novo* variant identification in this study as well as of broad utility for studies using LCLs. Therefore, we developed a supervised random forest model, Artifact Removal by Classifier (ARC), to distinguish true rare *de novo* variants (RDNVs) from LCL-specific genetic aberrations as well as artifacts such as sequencing and mapping errors.

We used 76 pairs of monozygotic (MZ) twins with LCL DNA from iHART to train ARC under the assumption that true *de novo* variants would be present in both twin pairs but LCL-derived artifacts would not. ARC incorporates 48 features representing intrinsic genomic properties, (e.g., GC content, *de novo* hotspots; Michaelson et al., 2012), sample-specific properties (e.g., number of *de novo* SNVs), signatures of transformation of peripheral B lymphocytes by Epstein-Barr virus (e.g., number of *de novo* SNVs in immunoglobulin genes), or variant properties (e.g., GATK variant metrics) (Figure 3A). To evaluate ARC, we applied it to WGS from LCL-derived DNA in 17 patients and compared it with WGS derived from whole blood (WB) in the same patients. The resulting random forest classifier achieved an area under the receiver operating characteristic (ROC) curve of 0.99 and 0.98 in the training and test sets, respectively (Figures 3B, 3C, and S3), indicating that ARC very successfully distinguishes true and false *de novo* variants.

Application of ARC in the 1,177 children for whom both biological parents were also sequenced successfully eliminated the significantly higher rate of RDNVs in LCL samples (Figures S4A–S4C) and resulted in the expected genome-wide *de novo* mutation rate (mean = 60.1 RDNVs per child; Figure S4B) (Besenbacher et al., 2016; Conrad et al., 2011; Kong et al., 2012; Michaelson et al., 2012; Turner et al., 2016; Yuen et al., 2017). Running ARC similarly corrected mutation rates to reveal that iHART children exhibit the well-known effect of paternal age on *de novo* mutation rates (increase of 1.46 RDNVs per year of paternal age; STAR Methods; Figure S4D) (Deciphering Developmental Disorders Study, 2017; Francioli et al., 2015; Goldmann et al., 2016; Michaelson et al., 2012). These RDNV properties match expectation, confirming that we had high-quality RDNVs for downstream analyses.

Evidence for Depletion of Rare *De Novo* ASD Risk in Multiplex Families

We hypothesized that the iHART multiplex families would be enriched for inherited risk variants relative to previous studies of simplex families in whom *de novo* variants primarily contribute to disease risk. Leppa et al. (2016) previously found an enrichment of rare *de novo* CNVs in affected compared with unaffected children in simplex SSC families but not in multiplex AGRE families. Consistent with that finding, we observed no significant association for *de novo* missense variants ($p = 0.56$, quasi-Poisson linear regression) or PTVs ($p = 0.87$, quasi-Poisson linear regression) in affected individuals in iHART multiplex families (Figure 3D). The rate of rare *de novo* PTVs in affected children from multiplex families ($Aff_{iHART} = 0.07$) was approximately half of that in simplex families ($Aff_{Kosmicki} = 0.13$) (Iossifov et al., 2014; Kosmicki et al., 2017) and equivalent to the rate in

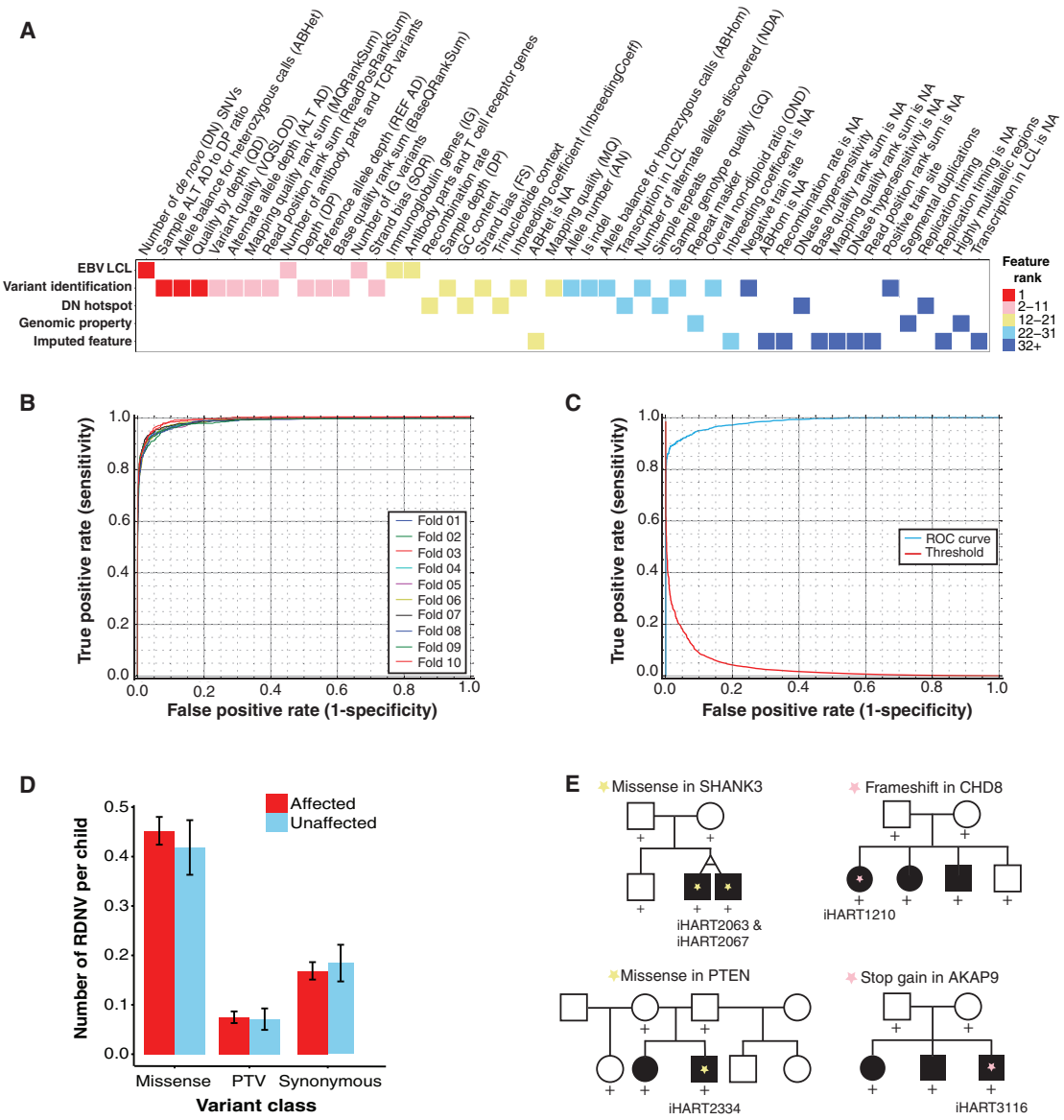

Figure 3. Rare *De Novo* Variants in iHART

(A) Heatmap reflecting the importance ranking for all 48 ARC features listed on the x axis in order of rank and sorted on the y axis by feature category (signatures of transformation of peripheral B lymphocytes by Epstein-Barr virus [EBV LCL], properties of variant identification, *de novo* hotspots, intrinsic genomic property, or imputed feature).

(B) ROC curves for 10-fold cross-validation for the ARC training set; area under the curve (AUC) = 0.99.

(C) ROC curve and threshold (threshold values on which true/false positive rates are calculated) for the ARC test set; ROC AUC = 0.98.

(D) The rate of RDNVs per child is displayed for 575 affected (red) and 141 unaffected (blue) children (716 fully phase-able samples after excluding MZ twins and ARC outliers) by variant consequence. Rates determined after ARC. Mean ± SE rates are shown.

(E) Pedigrees for iHART families containing RDNVs in previously established ASD risk genes. Children harboring the RDNV of interest are labeled with their iHART sample ID and a star symbol. The missense variants in *SHANK3* and *PTEN* are predicted to damage the encoded protein (Mis3).

unaffected children ($Unaff_{iHART}$ = 0.07) (Table S2). We estimated that our current cohort had more than 70% power to detect a rate difference for *de novo* PTVs in affected versus unaffected individuals (Monte Carlo integration; STAR Methods), suggesting a true difference in the underlying architecture of multiplex families compared with simplex families. Despite not observing a global excess for damaging RDNVs in affected children, we do identify pathogenic *de novo* variants in previously established ASD risk genes (STAR Methods; Figure 3E). Interestingly, we observe these mutations in some, but usually not all, affected family members, in line with a complex etiology where additional rare or common risk loci explain ASD in affected siblings, also in agreement with previous observations based only on large *de novo* CNVs (Leppa et al., 2016).

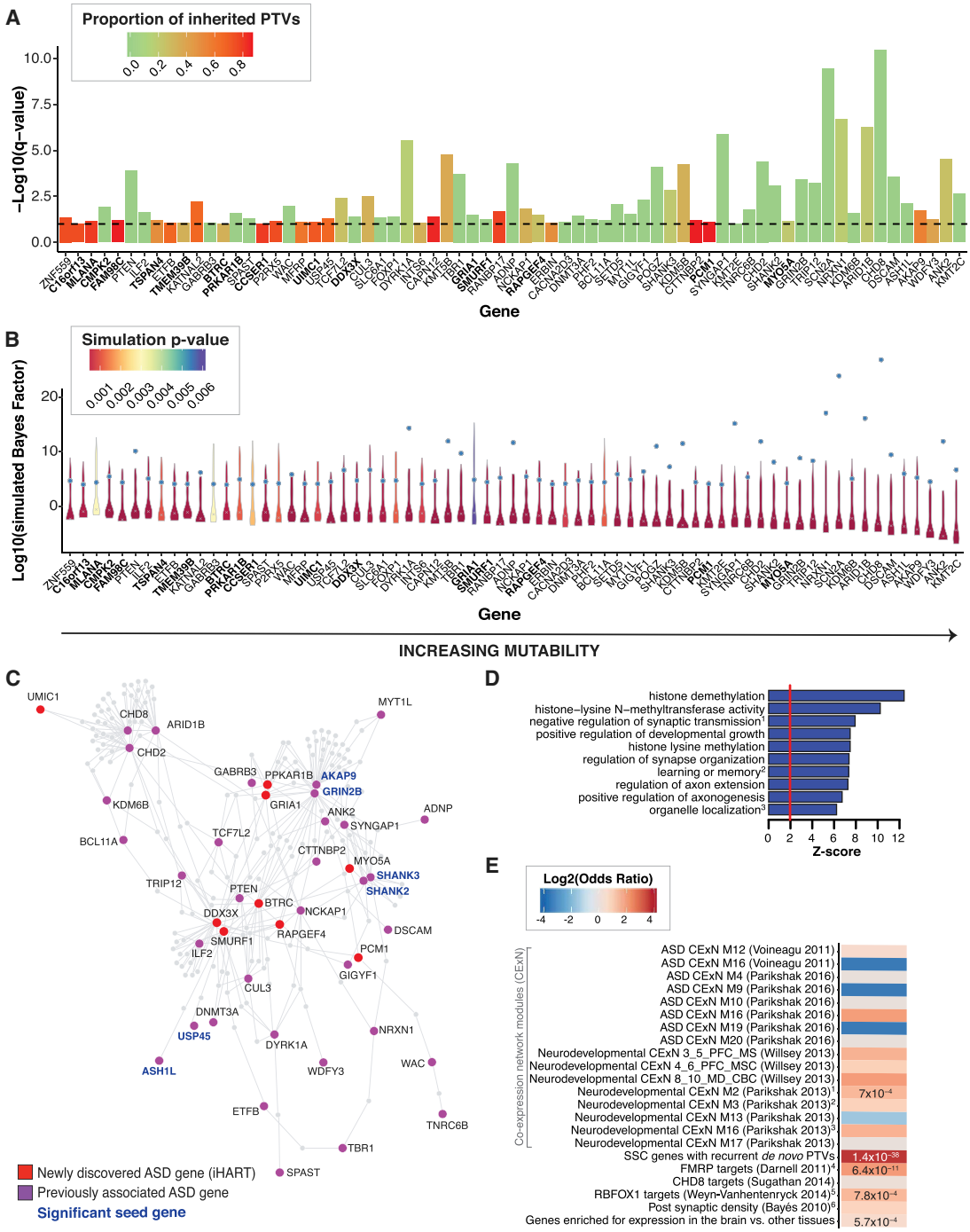

Figure 4. 69 ASD Risk Genes Identified by TADA Mega-analysis

(A and B) The 69 genes identified in the iHART TADA mega-analysis (FDR < 0.1) are displayed in order of increasing gene mutability; the 16 novel genes are shown in bold.

(A) The per-gene TADA FDR is displayed as a bar reaching the −log10(q value). The dashed horizontal line marks the FDR = 0.1 threshold. Bars are colored by the proportion of inherited PTVs for each gene (inherited PTVs/[inherited PTVs + *de novo* PTVs + *de novo* Mis3 + *de novo* small deletions]).

(B) Violin plots of the simulated Bayes factors (displayed as log10(simulated Bayes factor), 111 quantiles from the 1.1 million simulations) for each gene. The violin plots are colored by simulation p value (maximum p value = 0.006). For each gene, the gray x indicates the median of the simulated Bayes factors, and the blue dot is the Bayes factor obtained in the iHART TADA mega-analysis. The larger the distance between the median simulated Bayes factor and the observed TADA mega-analysis Bayes factor, the lower the probability of having achieved the observed Bayes factor by chance.

(legend continued on next page)

To expand this analysis to non-coding regions, we analyzed promoters, but did not find enrichment for rare *de novo* promoter variants when looking globally (STAR Methods; $p = 0.33$, quasi-Poisson linear regression) or when restricting the analysis to promoters of known ASD risk genes (STAR Methods; $p = 0.42$, quasi-Poisson linear regression). We also increased power by combining our cohort with 517 affected and 518 unaffected children with WGS data from the SSC and still found no evidence for enrichment in promoters (STAR Methods; all genes, $p = 0.25$; ASD risk genes, $p = 0.31$; quasi-Poisson linear regression). These data are accordant with recent results in simplex families (Werling et al., 2018), which suggests that the effect sizes in non-coding regions are, on aggregate, too small to detect with current sample sizes.

Identification of 16 Novel ASD Risk Genes Enriched for Inherited Variation

We next used a powerful Bayesian framework, the TADA test (He et al., 2013), to combine inherited and *de novo* signals to identify ASD risk genes (STAR Methods). To further improve power, we combined qualifying variants (STAR Methods) from the iHART cohort with the most recent ASD TADA mega-analysis (Sanders et al., 2015; Table S3). Our TADA mega-analysis identified 69 genes significantly associated with ASD at FDR < 0.1 (Figure 4A; Tables 1 and S3), 16 of which had not been identified previously (Figure 4A; Tables 1 and S3). The 16 novel ASD risk genes are enriched for genes in which a higher proportion of risk variants are inherited versus *de novo* (STAR Methods; Figure 4A). For 6 of the 16 novel genes (*UIMC1*, *C16orf13*, *MLANA*, *CCSER1*, *PCM1*, and *FAM98C*) and 5 of the 53 previously associated ASD risk genes (*RANBP17*, *ZNF559*, *P2RX5*, *CTTNBP2*, and *CAPN12*), 70% or more of the qualifying variants are inherited PTVs (Fisher's exact test, $p = 0.015$; OR = 5.57; 95% CI, 1.17–28.35).

Because TADA was previously applied to simplex families, the null distribution of the TADA statistic was not known for multiplex families. To ensure that we did not obtain false positives (type I errors) because of family structure alone, we estimated this distribution by simulating Mendelian transmission and *de novo* mutation across family structures using the observed variant counts (STAR Methods). As expected, genes with the lowest FDR in the TADA mega-analysis showed the largest simulated Bayes factors and lowest p values (Figures S5A and S5B); the three association statistics consistently reflect ASD risk association (the smaller the FDR or p value and the larger the Bayes factor, the stronger the association). All 69 genes with an FDR < 0.1 in the TADA mega-analysis obtained a simulated p value of less than 0.006 (median $p = 1 \times 10^{-3}$). The lowest simulation p value was for *CHD8* ($p = 9 \times 10^{-7}$; Figure 4B), which is a well-established ASD gene. We also leveraged the simulation p values and applied a stringent Bonferroni correction ($p < 2.7 \times 10^{-6}$) to highlight a high-confidence subset of 24 genes (STAR Methods; Tables 1 and S3). Stringent Bonferroni correction had not been utilized previously to identify genome-wide significant ASD risk genes. The most comparable approach was applying Fisher's exact test to variants found in a large *CHD8* resequencing cohort ($p = 1.01 \times 10^{-5}$) (Bernier et al., 2014).

The low relative risk estimated for inherited PTVs (De Rubeis et al., 2014) means that genes with primarily inherited risk variants will typically require more ASD carriers than those with primarily *de novo* risk to reach the same level of association. We identified 119 genes at a relaxed statistical threshold FDR < 0.2, 84 of which were identified previously at this threshold (Sanders et al., 2015). For 15 of the 35 genes that had not reached FDR < 0.2 in the previous study (Sanders et al., 2015), the majority (≥70%) of qualifying risk variants are inherited PTVs; in contrast, this was only the case for 8 of the 84 genes identified previously (FDR < 0.2) (Fisher's exact test, $p = 7.45 \times 10^{-5}$; OR = 6.98; 95% CI, 2.39–21.96). Consistently, for these 35 genes, we observe inherited PTV Bayes factors higher than those obtained in the previous TADA mega-analysis performed in largely simplex families (Sanders et al., 2015) (Kruskal-Wallis test, $p = 0.0003$; Figure S6A). For five of these 35 genes (*PCM1*, *STARD9*, *GRM6*, *RHPN1*, and *SLC10A1*) and two of the remaining 84 genes (*CTTNBP2* and *ZNF559*), the largest association signal is from inherited PTVs. Thus, these 35 genes are enriched for genes whose association signal is primarily driven by inherited PTVs (Fisher's exact test, $p = 0.02$; OR = 6.70; 95% CI, 1.03–73.81) (STAR Methods), further indicating that there is a substantial, previously unrecognized signal from rare inherited variants.

Biological Insights from Known and Novel ASD Genes

Gene set enrichment analyses (STAR Methods) indicated that the set of 69 high-confidence ASD risk genes identified in the TADA mega-analysis was enriched in a highly co-expressed group of transcriptionally co-regulated genes active during human cerebral cortical neurogenesis (module M2; Parikshak et al., 2013), FMRP targets (Darnell et al., 2011), RBFOX1 targets (Weyn-Vanhentenryck et al., 2014), and genes enriched for expression in the brain versus other tissues (STAR Methods; Figure 4E). We also integrated new data from single-cell sequencing of 40,000 cells from the human brain (Polioudakis et al., 2019) and previously published single-cell sequencing data (Lake et al., 2018; Nowakowski et al., 2017), which reveals an overall enrichment in mid-gestation and adult glutamatergic projection

(C) Indirect PPI network formed by the 69 ASD risk genes identified by TADA (FDR < 0.1). Proteins encoded by a previously known ASD risk gene (Sanders et al., 2015)) are shown in purple, and newly identified ASD risk genes (iHART TADA mega-analysis) are shown in red. Gene labels for the six significant seed genes are shown in bold blue font.

(D) Gene ontology enrichment for the 69 ASD risk genes with known biological pathways. Three of the enriched pathways contain one or more of the 16 novel ASD risk genes (all risk genes in these pathway are listed and novel risk genes have an asterisk): (1) negative regulation of synaptic transmission includes *ADNP*, *SLC6A1*, and *RAPGEF4**; (2) learning and memory includes *ADNP*, *GRIA1**, *NRXN1*, *PRKAR1B**, *SLC6A1*, and *SYNGAP1*; and (3) organelle organization includes *MYO5A**, *PCM1**, and *TCF7L2*.

(E) Gene set enrichment results for the 69 ASD risk genes displayed by the log2(odds ratio), with p values listed for gene sets surviving multiple test correction ($p < 0.002$); the SSC gene set was included as a positive control. In addition to the gene set "genes enriched for expression in the brain versus other tissues", which contains almost all of the 16 novel ASD risk genes, six additional gene sets contain one or more of the 16 novel ASD risk genes: (1) *TMEM39B* and *PCM1*; (2) *CCSER1* and *UIMC1*; (3) *BTRC*, *PRKAR1B*, and *MYO5A*; (4) *RAPGEF4* and *MYO5A*; (5) *BTRC*; and (6) *DDX3X*, *GRIA1*, *RAPGEF4*, and *MYO5A*.

Table 1. 69 ASD Risk Genes Identified in the iHART TADA Mega-analysis

dnPTV count	FDR ≤ 0.01	0.01 < FDR ≤ 0.05	0.05 < FDR ≤ 0.1
≥2	CHD8, SCN2A, ARID1B, SYNGAP1, DYRK1A, CHD2, ANK2, KDM5B, ADNP, POGZ, KMT5B, TBR1, GRIN2B, DSCAM, KMT2C, TCF7L2, TRIP12, ASH1L, CUL3, KATNAL2, GIGYF1	TNRC6B, WAC, NCKAP1, RANBP17, KDM6B, ILF2, SPAST, FOXP1, AKAP9, CMPK2*, DDX3X*	WDFY3, PHF2, BCL11A, KMT2E, CACNA2D3[a]
1	NRXN1, SHANK2, PTEN, SHANK3, SETD5	DNMT3A, MYT1L, RAPGEF4*, PRKAR1B*	MFRP, GABRB3, P2RX5, ETFB, CTTNBP2, INTS6, USP45, ERBIN, TMEM39B*, TSPAN4*, MLANA*, SMURF1*, C16orf13*, BTRC*, CCSER1*, FAM98C*
0	–	SLC6A1, ZNF559, CAPN12, GRIA1*	PCM1*, MYO5A*, UIMC1*

All 69 genes significantly associated with ASD risk (FDR < 0.1) by the iHART TADA mega-analysis are displayed by the number of *de novo* PTVs identified in the gene. The 16 newly ASD-associated genes are shown with an asterisk. The 24 underlined genes are the subset of highly confident genes that reach genome-wide significance after Bonferroni correction.

[a]The *CACNA2D3* gene had an FDR < 0.1 in this iHART TADA-mega analysis but not in the previous mega analysis (Sanders et al., 2015); however, it has been reported previously (De Rubeis et al., 2014) and, thus, is not considered a novel ASD risk gene.

neurons for both the previously established (Sanders et al., 2015) and 16 newly identified ASD risk genes (STAR Methods; Figures S6C and S6D). Despite enrichment of ASD genes as a class in glutamatergic projection neurons, some genes are more broadly expressed across neuronal cell types, many with high expression in interneurons, and others are expressed in non-neuronal cell types such as pericytes or oligodendrocyte progenitor cells (Polioudakis et al., 2019).

Many of the 16 new ASD risk genes from this study fall into biological pathways or gene sets of interest, including negative regulation of synaptic transmission (*RAPGEF4*), learning and memory (*GRIA1* and *PRKAR1B*), and cytoskeletal organization (*PCM1* and *MYO5A*) (Figure 4D). Other examples include *PRKAR1B*, which is in a gene co-expression module comprised of structural synaptic proteins that are highly co-expressed during human cerebral cortical neurogenesis and in which 60 genes harboring RDNVs in ASD probands from early exome sequencing studies are over-represented (Parikshak et al., 2013), and three genes that are found in the postsynaptic density of the human neocortex (Bayés et al., 2011): *GRIA1*, *RAPGEF4*, and *DDX3X*. *RAPGEF4* is also a known FMRP target (Darnell et al., 2011) and was previously suggested as a potential ASD candidate gene but lacked strong statistical support (Bacchelli et al., 2003). *DDX3X* was recently reported to account for 1%–3% of unexplained intellectual disability in females (Snijders Blok et al., 2015). Finally, 9 of these 16 new ASD risk genes form a significant indirect PPI network in concert with previously associated ASD genes (STAR Methods; seed indirect degrees mean permutation p = 0.016; CI degrees mean p = 0.024) (Figure 4C).

Pathways harboring primarily *de novo* variation are dominated by transcriptional and chromatin regulation (De Rubeis et al., 2014). Using gene ontology enrichment analysis, we asked whether inherited ASD risk variants cluster in distinct biological pathways and whether those pathways are the same or different from those implicated by *de novo* variation. Indeed, genes where the majority of the signal is from inherited variants reveal different pathways than those published based on *de novo* risk, including novel pathways related to ion transport (z = 3.7), cell cycle (z = 4.2), and the microtubule cytoskeleton (z = 5.7) (Figure S6E).

ASD Risk Genes Form a PPI Network with Candidate Genes Harboring High-Risk Inherited Variation

We next asked whether the proteins encoded by the 69 ASD risk genes identified in the TADA mega-analysis (FDR < 0.1) interact with the 98 candidate genes harboring high-risk inherited variants. The resulting PPI network formed by these 165 unique genes is significant for all reported network properties ($p < 0.05$; STAR Methods; Figures 5A and S6B). This network reveals interactions between genes with different levels of statistical support, ranging from high-risk inherited candidate genes and established ASD-risk genes to new ASD-risk genes, which suggests that many of these 98 candidate genes are true ASD risk genes. This network is preserved even when we limit the PPI analysis to genes emerging from the version of the TADA mega-analysis that excluded *de novo* variants from the iHART cohort (FDR < 0.1; Table S3), with the seed direct and indirect degree means both reaching significance (p = 0.013 and p = 0.0009, respectively). Thus, inherited risk variants critically contribute to this network.

Given that a large number of predicted ASD risk genes remain unidentified (Ronemus et al., 2014), we applied NetSig to identify high probability candidate genes via integration of PPI and association statistics (Horn et al., 2018). We identified 596 genes that were significantly more directly connected to ASD risk genes than expected by chance (Figure 5B; STAR Methods; Table S4), 38 of which are enriched in a developmental co-expression module shown previously to contain *de novo* variants in ASD probands (module M2; Parikshak et al., 2013; p = 0.0003; OR = 1.98; 95% confidence interval = 1.37–2.81). Interestingly, proteins in the network seeded by 98 high-risk inherited genes interact with NetSig candidates more than expected by chance, both directly (p = 0.02; OR = 12.80; 95% confidence interval = 1.07–111.92) and indirectly ($p = 4.24 \times 10^{-16}$; OR = 4.90; 95% confidence interval = 3.45–6.85) (STAR Methods; Figure 5B), providing further evidence that the genes identified by the analysis of high-risk inherited variants are likely to include true ASD risk genes.

Zebrafish Modeling of NR3C2 Syndromic ASD

Because previous evidence for *NR3C2* was inconsistent (De Rubeis et al., 2014; Sanders et al., 2015) but supported by our analyses, we sought to firmly establish *NR3C2* as an ASD risk

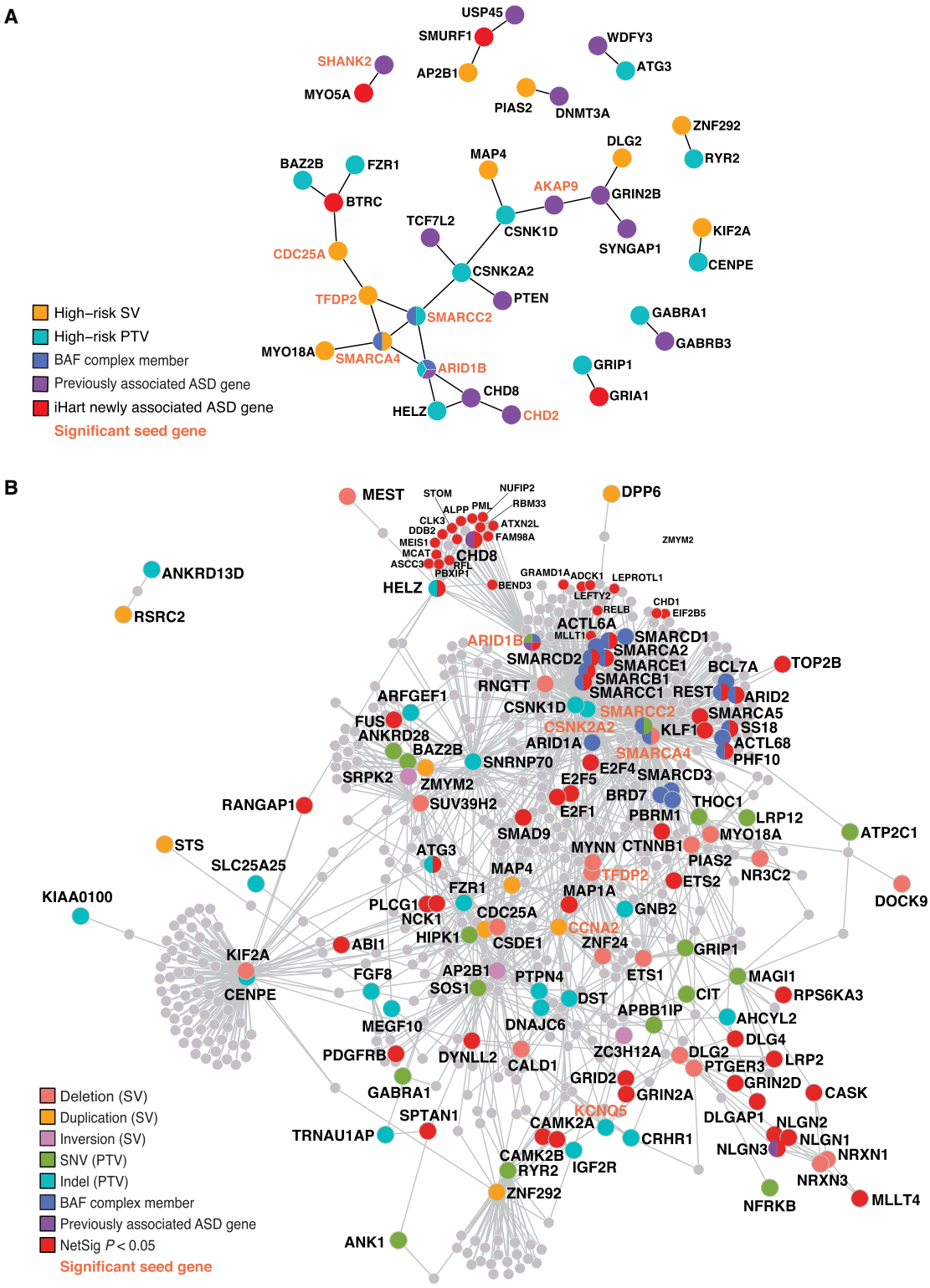

Figure 5. PPI Networks Formed by ASD Risk Genes

(A and B) Proteins encoded by previously known ASD risk genes (Sanders et al., 2015) are shown in purple, those belonging to the BAF complex are blue, and those belonging to more than one category are shown with all colors that apply. Gene labels for significant seed genes are shown in bold and orange font.

(A) Direct PPI network formed by constrained genes harboring high-risk inherited variants (98 genes) and ASD risk genes identified in the TADA mega-analysis (69 genes, FDR < 0.1). The direct PPI network formed by these 165 unique genes is significant for three connectivity metrics: the direct edges count ($p = 0.036$), the

(legend continued on next page)

gene by *in vivo* zebrafish modeling. We created a predicted null mutation in the single zebrafish *nr3c2* ortholog using CRISPR/Cas9 (Hwang et al., 2013; Figures S7A and S7B). Homozygous mutant animals are viable, fertile, and morphologically indistinguishable from their wild-type (WT) siblings. We first asked whether *nr3c2* mutant zebrafish exhibit abnormal social behaviors by developing and validating (STAR Methods; Figures S7C–S7H) a modified version of a previously described social preference assay (Figure 6A; Dreosti et al., 2015). We found that WT animals display a social preference for conspecifics (Figures S7C and S7F) at 3 weeks of age or older (data not shown), as reported previously (Dreosti et al., 2015). We found that, on average, $nr3c2^{+/+}$ and $nr3c2^{+/-}$ animals showed a social preference but $nr3c2^{-/-}$ animals did not (Figures 6B and 6C). There was no significant difference in the size of $nr3c2^{-/-}$ animals compared with their $nr3c2^{+/+}$ or $nr3c2^{+/-}$ siblings (Figure S7I), suggesting that the mutant phenotype was not simply due to developmental delay. This result indicates that $nr3c2^{-/-}$ animals have a social behavioral deficit.

Second, because ASD is often comorbid with disrupted sleep (Maxwell-Horn and Malow, 2017), we assayed sleep/wake behaviors (Prober et al., 2006) in 5- to 7-day-old *nr3c2* mutants. We found that $nr3c2^{-/-}$ animals were more active and slept less at night compared with their $nr3c2^{+/-}$ and $nr3c2^{+/+}$ siblings (Figures 6D–6F, 6H, and 6I). This effect was due to increased sleep latency, longer wake bouts, and shorter sleep bouts (Figures 6G, 6J, and 6K), indicating defects in both sleep initiation and maintenance, similar to sleep phenotypes observed in individuals with ASD (Ballester et al., 2018; Maxwell-Horn and Malow, 2017). Thus, *nr3c2* mutant zebrafish exhibit both social deficits and sleep disturbances, parallel to core and comorbid phenotypes observed in humans with ASD, which is consistent with the genetic evidence implicating *NR3C2* as an ASD risk gene.

DISCUSSION

To date, *de novo* variants have provided compelling evidence for dozens of ASD risk genes, but studies in primarily simplex families have yielded little, if any, inherited risk signal. Here we used WGS to identify over a dozen new genes that are significantly associated with ASD risk, the majority of which exhibit a contribution from rare inherited mutations. The identification of more than a dozen novel ASD risk genes was facilitated by studying families ascertained to contain two or more children with ASD, where inherited risk variants are likely to contribute to the observed ASD recurrence (Ronemus et al., 2014; Sebat et al., 2007; Virkud et al., 2009). We provide strong support for 69 ASD risk genes, 24 of which reach genome-wide significance after Bonferroni correction (Table 1). This substantially extends previous work; only a few genes had previously passed this threshold. The fact that we did not find global differences in the rate of rare inherited variants between affected and unaffected children is consistent with both (1) the known lower effect size of inherited ASD risk variation (compared with *de novo* pathogenic mutations) and (2) the expectation that, in multiplex families, the unaffected siblings (like their unaffected parents) also carry ASD risk variation (reduced penetrance), necessitating large sample sizes. Nevertheless, we identified a significant excess of constrained genes harboring inherited PTVs transmitted to all affected children but not transmitted to any unaffected children and found that these genes converge in a PPI network. This significant PPI network is seeded by known ASD risk genes, including multiple members of the BAF complex and other chromatin modifiers, and is also enriched for proteins that interact with additional ASD risk genes, many of which are involved in cortical neurogenesis (Parikshak et al., 2013). Single-cell sequencing data reveal that many of these ASD risk genes are expressed in developing glutamatergic neurons (Figures S6C and S6D), lending further support to the role of ASD risk genes in neurogenesis.

We employed WGS to enable the detection of non-coding variants and structural variation at high resolution and identified small non-coding regulatory deletions for both *DLG2* and *NR3C2*. The shared phenotypic features among the *NR3C2* variant carriers are consistent with a new syndromic form of ASD (Table S1). We were able to infer biological importance of the *NR3C2* putative regulatory deletion from its open chromatin state in the human developing brain (de la Torre-Ubieta et al., 2018) and phenotypic concordance to the family harboring the coding PTV. We also modeled this syndromic ASD in zebrafish, finding that the mutant animals exhibit both social deficits and sleep disturbances. We also identified a recurrent deletion significantly associated with ASD that disrupts the *DLG2* promoter, which further emphasizes the utility of WGS in identifying small functional deletions in non-coding regulatory regions.

More broadly, we found no global enrichment for non-coding variation in promoters, structural variant or otherwise, in affected versus unaffected children. Consistently, a previous investigation of 53 simplex families found a small enrichment ($p = 0.03$) for private and *de novo* disruptive variants in fetal brain DNase I hypersensitive sites in probands. However, this signal was limited to DNase I hypersensitive sites within 50 kb of genes that had been associated previously with ASD risk (Turner et al., 2016). More recent studies are consistent with our lack of enrichment for rare, non-coding variation (Werling et al., 2018). Advances in methods for analyzing the non-coding genome, similar to what has been done to identify functional PTVs (e.g., constraint metrics such as pLI), as well as increased sample sizes are necessary to improve power for identifying non-coding risk variants.

As previous studies have shown, inherited variation alone does not explain all instances of ASD within multiplex families, consistent with complex genetic contributions that include *de novo* mutations (Leppa et al., 2016). Given our success in uncovering many ASD risk genes whose signal is derived at least partially from inherited variation, even modest increases in sample sizes from families with multiple affected children will likely confirm many new genes. Our machine learning classifier,

seed direct degrees mean ($p = 0.046$), and the CI degrees mean ($p = 0.005$). Proteins encoded by a gene with a high-risk inherited SV are shown in gold, those with PTVs are shown in teal, and newly identified ASD risk genes by the iHART TADA mega-analysis are shown in red.
(B) Indirect PPI networks seeded by genes harboring high-risk inherited variants (98 genes). Proteins are colored according to the variant class identified, and NetSig significant genes ($p < 0.05$) are shown in red.

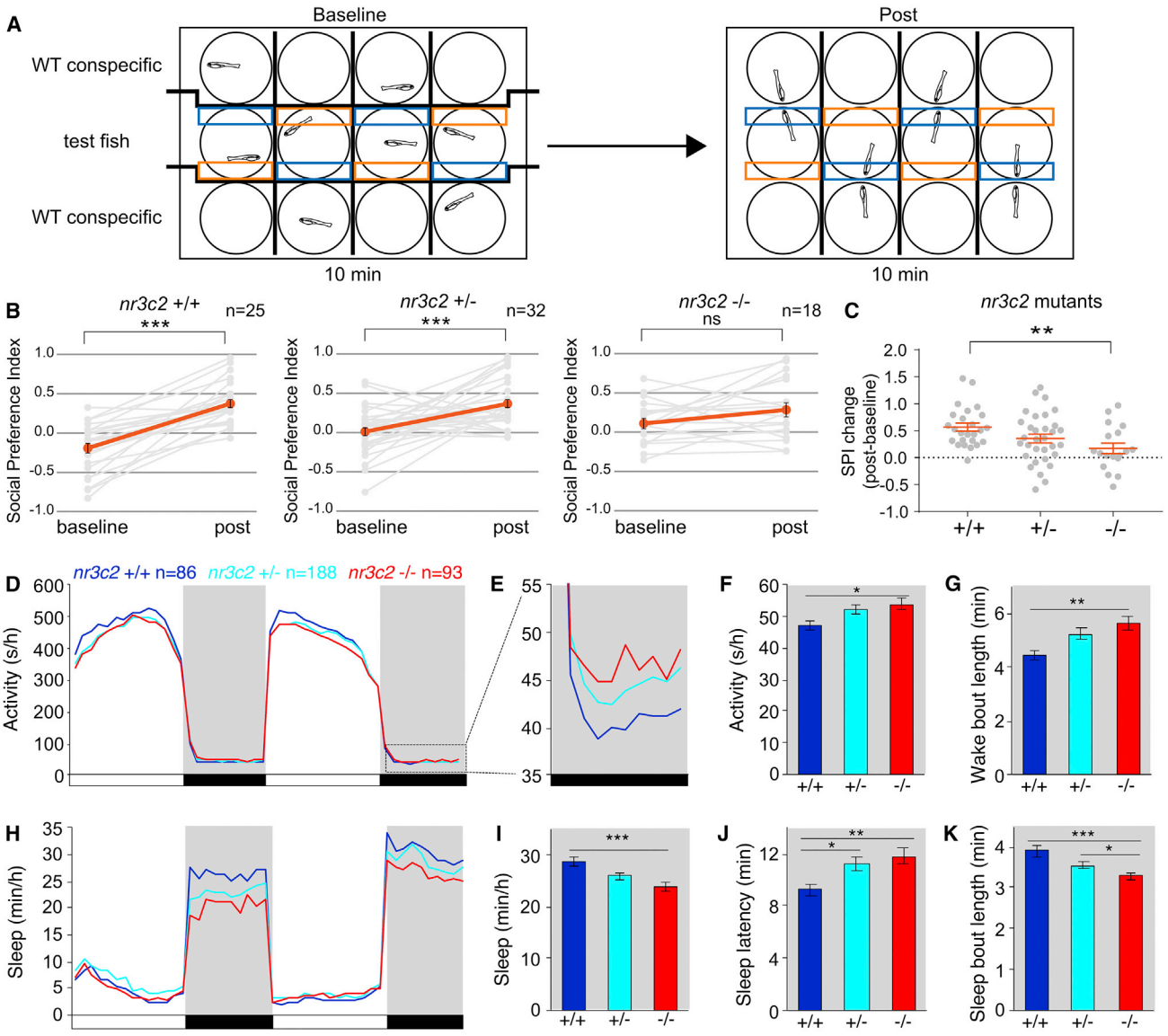

Figure 6. *nr3c2* Mutant Zebrafish Exhibit Impaired Social Preference Behavior and Disrupted Sleep at Night

(A) Schematic of the social preference behavioral assay. Boxes indicate regions used to quantify time spent by the test fish near (blue) and far (orange) from the conspecific. Thick lines indicate opaque dividers.

(B) *nr3c2*$^{+/+}$ and *nr3c2*$^{+/-}$ animals, on average, showed a significant preference for the conspecific but *nr3c2*$^{-/-}$ animals did not.

(C) The change in social preference index (SPI post – SPI baseline) was significantly smaller for *nr3c2*$^{-/-}$ animals compared with their *nr3c2*$^{+/+}$ siblings. Grey data represent individuals. Red data indicate mean ± standard error of the mean (SEM).

(D–K) Compared with their *nr3c2*$^{+/+}$ siblings at night, *nr3c2*$^{-/-}$ animals were 14% more active (D–F) and slept 17% less (H and I) because of 27% longer wake bouts (G) and 16% shorter sleep bouts (K). *nr3c2*$^{-/-}$ animals also showed a 28% longer sleep latency (time to first sleep bout at night) (J). There was no difference among the three genotypes in the number of sleep bouts at night or in any of these measures during the day (data not shown). The boxed region in (D) is magnified in (E). White and black bars indicate day (14 h) and night (10 h). Grey shading indicates night. Line graphs show mean, and bar graphs show mean ± SEM for 5 pooled experiments.

n = number of animals. *p < 0.05; **p < 0.01; ***p < 0.001, ns, not significant by paired t test (B), one-way ANOVA with Tukey's HSD post hoc test (C), or one-way ANOVA with Holm-Sidak post hoc test (F, G, and I–K). See also Figure S7.

ARC, will also enable increases in sample sizes when only LCL-derived DNA is available by distinguishing sequencing and cell line artifacts from true *de novo* variation.

As sample sizes grow, we can confirm whether our observed differences between simplex versus multiplex families are generalizable, but our data suggest substantial differences in their genetic architecture. Furthermore, with larger cohorts, we may be able to explore additive effects of both common and rare inherited variation and classify risk genes based on inheritance—(1) *de novo*, (2) inherited, or (3) *de novo* and inherited—to

establish whether these distinct gene classes are associated with phenotypic severity and/or specific biological pathways.

One striking finding of our study is that genes where the majority of the autism signal is from inherited variants are in pathways related to ion transport, the cell cycle, and the microtubule cytoskeleton (Figure S6E). In contrast, genes harboring primarily *de novo* variation are enriched in pathways related to transcriptional and chromatin regulation. These observations suggest that inherited and *de novo* variation, the former expected to have smaller effects and reduced penetrance and the latter with larger effects (Kosmicki et al., 2017), may impact distinct biological processes. Nevertheless, the ASD risk genes identified here contribute to cellular processes that are interconnected at the level of gene co-expression and PPI networks, a pattern of interaction that, we hypothesize, will be replicated in future studies having more power to assess variants on a broad continuum of effect sizes.

The iHART portal (http://www.ihart.org/home) provides researchers access to these data, facilitating additional analyses of these samples and integration with future cohorts.

STAR★METHODS

Detailed methods are provided in the online version of this paper and include the following:

- KEY RESOURCES TABLE
- LEAD CONTACT AND MATERIALS AVAILABILITY
- EXPERIMENTAL MODEL AND SUBJECT DETAILS
  - ASD multiplex family samples
  - Control cohorts
  - Zebrafish studies
- METHOD DETAILS
  - Whole-genome sequencing and data processing
  - Quality control assessment
  - Detection of large structural variants
  - Defining rare inherited and private variants
  - Non-coding analyses
  - High-risk inherited variant analysis
  - Gene set enrichment
  - DLG2 association and haplotype prediction
  - Artifact Removal by Classifier (ARC)
  - De novo mutation rate versus paternal age
  - Rates for rare *de novo* mutations
  - Power calculations for RDNVs
  - Defining pathogenic *de novo* variants
  - TADA mega-analysis
  - TADA simulations
  - Genes with large inherited PTV contribution
  - Single cell RNA-seq
  - Identifying candidate ASD genes with NetSig
  - Zebrafish experiments
- QUANTIFICATION AND STATISTICAL ANALYSIS
  - Determining rate differences between groups
  - TADA and TADA simulations
  - Zebrafish statistics
- DATA AND CODE AVAILABILITY
  - Interactive genotype/phenotype search engine
  - Zebrafish data

SUPPLEMENTAL INFORMATION

Supplemental Information can be found online at https://doi.org/10.1016/j.cell.2019.07.015.

ACKNOWLEDGMENTS

We thank Stephanie A. Arteaga, Stephanie N. Kravitz, Cheyenne L. Schloffman, Min Sun, Tor Solli-Nowlan, T. Chang, Hyejung Won, Sasha Sharma, Marlena Duda, Greg Madden McInnes, Ravina Jain, Valentí Moncunill, Josep M. Mercader, Montserrat Puiggròs, Hailey H. Choi, Anika Gupta, and David Torrents for technical support and Hannah Hurley and Amina Kinkhabwala for assistance with zebrafish experiments. We are grateful to The Hartwell Foundation for supporting the creation of the iHART database. We are grateful to the Simons Foundation for additional support for genome sequencing. We are grateful to the PRACE Research Infrastructure resource MareNostrum III based in Spain at the Barcelona Supercomputing Center. We thank the New York Genome Center for conducting sequencing and initial quality control. We thank A. Gordon, J. Huang, J. Sebat, and D. Antaki for help with resolving the DLG2 structural variant. We thank Amazon Web Services for their grant support for the computational infrastructure and storage for the iHART database. We thank J. Sul for helpful discussions and for suggesting a machine learning approach. This work has been supported by grants from The Hartwell Foundation and the NIH (U24MH081810, R01MH064547, NS101158, NS070911, NS101665, NS095824, S10OD011939, P30AG10161, R01AG17917, and U01AG61356) and from the Stanford Precision Health and Integrated Diagnostics Center and from the Stanford Bio-X Center. We are grateful to all of the families at the participating SSC sites as well as the principal investigators (A. Beaudet, R. Bernier, J. Constantino, E. Cook, E. Fombonne, D. Geschwind, R. Goin-Kochel, E. Hanson, D. Grice, A. Klin, D. Ledbetter, C. Lord, C. Martin, D. Martin, R. Maxim, J. Miles, O. Ousley, K. Pelphrey, B. Peterson, J. Piggot, C. Saulnier, M. State, W. Stone, J. Sutcliffe, C. Walsh, Z. Warren, and E. Wijsman). We appreciate obtaining access to genetic data on SFARI Base. Approved researchers can obtain the SSC population dataset described in this study (https://www.sfari.org/2015/12/11/whole-genome-analysis-of-the-simons-simplex-collection-ssc-2/#chapter-wgs-of-500-additional-ssc-families) by applying at https://base.sfari.org.

AUTHOR CONTRIBUTIONS

E.K.R. and L.P.C. contributed to the analytical plans, performed analyses, and interpreted results. J.K.L. selected and submitted samples for sequencing. E.K.R., J.Y.J., L.K.W., and J.K.L. performed quality control checks. L.K.W. wrote scripts for data processing and helped interpret results. L.P.C., D.K.H., J.Y.J., E.K.R., and D.P.W. developed ARC. C.H. interpreted results and ran TADA simulations. E.K.R. and C.H. ran high-risk inherited simulations. J.Y.J. and D.P.W. designed the access systems. J.Y.J. performed joint genotyping, VCF annotation, and data transfers. L.P.C. and D.K.H. processed SVs, and L.P.C. wrote the SV cross-algorithm comparison pipeline. D.P. performed single-cell analyses. M.J.G. analyzed phenotypes. V.M.L. helped with array-based CNV analyses. C.S., J.X., and D.A.P. performed and analyzed zebrafish experiments. D.P.W. identified and supplied funding. E.K.R. and D.H.G. took the lead in writing the manuscript, and all authors reviewed, edited, and approved the manuscript. D.H.G. and D.P.W. supervised the experimental design and analysis and interpreted results.

DECLARATION OF INTERESTS

The authors declare no competing interests.

Received: November 15, 2018
Revised: April 8, 2019
Accepted: July 11, 2019
Published: August 8, 2019

REFERENCES

Abecasis, G.R., Altshuler, D., Auton, A., Brooks, L.D., Durbin, R.M., Gibbs, R.A., Hurles, M.E., and McVean, G.A.; 1000 Genomes Project Consortium (2010). A map of human genome variation from population-scale sequencing. Nature *467*, 1061–1073.

Adzhubei, I.A., Schmidt, S., Peshkin, L., Ramensky, V.E., Gerasimova, A., Bork, P., Kondrashov, A.S., and Sunyaev, S.R. (2010). A method and server for predicting damaging missense mutations. Nat. Methods *7*, 248–249.

American Psychiatric Association (2013). Diagnostic and Statistical Manual of Mental Disorders, Fifth Edition (American Psychiatric Publishing).

An, J.Y., Lin, K., Zhu, L., Werling, D.M., Dong, S., Brand, H., Wang, H.Z., Zhao, X., Schwartz, G.B., Collins, R.L., et al. (2018). Genome-wide de novo risk score implicates promoter variation in autism spectrum disorder. Science *362*, eaat6576.

Auton, A., Brooks, L.D., Durbin, R.M., Garrison, E.P., Kang, H.M., Korbel, J.O., Marchini, J.L., McCarthy, S., McVean, G.A., and Abecasis, G.R.; 1000 Genomes Project Consortium (2015). A global reference for human genetic variation. Nature *526*, 68–74.

Bacchelli, E., Blasi, F., Biondolillo, M., Lamb, J.A., Bonora, E., Barnby, G., Parr, J., Beyer, K.S., Klauck, S.M., Poustka, A., et al.; International Molecular Genetic Study of Autism Consortium (IMGSAC) (2003). Screening of nine candidate genes for autism on chromosome 2q reveals rare nonsynonymous variants in the cAMP-GEFII gene. Mol. Psychiatry *8*, 916–924.

Ballester, P., Martinez, M.J., Javaloyes, A., Inda, M.M., Fernandez, N., Gazquez, P., Aguilar, V., Perez, A., Hernandez, L., Richdale, A.L., et al. (2018). Sleep Problems in Adults With Autism Spectrum Disorder and Intellectual Disability. Autism Res. *12*, 66–79.

Barnett, D.W., Garrison, E.K., Quinlan, A.R., Strömberg, M.P., and Marth, G.T. (2011). BamTools: a C++ API and toolkit for analyzing and managing BAM files. Bioinformatics *27*, 1691–1692.

Battle, A., Brown, C.D., Engelhardt, B.E., and Montgomery, S.B.; GTEx Consortium; Laboratory, Data Analysis &Coordinating Center (LDACC)—Analysis Working Group; Statistical Methods groups—Analysis Working Group; Enhancing GTEx (eGTEx) groups; NIH Common Fund; NIH/NCI; NIH/NHGRI; NIH/NIMH; NIH/NIDA; Biospecimen Collection Source Site—NDRI; Biospecimen Collection Source Site—RPCI; Biospecimen Core Resource—VARI; Brain Bank Repository—University of Miami Brain Endowment Bank; Leidos Biomedical—Project Management; ELSI Study; Genome Browser Data Integration &Visualization—EBI; Genome Browser Data Integration &Visualization—UCSC Genomics Institute, University of California Santa Cruz; Lead analysts; Laboratory, Data Analysis &Coordinating Center (LDACC); NIH program management; Biospecimen collection; Pathology; eQTL manuscript working group (2017). Genetic effects on gene expression across human tissues. Nature *550*, 204–213.

Bayés, A., van de Lagemaat, L.N., Collins, M.O., Croning, M.D., Whittle, I.R., Choudhary, J.S., and Grant, S.G. (2011). Characterization of the proteome, diseases and evolution of the human postsynaptic density. Nat. Neurosci. *14*, 19–21.

Belgard, T.G., and Geschwind, D.H. (2013). Retooling spare parts: gene duplication and cognition. Nat. Neurosci. *16*, 6–8.

Bennett, D.A., Buchman, A.S., Boyle, P.A., Barnes, L.L., Wilson, R.S., and Schneider, J.A. (2018). Religious Orders Study and Rush Memory and Aging Project. J. Alzheimers Dis. *64* (s1), S161–S189.

Bernier, R., Golzio, C., Xiong, B., Stessman, H.A., Coe, B.P., Penn, O., Witherspoon, K., Gerdts, J., Baker, C., Vulto-van Silfhout, A.T., et al. (2014). Disruptive CHD8 mutations define a subtype of autism early in development. Cell *158*, 263–276.

Besenbacher, S., Sulem, P., Helgason, A., Helgason, H., Kristjansson, H., Jonasdottir, A., Jonasdottir, A., Magnusson, O.T., Thorsteinsdottir, U., Masson, G., et al. (2016). Multi-nucleotide de novo Mutations in Humans. PLoS Genet. *12*, e1006315.

Brandler, W.M., Antaki, D., Gujral, M., Noor, A., Rosanio, G., Chapman, T.R., Barrera, D.J., Lin, G.N., Malhotra, D., Watts, A.C., et al. (2016). Frequency and Complexity of De Novo Structural Mutation in Autism. Am. J. Hum. Genet. *98*, 667–679.

Brandler, W.M., Antaki, D., Gujral, M., Kleiber, M.L., Whitney, J., Maile, M.S., Hong, O., Chapman, T.R., Tan, S., Tandon, P., et al. (2018). Paternally inherited cis-regulatory structural variants are associated with autism. Science *360*, 327–331.

C Yuen, R.K., Merico, D., Bookman, M., L Howe, J., Thiruvahindrapuram, B., Patel, R.V., Whitney, J., Deflaux, N., Bingham, J., Wang, Z., et al. (2017). Whole genome sequencing resource identifies 18 new candidate genes for autism spectrum disorder. Nat. Neurosci. *20*, 602–611.

Chen, K., Wallis, J.W., McLellan, M.D., Larson, D.E., Kalicki, J.M., Pohl, C.S., McGrath, S.D., Wendl, M.C., Zhang, Q., Locke, D.P., et al. (2009). BreakDancer: an algorithm for high-resolution mapping of genomic structural variation. Nat. Methods *6*, 677–681.

Coe, B.P., Witherspoon, K., Rosenfeld, J.A., van Bon, B.W., Vulto-van Silfhout, A.T., Bosco, P., Friend, K.L., Baker, C., Buono, S., Vissers, L.E., et al. (2014). Refining analyses of copy number variation identifies specific genes associated with developmental delay. Nat. Genet. *46*, 1063–1071.

Colvert, E., Tick, B., McEwen, F., Stewart, C., Curran, S.R., Woodhouse, E., Gillan, N., Hallett, V., Lietz, S., Garnett, T., et al. (2015). Heritability of Autism Spectrum Disorder in a UK Population-Based Twin Sample. JAMA Psychiatry *72*, 415–423.

Conrad, D.F., Keebler, J.E., DePristo, M.A., Lindsay, S.J., Zhang, Y., Casals, F., Idaghdour, Y., Hartl, C.L., Torroja, C., Garimella, K.V., et al.; 1000 Genomes Project (2011). Variation in genome-wide mutation rates within and between human families. Nat. Genet. *43*, 712–714.

Constantino, J.N., Zhang, Y., Frazier, T., Abbacchi, A.M., and Law, P. (2010). Sibling recurrence and the genetic epidemiology of autism. Am. J. Psychiatry *167*, 1349–1356.

Cooper, G.M., Coe, B.P., Girirajan, S., Rosenfeld, J.A., Vu, T.H., Baker, C., Williams, C., Stalker, H., Hamid, R., Hannig, V., et al. (2011). A copy number variation morbidity map of developmental delay. Nat. Genet. *43*, 838–846.

Darnell, J.C., Van Driesche, S.J., Zhang, C., Hung, K.Y., Mele, A., Fraser, C.E., Stone, E.F., Chen, C., Fak, J.J., Chi, S.W., et al. (2011). FMRP stalls ribosomal translocation on mRNAs linked to synaptic function and autism. Cell *146*, 247–261.

de la Torre-Ubieta, L., Stein, J.L., Won, H., Opland, C.K., Liang, D., Lu, D., and Geschwind, D.H. (2018). The Dynamic Landscape of Open Chromatin during Human Cortical Neurogenesis. Cell *172*, 289–304.e18.

De Rubeis, S., He, X., Goldberg, A.P., Poultney, C.S., Samocha, K., Cicek, A.E., Kou, Y., Liu, L., Fromer, M., Walker, S., et al.; DDD Study; Homozygosity Mapping Collaborative for Autism; UK10K Consortium (2014). Synaptic, transcriptional and chromatin genes disrupted in autism. Nature *515*, 209–215.

Deciphering Developmental Disorders Study (2017). Prevalence and architecture of de novo mutations in developmental disorders. Nature *542*, 433–438.

DePristo, M.A., Banks, E., Poplin, R., Garimella, K.V., Maguire, J.R., Hartl, C., Philippakis, A.A., del Angel, G., Rivas, M.A., Hanna, M., et al. (2011). A framework for variation discovery and genotyping using next-generation DNA sequencing data. Nat. Genet. *43*, 491–498.

Developmental Disabilities Monitoring Network Surveillance Year 2010 Principal Investigators and Centers for Disease Control and Prevention (CDC) (2014). Prevalence of autism spectrum disorder among children aged 8 years - autism and developmental disabilities monitoring network, 11 sites, United States, 2010. MMWR Surveill. Summ. *63*, 1–21.

Dreosti, E., Lopes, G., Kampff, A.R., and Wilson, S.W. (2015). Development of social behavior in young zebrafish. Front. Neural Circuits *9*, 39.

Drmanac, R., Sparks, A.B., Callow, M.J., Halpern, A.L., Burns, N.L., Kermani, B.G., Carnevali, P., Nazarenko, I., Nilsen, G.B., Yeung, G., et al. (2010). Human genome sequencing using unchained base reads on self-assembling DNA nanoarrays. Science *327*, 78–81.

Francioli, L.C., Polak, P.P., Koren, A., Menelaou, A., Chun, S., Renkens, I., van Duijn, C.M., Swertz, M., Wijmenga, C., van Ommen, G., et al.; Genome of the

Netherlands Consortium (2015). Genome-wide patterns and properties of de novo mutations in humans. Nat. Genet. *47*, 822–826.

Gaugler, T., Klei, L., Sanders, S.J., Bodea, C.A., Goldberg, A.P., Lee, A.B., Mahajan, M., Manaa, D., Pawitan, Y., Reichert, J., et al. (2014). Most genetic risk for autism resides with common variation. Nat. Genet. *46*, 881–885.

Geschwind, D.H., and Flint, J. (2015). Genetics and genomics of psychiatric disease. Science *349*, 1489–1494.

Glessner, J.T., Wang, K., Cai, G., Korvatska, O., Kim, C.E., Wood, S., Zhang, H., Estes, A., Brune, C.W., Bradfield, J.P., et al. (2009). Autism genome-wide copy number variation reveals ubiquitin and neuronal genes. Nature *459*, 569–573.

Goldmann, J.M., Wong, W.S., Pinelli, M., Farrah, T., Bodian, D., Stittrich, A.B., Glusman, G., Vissers, L.E., Hoischen, A., Roach, J.C., et al. (2016). Parent-of-origin-specific signatures of de novo mutations. Nat. Genet. *48*, 935–939.

Handsaker, R.E., Korn, J.M., Nemesh, J., and McCarroll, S.A. (2011). Discovery and genotyping of genome structural polymorphism by sequencing on a population scale. Nat. Genet. *43*, 269–276.

Handsaker, R.E., Van Doren, V., Berman, J.R., Genovese, G., Kashin, S., Boettger, L.M., and McCarroll, S.A. (2015). Large multiallelic copy number variations in humans. Nat. Genet. *47*, 296–303.

Harrow, J., Frankish, A., Gonzalez, J.M., Tapanari, E., Diekhans, M., Kokocinski, F., Aken, B.L., Barrell, D., Zadissa, A., Searle, S., et al. (2012). GENCODE: the reference human genome annotation for The ENCODE Project. Genome research *22*, 1760–1774.

He, X., Sanders, S.J., Liu, L., De Rubeis, S., Lim, E.T., Sutcliffe, J.S., Schellenberg, G.D., Gibbs, R.A., Daly, M.J., Buxbaum, J.D., et al. (2013). Integrated model of de novo and inherited genetic variants yields greater power to identify risk genes. PLoS Genet. *9*, e1003671.

Hoekstra, R.A., Bartels, M., Verweij, C.J., and Boomsma, D.I. (2007). Heritability of autistic traits in the general population. Arch. Pediatr. Adolesc. Med. *161*, 372–377.

Hormozdiari, F., Penn, O., Borenstein, E., and Eichler, E.E. (2015). The discovery of integrated gene networks for autism and related disorders. Genome Res. *25*, 142–154.

Horn, H., Lawrence, M.S., Chouinard, C.R., Shrestha, Y., Hu, J.X., Worstell, E., Shea, E., Ilic, N., Kim, E., Kamburov, A., et al. (2018). NetSig: network-based discovery from cancer genomes. Nat. Methods *15*, 61–66.

Hwang, W.Y., Fu, Y., Reyon, D., Maeder, M.L., Tsai, S.Q., Sander, J.D., Peterson, R.T., Yeh, J.R., and Joung, J.K. (2013). Efficient genome editing in zebrafish using a CRISPR-Cas system. Nat. Biotechnol. *31*, 227–229.

Iossifov, I., Ronemus, M., Levy, D., Wang, Z., Hakker, I., Rosenbaum, J., Yamrom, B., Lee, Y.H., Narzisi, G., Leotta, A., et al. (2012). De novo gene disruptions in children on the autistic spectrum. Neuron *74*, 285–299.

Iossifov, I., O'Roak, B.J., Sanders, S.J., Ronemus, M., Krumm, N., Levy, D., Stessman, H.A., Witherspoon, K.T., Vives, L., Patterson, K.E., et al. (2014). The contribution of de novo coding mutations to autism spectrum disorder. Nature *515*, 216–221.

Jun, G., Flickinger, M., Hetrick, K.N., Romm, J.M., Doheny, K.F., Abecasis, G.R., Boehnke, M., and Kang, H.M. (2012). Detecting and estimating contamination of human DNA samples in sequencing and array-based genotype data. Am. J. Hum. Genet. *91*, 839–848.

Karczewski, K.J., Francioli, L.C., Tiao, G., Cummings, B.B., Alföldi, J., Wang, Q., Collins, R.L., Laricchia, K.M., Ganna, A., Birnbaum, D.P., et al. (2019). Variation across 141,456 human exomes and genomes reveals the spectrum of loss-of-function intolerance across human protein-coding genes. bioRxiv. https://doi.org/10.1101/531210.

Klei, L., Sanders, S.J., Murtha, M.T., Hus, V., Lowe, J.K., Willsey, A.J., Moreno-De-Luca, D., Yu, T.W., Fombonne, E., Geschwind, D., et al. (2012). Common genetic variants, acting additively, are a major source of risk for autism. Mol. Autism *3*, 9.

Kong, A., Frigge, M.L., Masson, G., Besenbacher, S., Sulem, P., Magnusson, G., Gudjonsson, S.A., Sigurdsson, A., Jonasdottir, A., Jonasdottir, A., et al. (2012). Rate of de novo mutations and the importance of father's age to disease risk. Nature *488*, 471–475.

Kosmicki, J.A., Samocha, K.E., Howrigan, D.P., Sanders, S.J., Slowikowski, K., Lek, M., Karczewski, K.J., Cutler, D.J., Devlin, B., Roeder, K., et al. (2017). Refining the role of de novo protein-truncating variants in neurodevelopmental disorders by using population reference samples. Nat. Genet. *49*, 504–510.

Krishnan, A., Zhang, R., Yao, V., Theesfeld, C.L., Wong, A.K., Tadych, A., Volfovsky, N., Packer, A., Lash, A., and Troyanskaya, O.G. (2016). Genome-wide prediction and functional characterization of the genetic basis of autism spectrum disorder. Nat. Neurosci. *19*, 1454–1462.

Krumm, N., Turner, T.N., Baker, C., Vives, L., Mohajeri, K., Witherspoon, K., Raja, A., Coe, B.P., Stessman, H.A., He, Z.X., et al. (2015). Excess of rare, inherited truncating mutations in autism. Nat. Genet. *47*, 582–588.

Lage, K., Karlberg, E.O., Størling, Z.M., Olason, P.I., Pedersen, A.G., Rigina, O., Hinsby, A.M., Tümer, Z., Pociot, F., Tommerup, N., et al. (2007). A human phenome-interactome network of protein complexes implicated in genetic disorders. Nat. Biotechnol. *25*, 309–316.

Lajonchere, C.M.; AGRE Consortium (2010). Changing the landscape of autism research: the autism genetic resource exchange. Neuron *68*, 187–191.

Lake, B.B., Chen, S., Sos, B.C., Fan, J., Kaeser, G.E., Yung, Y.C., Duong, T.E., Gao, D., Chun, J., Kharchenko, P.V., and Zhang, K. (2018). Integrative single-cell analysis of transcriptional and epigenetic states in the human adult brain. Nat. Biotechnol. *36*, 70–80.

Larsch, J., and Baier, H. (2018). Biological motion as an innate perceptual mechanism driving social affiliation. Curr. Biol. *28*, 3523–3532.e4.

Layer, R.M., Chiang, C., Quinlan, A.R., and Hall, I.M. (2014). LUMPY: a probabilistic framework for structural variant discovery. Genome Biol. *15*, R84.

Lek, M., Karczewski, K.J., Minikel, E.V., Samocha, K.E., Banks, E., Fennell, T., O'Donnell-Luria, A.H., Ware, J.S., Hill, A.J., Cummings, B.B., et al.; Exome Aggregation Consortium (2016). Analysis of protein-coding genetic variation in 60,706 humans. Nature *536*, 285–291.

Leppa, V.M., Kravitz, S.N., Martin, C.L., Andrieux, J., Le Caignec, C., Martin-Coignard, D., DyBuncio, C., Sanders, S.J., Lowe, J.K., Cantor, R.M., and Geschwind, D.H. (2016). Rare Inherited and De Novo CNVs Reveal Complex Contributions to ASD Risk in Multiplex Families. Am. J. Hum. Genet. *99*, 540–554.

Levy, D., Ronemus, M., Yamrom, B., Lee, Y.H., Leotta, A., Kendall, J., Marks, S., Lakshmi, B., Pai, D., Ye, K., et al. (2011). Rare de novo and transmitted copy-number variation in autistic spectrum disorders. Neuron *70*, 886–897.

Li, H., and Durbin, R. (2009). Fast and accurate short read alignment with Burrows-Wheeler transform. Bioinformatics *25*, 1754–1760.

Li, H., Handsaker, B., Wysoker, A., Fennell, T., Ruan, J., Homer, N., Marth, G., Abecasis, G., and Durbin, R.; 1000 Genome Project Data Processing Subgroup (2009). The Sequence Alignment/Map format and SAMtools. Bioinformatics *25*, 2078–2079.

MacDonald, J.R., Ziman, R., Yuen, R.K., Feuk, L., and Scherer, S.W. (2014). The Database of Genomic Variants: a curated collection of structural variation in the human genome. Nucleic Acids Res. *42*, D986–D992.

Marshall, C.R., Noor, A., Vincent, J.B., Lionel, A.C., Feuk, L., Skaug, J., Shago, M., Moessner, R., Pinto, D., Ren, Y., et al. (2008). Structural variation of chromosomes in autism spectrum disorder. Am. J. Hum. Genet. *82*, 477–488.

Martin, C.L., Duvall, J.A., Ilkin, Y., Simon, J.S., Arreaza, M.G., Wilkes, K., Alvarez-Retuerto, A., Whichello, A., Powell, C.M., Rao, K., et al. (2007). Cytogenetic and molecular characterization of A2BP1/FOX1 as a candidate gene for autism. Am. J. Med. Genet. B Neuropsychiatr. Genet. *144B*, 869–876.

Maxwell-Horn, A., and Malow, B.A. (2017). Sleep in Autism. Semin. Neurol. *37*, 413–418.

McKenna, A., Hanna, M., Banks, E., Sivachenko, A., Cibulskis, K., Kernytsky, A., Garimella, K., Altshuler, D., Gabriel, S., Daly, M., and DePristo, M.A. (2010). The Genome Analysis Toolkit: a MapReduce framework for analyzing next-generation DNA sequencing data. Genome Res. *20*, 1297–1303.

McLaren, W., Gil, L., Hunt, S.E., Riat, H.S., Ritchie, G.R., Thormann, A., Flicek, P., and Cunningham, F. (2016). The Ensembl Variant Effect Predictor. Genome Biol. *17*, 122.

Mefford, H.C., Sharp, A.J., Baker, C., Itsara, A., Jiang, Z., Buysse, K., Huang, S., Maloney, V.K., Crolla, J.A., Baralle, D., et al. (2008). Recurrent rearrangements of chromosome 1q21.1 and variable pediatric phenotypes. N. Engl. J. Med. *359*, 1685–1699.

Michaelson, J.J., Shi, Y., Gujral, M., Zheng, H., Malhotra, D., Jin, X., Jian, M., Liu, G., Greer, D., Bhandari, A., et al. (2012). Whole-genome sequencing in autism identifies hot spots for de novo germline mutation. Cell *151*, 1431–1442.

Miller, D.T., Adam, M.P., Aradhya, S., Biesecker, L.G., Brothman, A.R., Carter, N.P., Church, D.M., Crolla, J.A., Eichler, E.E., Epstein, C.J., et al. (2010). Consensus statement: chromosomal microarray is a first-tier clinical diagnostic test for individuals with developmental disabilities or congenital anomalies. Am. J. Hum. Genet. *86*, 749–764.

Moncunill, V., Gonzalez, S., Beà, S., Andrieux, L.O., Salaverria, I., Royo, C., Martinez, L., Puiggròs, M., Segura-Wang, M., Stütz, A.M., et al. (2014). Comprehensive characterization of complex structural variations in cancer by directly comparing genome sequence reads. Nat. Biotechnol. *32*, 1106–1112.

Moy, S.S., Nonneman, R.J., Shafer, G.O., Nikolova, V.D., Riddick, N.V., Agster, K.L., Baker, L.K., and Knapp, D.J. (2013). Disruption of social approach by MK-801, amphetamine, and fluoxetine in adolescent C57BL/6J mice. Neurotoxicol. Teratol. *36*, 36–46.

Nithianantharajah, J., Komiyama, N.H., McKechanie, A., Johnstone, M., Blackwood, D.H., St Clair, D., Emes, R.D., van de Lagemaat, L.N., Saksida, L.M., Bussey, T.J., and Grant, S.G. (2013). Synaptic scaffold evolution generated components of vertebrate cognitive complexity. Nat. Neurosci. *16*, 16–24.

Nowakowski, T.J., Bhaduri, A., Pollen, A.A., Alvarado, B., Mostajo-Radji, M.A., Di Lullo, E., Haeussler, M., Sandoval-Espinosa, C., Liu, S.J., Velmeshev, D., et al. (2017). Spatiotemporal gene expression trajectories reveal developmental hierarchies of the human cortex. Science *358*, 1318–1323.

O'Roak, B.J., Vives, L., Girirajan, S., Karakoc, E., Krumm, N., Coe, B.P., Levy, R., Ko, A., Lee, C., Smith, J.D., et al. (2012). Sporadic autism exomes reveal a highly interconnected protein network of de novo mutations. Nature *485*, 246–250.

Ozonoff, S., Young, G.S., Carter, A., Messinger, D., Yirmiya, N., Zwaigenbaum, L., Bryson, S., Carver, L.J., Constantino, J.N., Dobkins, K., et al. (2011). Recurrence risk for autism spectrum disorders: a Baby Siblings Research Consortium study. Pediatrics *128*, e488–e495.

Parikshak, N.N., Luo, R., Zhang, A., Won, H., Lowe, J.K., Chandran, V., Horvath, S., and Geschwind, D.H. (2013). Integrative functional genomic analyses implicate specific molecular pathways and circuits in autism. Cell *155*, 1008–1021.

Parikshak, N.N., Gandal, M.J., and Geschwind, D.H. (2015). Systems biology and gene networks in neurodevelopmental and neurodegenerative disorders. Nat. Rev. Genet. *16*, 441–458.

Parikshak, N.N., Swarup, V., Belgard, T.G., Irimia, M., Ramaswami, G., Gandal, M.J., Hartl, C., Leppa, V., Ubieta, L.T., Huang, J., et al. (2016). Genome-wide changes in lncRNA, splicing, and regional gene expression patterns in autism. Nature *540*, 423–427.

Pinto, D., Delaby, E., Merico, D., Barbosa, M., Merikangas, A., Klei, L., Thiruvahindrapuram, B., Xu, X., Ziman, R., Wang, Z., et al. (2014). Convergence of genes and cellular pathways dysregulated in autism spectrum disorders. Am. J. Hum. Genet. *94*, 677–694.

Polioudakis, D., de la Torre-Ubieta, L., Langerman, J., Elkins, A.G., Shi, X., Stein, J.L., Vuong, C.K., Nichterwitz, S., Gevorgian, M., Opland, C.K., et al. (2019). A Single-Cell Transcriptomic Atlas of Human Neocortical Development during Mid-gestation. Neuron. Published online July 11, 2019. https://doi.org/10.1016/j.neuron.2019.06.011.

Prober, D.A., Rihel, J., Onah, A.A., Sung, R.J., and Schier, A.F. (2006). Hypocretin/orexin overexpression induces an insomnia-like phenotype in zebrafish. J. Neurosci. *26*, 13400–13410.

Purcell, S., Neale, B., Todd-Brown, K., Thomas, L., Ferreira, M.A., Bender, D., Maller, J., Sklar, P., de Bakker, P.I., Daly, M.J., and Sham, P.C. (2007). PLINK: a tool set for whole-genome association and population-based linkage analyses. Am. J. Hum. Genet. *81*, 559–575.

Quinlan, A.R., and Hall, I.M. (2010). BEDTools: a flexible suite of utilities for comparing genomic features. Bioinformatics *26*, 841–842.

Ronemus, M., Iossifov, I., Levy, D., and Wigler, M. (2014). The role of de novo mutations in the genetics of autism spectrum disorders. Nat. Rev. Genet. *15*, 133–141.

Rossin, E.J., Lage, K., Raychaudhuri, S., Xavier, R.J., Tatar, D., Benita, Y., Cotsapas, C., and Daly, M.J.; International Inflammatory Bowel Disease Genetics Consortium (2011). Proteins encoded in genomic regions associated with immune-mediated disease physically interact and suggest underlying biology. PLoS Genet. *7*, e1001273.

Samocha, K.E., Robinson, E.B., Sanders, S.J., Stevens, C., Sabo, A., McGrath, L.M., Kosmicki, J.A., Rehnström, K., Mallick, S., Kirby, A., et al. (2014). A framework for the interpretation of de novo mutation in human disease. Nat. Genet. *46*, 944–950.

Sanders, S.J., Ercan-Sencicek, A.G., Hus, V., Luo, R., Murtha, M.T., Moreno-De-Luca, D., Chu, S.H., Moreau, M.P., Gupta, A.R., Thomson, S.A., et al. (2011). Multiple recurrent de novo CNVs, including duplications of the 7q11.23 Williams syndrome region, are strongly associated with autism. Neuron *70*, 863–885.

Sanders, S.J., Murtha, M.T., Gupta, A.R., Murdoch, J.D., Raubeson, M.J., Willsey, A.J., Ercan-Sencicek, A.G., DiLullo, N.M., Parikshak, N.N., Stein, J.L., et al. (2012). De novo mutations revealed by whole-exome sequencing are strongly associated with autism. Nature *485*, 237–241.

Sanders, S.J., He, X., Willsey, A.J., Ercan-Sencicek, A.G., Samocha, K.E., Cicek, A.E., Murtha, M.T., Bal, V.H., Bishop, S.L., Dong, S., et al.; Autism Sequencing Consortium (2015). Insights into Autism Spectrum Disorder Genomic Architecture and Biology from 71 Risk Loci. Neuron *87*, 1215–1233.

Sandin, S., Lichtenstein, P., Kuja-Halkola, R., Larsson, H., Hultman, C.M., and Reichenberg, A. (2014). The familial risk of autism. JAMA *311*, 1770–1777.

Scheet, P., and Stephens, M. (2006). A fast and flexible statistical model for large-scale population genotype data: applications to inferring missing genotypes and haplotypic phase. Am. J. Hum. Genet. *78*, 629–644.

Schneider, C.A., Rasband, W.S., and Eliceiri, K.W. (2012). NIH Image to ImageJ: 25 years of image analysis. Nat. Methods *9*, 671–675.

Sebat, J., Lakshmi, B., Malhotra, D., Troge, J., Lese-Martin, C., Walsh, T., Yamrom, B., Yoon, S., Krasnitz, A., Kendall, J., et al. (2007). Strong association of de novo copy number mutations with autism. Science *316*, 445–449.

Skuse, D.H., Mandy, W.P., and Scourfield, J. (2005). Measuring autistic traits: heritability, reliability and validity of the Social and Communication Disorders Checklist. Br. J. Psychiatry *187*, 568–572.

Snijders Blok, L., Madsen, E., Juusola, J., Gilissen, C., Baralle, D., Reijnders, M.R., Venselaar, H., Helsmoortel, C., Cho, M.T., Hoischen, A., et al.; DDD Study (2015). Mutations in DDX3X Are a Common Cause of Unexplained Intellectual Disability with Gender-Specific Effects on Wnt Signaling. Am. J. Hum. Genet. *97*, 343–352.

Sugathan, A., Biagioli, M., Golzio, C., Erdin, S., Blumenthal, I., Manavalan, P., Ragavendran, A., Brand, H., Lucente, D., Miles, J., et al. (2014). CHD8 regulates neurodevelopmental pathways associated with autism spectrum disorder in neural progenitors. Proc. Natl. Acad. Sci. USA *111*, E4468–E4477.

Turner, T.N., Hormozdiari, F., Duyzend, M.H., McClymont, S.A., Hook, P.W., Iossifov, I., Raja, A., Baker, C., Hoekzema, K., Stessman, H.A., et al. (2016). Genome Sequencing of Autism-Affected Families Reveals Disruption of Putative Noncoding Regulatory DNA. Am. J. Hum. Genet. *98*, 58–74.

Van der Auwera, G.A., Carneiro, M.O., Hartl, C., Poplin, R., Del Angel, G., Levy-Moonshine, A., Jordan, T., Shakir, K., Roazen, D., Thibault, J., et al. (2013). From FastQ data to high confidence variant calls: the Genome

Analysis Toolkit best practices pipeline. Curr. Protoc. Bioinformatics *43*, 11.10.11–33.

Vandeweyer, G., Helsmoortel, C., Van Dijck, A., Vulto-van Silfhout, A.T., Coe, B.P., Bernier, R., Gerdts, J., Rooms, L., van den Ende, J., Bakshi, M., et al. (2014). The transcriptional regulator ADNP links the BAF (SWI/SNF) complexes with autism. Am. J. Med. Genet. C. Semin. Med. Genet. *166C*, 315–326.

Virkud, Y.V., Todd, R.D., Abbacchi, A.M., Zhang, Y., and Constantino, J.N. (2009). Familial aggregation of quantitative autistic traits in multiplex versus simplex autism. Am. J. Med. Genet. B Neuropsychiatr. Genet. *150B*, 328–334.

Voineagu, I., Wang, X., Johnston, P., Lowe, J.K., Tian, Y., Horvath, S., Mill, J., Cantor, R.M., Blencowe, B.J., and Geschwind, D.H. (2011). Transcriptomic analysis of autistic brain reveals convergent molecular pathology. Nature *474*, 380–384.

Wang, K., Li, M., and Hakonarson, H. (2010). ANNOVAR: functional annotation of genetic variants from high-throughput sequencing data. Nucleic Acids Res. *38*, e164.

Werling, D.M., and Geschwind, D.H. (2015). Recurrence rates provide evidence for sex-differential, familial genetic liability for autism spectrum disorders in multiplex families and twins. Mol. Autism *6*, 27.

Werling, D.M., Brand, H., An, J.Y., Stone, M.R., Zhu, L., Glessner, J.T., Collins, R.L., Dong, S., Layer, R.M., Markenscoff-Papadimitriou, E., et al. (2018). An analytical framework for whole-genome sequence association studies and its implications for autism spectrum disorder. Nat. Genet. *50*, 727–736.

Weyn-Vanhentenryck, S.M., Mele, A., Yan, Q., Sun, S., Farny, N., Zhang, Z., Xue, C., Herre, M., Silver, P.A., Zhang, M.Q., et al. (2014). HITS-CLIP and integrative modeling define the Rbfox splicing-regulatory network linked to brain development and autism. Cell Rep. *6*, 1139–1152.

Willsey, A.J., Sanders, S.J., Li, M., Dong, S., Tebbenkamp, A.T., Muhle, R.A., Reilly, S.K., Lin, L., Fertuzinhos, S., Miller, J.A., et al. (2013). Coexpression networks implicate human midfetal deep cortical projection neurons in the pathogenesis of autism. Cell *155*, 997–1007.

Zimmermann, F.F., Gaspary, K.V., Siebel, A.M., and Bonan, C.D. (2016). Oxytocin reversed MK-801-induced social interaction and aggression deficits in zebrafish. Behav. Brain Res. *311*, 368–374.

Zook, J.M., Chapman, B., Wang, J., Mittelman, D., Hofmann, O., Hide, W., and Salit, M. (2014). Integrating human sequence data sets provides a resource of benchmark SNP and indel genotype calls. Nat. Biotechnol. *32*, 246–251.

STAR★METHODS

KEY RESOURCES TABLE

REAGENT or RESOURCE	SOURCE	IDENTIFIER
Biological Samples		
AGRE DNA samples	AGRE	https://www.autismspeaks.org/agre
Chemicals, Peptides, and Recombinant Proteins		
MK-801	Sigma Aldrich	Cat# M107
Ethanol	Koptec	Cat# V1016
Critical Commercial Assays		
Illumina Infinium Human Exome-12 v1.2	Illumina	Cat# WG-353-1204
Infinium CoreExome-24 Kit	Illumina	Cat# 20024662
Illumina TruSeq Nano library kits	Illumina	Cat# 20015964
Deposited Data		
Raw and analyzed data: WGS	This paper	http://www.ihart.org/access
Exome Variant Server, NHLBI GO Exome Sequencing Project (ESP)	Exome Variant Server, NHLBI GO Exome Sequencing Project (ESP), Seattle, WA (URL: https://evs.gs.washington.edu/EVS/) [Oct 2017].	https://evs.gs.washington.edu/EVS/RRID:SCR_012761
Exome Aggregation Consortium (ExAC)	Lek et al., 2016	http://exac.broadinstitute.org/RRID:SCR_004068
Complete Genomics Genomes	Drmanac et al., 2010	https://www.completegenomics.com/public-data/69-genomes/
1000 Genomes Project	Auton et al., 2015	https://www.internationalgenome.org/RRID:SCR_008801
Genome Aggregation Database (gnomAD) (version 2.0.2)	Karczewski et al., 2019	https://gnomad.broadinstitute.org/downloads RRID:SCR_014964
Database of Genomic Variants (DGV)	MacDonald et al., 2014 [release date 2015-07-23]	http://dgv.tcag.ca/dgv/app/home RRID:SCR_004896
Human Reference Genome (Hg19; 1000 Genomes Project Phase 3 reference assembly)	N/A	https://www.internationalgenome.org/category/grch37/
Illumina genotyping array data for AGRE CNV calls	Leppa et al., 2016	NDAR: Submission ID 393 (https://nda.nih.gov/study.html?id=393)
Genome in a bottle (GIAB)	Zook et al., 2014	ftp://ftp-trace.ncbi.nlm.nih.gov/giab/ftp/data/NA12878/analysis/NIST_union_callsets_06172013/NISTIntegratedCalls_14datasets_131103_allcall_UGHapMerge_HomRef_VQSRv2.18_all_bias_nouncert_excludesimplerep_excludesegdups_excludedecoy_excludeRepSeqSTRs_noCNVs.vcf.gz
Simons Simplex Collection (SSC), Pilot set and Phase 1 WGS quads	N/A	https://www.sfari.org/resource/sfari-base/RRID:SCR_004644
pLI constrained gene scores (nonpsych)	Lek et al., 2016	ftp://ftp.broadinstitute.org/pub/ExAC_release/release0.3/functional_gene_constraint/
gnomAD observed/expected (o/e) constrained gene scores	Karczewski et al., 2019	https://storage.googleapis.com/gnomad-public/release/2.1.1/constraint/gnomad.v2.1.1.lof_metrics.by_gene.txt.bgz
GTEx data v6	Battle et al., 2017	dbGap # phs000424.v6.p1 RRID:SCR_013042
ARC annotation source files	This paper	https://github.com/walllab/iHART-ARC/tree/master/Annotation_Source_Files
PolyPhen-2 v2.2.2r395 HDIV predictions from the Whole Human Exome Sequence Space (WHESS dataset)	Adzhubei et al., 2010	http://genetics.bwh.harvard.edu/pph2/dbsearch.shtml RRID:SCR_013189

(*Continued on next page*)

Continued

REAGENT or RESOURCE	SOURCE	IDENTIFIER
Gencode v19	Harrow et al., 2012	https://www.gencodegenes.org/human/release_19.html RRID:SCR_014966
Exome mutation rates (PTV and Mis3)	Samocha et al., 2014	N/A
InWeb	Lage et al., 2007	http://www.lagelab.org/wp-content/uploads/2017/06/NetSig_Code.zip
Experimental Models: Organisms/Strains		
zebrafish *nr3c2 ct#867* mutant	This paper	RRID: ZDB-ALT-190607-1
Oligonucleotides		
Primer: *nr3c2* mutant Forward: CTTCCCTG CAGAGCTCAAAG	This paper	N/A
Primer: *nr3c2* mutant Reverse: ATAGCCAG CGAACACCACTT	This paper	N/A
Recombinant DNA		
Software and Algorithms		
ANNOVAR (version 20160201)	Wang et al., 2010	http://annovar.openbioinformatics.org/en/latest/ RRID:SCR_012821
PLINK (version 1.07)	Purcell et al., 2007	http://zzz.bwh.harvard.edu/plink/RRID:SCR_001757
verifyIDintensity (VII)	Jun et al., 2012	https://github.com/gjun/verifyIDintensity
Burrows-Wheeler Aligner (bwa-mem, version 0.7.8)	Li and Durbin, 2009	http://bio-bwa.sourceforge.net/RRID:SCR_010910
BamTools (version 2.3.0)	Barnett et al., 2011	https://github.com/pezmaster31/bamtools RRID:SCR_015987
PicardTools (version 1.119)	N/A	http://broadinstitute.github.io/picard/RRID: SCR_006525
GATK (version 3.2-2)	McKenna et al., 2010	https://software.broadinstitute.org/gatk/RRID: SCR_001876
Variant Effect Predictor (version VEPv83)	McLaren et al., 2016	http://uswest.ensembl.org//useast.ensembl.org/info/docs/tools/vep/index.html?redirectsrc=//uswest.ensembl.org%2Finfo%2Fdocs%2Ftools%2Fvep%2Findex.html RRID:SCR_007931
SAMtools (version 1.2)	Li et al., 2009	http://www.htslib.org/doc/samtools.html RRID:SCR_002105
BreakDancer (version 1.1.2)	Chen et al., 2009	https://github.com/genome/breakdancer RRID:SCR_001799
LUMPY (version 0.2.11)	Layer et al., 2014	https://github.com/arq5x/lumpy-sv RRID:SCR_003253
GenomeSTRiP (version 1.04)	Handsaker et al., 2011; Handsaker et al., 2015	http://software.broadinstitute.org/software/genomestrip/
Somatic MUtation FINder (SMuFin)	Moncunill et al., 2014	http://cg.bsc.es/smufin/
Bamotate	Sanders et al., 2015	N/A
BEDTools (version 2.28.0)	Quinlan and Hall, 2010	https://bedtools.readthedocs.io/en/latest/ RRID:SCR_006646
Disease Association Protein-Protein Link Evaluator (DAPPLE)	Rossin et al., 2011	https://cloud.genepattern.org/gp/pages/login.jsf
fastPHASE	Scheet and Stephens, 2006	http://stephenslab.uchicago.edu/software.html#fastphase
Artifact Removal by Classifier (ARC)	This paper	https://github.com/walllab/iHART-ARC
Python scikit-learn package (version 0.18.1)	N/A	https://www.python.org/RRID:SCR_008394
Transmitted And *De novo* Association (TADA) test	He et al., 2013	http://www.compgen.pitt.edu/TADA/TADA_homepage.htm
NetSig	Horn et al., 2018	http://www.lagelab.org/wp-content/uploads/2017/06/NetSig_Code.zip

(*Continued on next page*)

Continued

REAGENT or RESOURCE	SOURCE	IDENTIFIER
R (version 3.5.1)	N/A	https://www.r-project.org/ RRID:SCR_001905
Megalign Pro	DNASTAR	https://www.dnastar.com/manuals/MegAlignPro/15.2/en/topic/welcome-to-megalign-pro
MATLAB (R2017b)	Mathworks	RRID:SCR_001622
Prism6	GraphPad	RRID:SCR_002798
ImageJ	Schneider et al., 2012	RRID:SCR_002285
Other		
Flat-bottom 12-well plate for zebrafish social preference assay	CytoOne	Cat# CC7672-7512
96-well plate for zebrafish sleep assay	GE Healthcare Life Sciences	Cat# 7701-1651
MicroAmp Optical Adhesive Film for zebrafish sleep assay	Thermo Fisher Scientific	Cat# 4311971
Illumina's HiSeq X	Illumina	Cat# SY-412-1001

LEAD CONTACT AND MATERIALS AVAILABILITY

The whole-genome sequencing data generated during this study are available from the Hartwell Foundation's Autism Research and Technology Initiative (iHART) following request and approval of the data use agreement available at http://www.ihart.org. We provide the code for ARC (Artifact Removal by Classifier), our random forest supervised model developed to distinguish true rare *de novo* variants from LCL-specific genetic aberrations or other types of artifacts such as sequencing and mapping errors, together with a full tutorial at https://github.com/walllab/iHART-ARC. The zebrafish mutant line generated in this study will be deposited to the Zebrafish International Resource Center (ct867, ZFIN ID: ZDB-ALT-190607-1). Further information and requests for resources and reagents should be directed to and will be fulfilled by the Lead Contact, Dennis Paul Wall (dpwall@stanford.edu).

EXPERIMENTAL MODEL AND SUBJECT DETAILS

ASD multiplex family samples

The UCLA and Stanford IRBs designated this study as "Not human subjects research" and therefore exempt from review; this was due to the study being limited to previously-existing coded data and specimens. Study subjects were carefully selected from the Autism Genetic Resource Exchange (AGRE) (Lajonchere, 2010) and chosen from families including two or more individuals with ASD (those with a "derived affected status" of "autism", "broad-spectrum", "nqa", "asd", or "spectrum"). Patients with known genetic causes of ASD (15p13 duplication, 15q deletion, 15q duplication, 16p deletion, 16p duplication, 22q duplication, mosaic for deleted Y, mosaic trisomy 12, Trisomy 21 (Down Syndrome), Fragile X) or syndromes with overlapping ASD-features (Gaucher Disease, Marfan's Syndrome, Sotos Syndrome) were excluded from sequencing. We prioritized ASD-families harboring affected female subjects. We also prioritized monozygotic-twin containing families, in part to facilitate the development of our machine learning model (Artifact Removal by Classifier (ARC)). A complete list of sequenced samples can be found in Table S1.

A total of 2,308 individuals from 493 ASD families from the Autism Genetic Resource Exchange (AGRE) (Table S1) passed quality control. Details for each of these 2,308 samples, including sex, ethnicity, phenotype, and familial relationship, can be found in Table S1. Unless otherwise specified (STAR Methods or Table S1), our analyses included a subset of 1,177 children (960 affected and 217 unaffected children) for whom both biological parents were sequenced.

Purified DNA was obtained from the Rutgers University Cell and DNA Repository (RUCDR; Piscataway, NJ). Where available, DNA from whole blood was used; however, for many samples, only lymphoblastoid cell line (LCL) DNA was available because DNA was not extracted from whole blood at the time of recruitment.

Control cohorts

Throughout this manuscript, we reference several control cohorts used for assessing variant frequencies in samples not ascertained for ASD. These cohorts are described below. The AD cohort was *only* used for the high-risk inherited simulation analysis. The Genome Aggregation Database (gnomAD) cohort was *only* used for the analysis of non-coding variants.

Publicly available databases

Unless otherwise specified, the publicly available databases (all annotations provided by ANNOVAR) referenced include: the NHLBI Exome Sequencing Project (ESP, esp6500siv2_all) (https://evs.gs.washington.edu/EVS/), the Exome Aggregation Consortium (ExAC_ALL annotation from version exac03nonpsych) (Lek et al., 2016), 46 unrelated, whole-genome sequenced (high coverage

on the Complete Genomics platform), non-disease samples (https://www.completegenomics.com/public-data/69-genomes/, cg46) (Drmanac et al., 2010) and the 1000 genomes project (1000 g2015aug_all) (Auton et al., 2015).

UCLA internal controls

Throughout this manuscript, the use of "UCLA internal controls" refers to a set of 379 unrelated, whole-genome sequenced (30x coverage on Illumina platform, processed by the same bioinformatics pipeline as was used for iHART) samples with a neurodegenerative disorder known as Progressive Supranuclear Palsy (PSP). There is no known etiological overlap or comorbidity between PSP and ASD.

Healthy Non-Phaseable (HNP) samples

Throughout this manuscript, the use of "HNPs" refers to the 922 healthy non-phaseable (no biological parents sequenced) iHART samples. The majority of these samples are parents of affected or unaffected children. Due to the fact that these samples likely harbor genetic ASD-risk variants, these HNPs provide a helpful estimate of allele frequencies but we generally apply more permissive allele frequency filtering to retain inherited risk variants.

Alzheimer's disease cohort

The Alzheimer's disease (AD) cohort (n = 1,173 unrelated samples) was selected as a control group for the high-risk inherited simulation analysis (Bennett et al., 2018). This AD cohort was selected because of the lack of ASD comorbidity and the late-onset of the disease which precludes ASD diagnoses in this cohort.

gnomAD

We used allele frequency estimates from gnomAD (version 2.0.2) (Karczewski et al., 2019) for the analysis of non-coding variants because these data include 15,708 genomes from unrelated individuals which facilitates allele frequency estimation in the non-coding regions of the genome.

Curated Database of Genomic Variants (cDGV)

To assess the population frequency of structural variants in a more precise manner, we manually curated the Database of Genomic Variants (DGV, release date 2015-07-23) (MacDonald et al., 2014). This curation involved removing studies that did not include sample identifications and/or only analyzed targeted genomic regions, as well as SVs detected in non-human samples or individuals diagnosed with intellectual disability (ID) or developmental delay (DD). The ID and DD samples from two studies (Coe et al. 2014 and Cooper et al., 2011) were flagged for exclusion by Evan Eichler's laboratory and their accession numbers were shared with us (E. Eichler, personal communication). This resulted in a total of 26,353 unique samples with DGV data. We then removed redundancies in DGV's SV types by collapsing all SV types in the remaining samples into five different categories: deletions ("deletion" + "loss"), duplications ("duplication" + "gain" + "tandem duplication"), insertions ("insertion" + "mobile element insertion" + "novel sequence insertion"), inversions, and unknown ("complex" + "gain+loss" + "sequence alteration"). We finally re-calculated the frequency of the different SV categories by continuous genomic intervals, avoiding double-counting SVs (of the same type) identified in the same sample and same region by different studies.

Zebrafish studies

Zebrafish experiments and husbandry followed standard protocols in accordance with Caltech Institutional Animal Care and Use Committee (IACUC) guidelines (animal protocol 1580). Zebrafish behaviors were studied before the onset of sexual differentiation and were performed using siblings with the same genetic background, differing only in *nr3c2* genotype, or in treatment with drugs and appropriate vehicle controls. WT and mutant stocks were derived from a TLAB hybrid strain. Animals were raised on a 14:10 hour light:dark cycle, and were housed in Petri dishes with 50 animals per dish in E3 medium (5 mM NaCl, 0.17 mM KCl, 0.33 mM $CaCl_2$, 0.33 mM $MgSO_4$) until 4 days post-fertilization. Animals were then either assayed for sleep/wake behaviors, or were transferred to 0.8 L tanks and fed rotifers (*Brachionus plicatilis*) twice per day until reaching 2 weeks of age. Animals were then fed brine shrimp (*Artemia salina*) until 3-4 weeks of age, at which point their social behavior was assayed. Animals were not involved in any previous procedures and were naive to the tests and drugs used. The zebrafish mutant generated in this study will be made available upon request.

METHOD DETAILS

Whole-genome sequencing and data processing

DNA samples were submitted to the New York Genome Center (NYGC) for whole-genome sequencing. DNA samples were examined for quality/quantity and subsequently genotyped using Illumina Infinium Human Exome-12 v1.2 or Infinium Human Core Exome microarrays (San Diego, CA) according to standard manufacturer protocols. Identity-by-descent estimation and sex checks in PLINK v1.07 (Purcell et al., 2007) were used to validate expected versus observed family relationships and confirm sample identity based on these genome-wide genotyping data. Contamination was assessed using verifyIDintensity (VII) (Jun et al., 2012); samples exceeding 3% contamination in two or more modes were excluded from sequencing.

Samples passing these array-based identity and quality checks were sequenced at NYGC using the Illumina TruSeq Nano library kits and Illumina's HiSeq X (San Diego, CA) according to standard manufacturer protocols.

All iHART WGS data were processed through the same bioinformatics pipeline; this pipeline was designed based on GATK's best practices (DePristo et al., 2011; Van der Auwera et al., 2013). The metadata for each sample are stored in a custom MySQL database

where each sample was tracked as it progressed through the sequencing and bioinformatic pipelines, and finally the quality assurance metrics were populated based on the resulting processed data. The first step in the pipeline was to align the raw short sequence reads to the human reference genome (human_g1k_v37.fasta). This was accomplished by processing the fastq files with the Burrows-Wheeler Aligner (bwa-mem, version 0.7.8) (Li and Durbin, 2009) to generate BAM files. BAM files were generated in a read-group-aware fashion (properly annotating sequence reads derived from the same flow cell and lane) and thus multiple BAM files were subsequently merged using BamTools (version 2.3.0) (Barnett et al., 2011) to generate a single BAM file per sample. The second step in the pipeline was to mark duplicate reads in the BAM file using the Picard MarkDuplicates tool (version 1.119; http://broadinstitute.github.io/picard/). The third step in the pipeline was to perform local realignment of reads around indels using GATK's IndelRealigner (version 3.2-2). The fourth step in the pipeline was to genotype each sample, generating a gVCF file. To achieve accuracy at this stage, base quality score recalibration was run using GATK (version 3.2-2) (McKenna et al., 2010). Subsequently, GATK's HaplotypeCaller (version 3.2-2) was run on each base-recalibrated BAM to identify the variant and non-variant bases in the genome. All four of these steps were performed at the NYGC, resulting in a BAM and a gVCF file for each sample.

The fifth step in the pipeline was to jointly call variants across all iHART samples to generate a VCF file. This was accomplished by combining gVCF files, 200 samples at a time using GATK's combineGVCFs (version 3.2-2), and then running GATK's GenotypeGVCFs (version 3.2-2). Step 5 was accomplished by splitting data by chromosome (which increases parallelization) and resulted in one cohort-wide VCF per chromosome. Finally, to help filter out low quality variants within the call set, GATK's Variant Quality Score Recalibration (VQSR, version 3.2-2) was run to generate well-calibrated quality scores. The final step in the pipeline was to annotate the resulting variant calls (SNVs and indels) in order to generate an annotated VCF file. This was accomplished by annotating with ANNOVAR (version 20160201) (Wang et al., 2010) and then with Variant Effect Predictor (version VEPv83) (McLaren et al., 2016). The resulting VCF contains gene-based, region-based, and filter-based annotations for each identified variant. For all the analyses described in this manuscript, we excluded VQSR failed variants and multi-allelic variants.

Quality control assessment

We performed standard quality control checks on our WGS data to ensure both sequencing/variant quality and sample identity. This included checking relatedness between samples, exclusion of duplicate samples, concordance between genotyping chip and WGS data, concordance between self-declared sex and observed biological sex, exclusion of samples with contamination from other samples, variant quality evaluation with GATK's VariantEval module (data not shown), and sequencing coverage. A total of 2,308 individuals from 493 ASD families from the Autism Genetic Resource Exchange (AGRE) passed quality control (Table S1).

Whole-genome sequence coverage

We used SAMtools v1.2 (Li et al., 2009) depth utility to calculate genome-wide (excluding gap regions in the human reference genome, downloaded from the UCSC table browser) per-base sequencing coverage for each sample. In order to reduce memory requirements, the reported depth was truncated at a maximum of 500 reads. Subsequently, we calculated two main summary statistics for each sample using custom scripts: (i) average coverage and (ii) percent of the genome (excluding gap regions) covered at 1X, 10X, 20X, 30X and 40X. On average, 98.97 $\pm$ 0.37 % of bases were covered at a depth of $\geq$ 10X (Figures S1A–S1E).

Variant inheritance classifications

Children with only a single parent sequenced are referred to as partially phase-able and children with both parents sequenced are referred to as fully phase-able. For each member of the iHART cohort with at least one parent sequenced (partially or fully phase-able affected or unaffected children), all identified variants were classified based on their observed inheritance (defined below). To perform this classification, we developed a custom script to simultaneously evaluate variant quality and inheritance within each family. Prior to this classification step, all VQSR failed variants and multi-allelic variants were excluded. Additionally, we set permissive quality control thresholds in order to retain sensitivity while removing variants with a high probability of being false positives. Variants were required to have a depth of $\geq$ 10x, a genotype quality of $\geq$ 25, and a ratio of alternative allele reads/total reads $\geq$ 0.2. We assumed that if a variant met these quality thresholds, then the assigned genotype was correct.

Every variant was categorized into one of eight inheritance types: (i) *de novo*, (ii) maternally inherited, (iii) paternally inherited, (iv) newly homozygous, (v) newly hemizygous, (vi) missing, (vii) unknown phase, or (viii) uncertain. While maternally inherited, paternally inherited, and *de novo* categories are self-explanatory, definitions for the remaining inheritance classifications are more complex. A homozygous variant observed in a child was called a newly homozygous variant if it was heterozygous in both parents. Similarly, a newly hemizygous variant on the X chromosome was defined as a hemizygous variant observed in a male child which was not identified as hemizygous in the corresponding father. A variant was classified as missing (./.) if the variant was called in at least one child in the iHART cohort but did not have sufficient coverage for GATK's haplotype caller to define a genotype. A variant was classified as unknown phase if a child had an inherited variant and only one biological parent was sequenced (unless on a sex chromosome where inheritance can be inferred) or if both parents carry the variant and thus the phase cannot be determined from this site alone. Finally, a variant was classified as uncertain if it could not be classified into another inheritance type; this includes: Mendelian error variants (e.g., heterozygous variants on male sex chromosomes), variants failing the quality control thresholds above (in a child or a parent), or a variant that couldn't be classified with confidence (e.g., a variant identified in a child but absent in its only sequenced parent could

be *de novo* or inherited). Unless otherwise specified, variants classified as missing, uncertain, or unknown phase were excluded from our analyses.

Detection of large structural variants

We developed a custom pipeline for high-resolution detection of large structural variants (SVs) from whole-genome sequence data (Figures S1F–S1H). This pipeline combines four different detection algorithms, including: BreakDancer (Chen et al., 2009), LUMPY (Layer et al., 2014), GenomeSTRiP (Handsaker et al., 2011, 2015), and Somatic MUtation FINder (SMuFin) (Moncunill et al., 2014) (STAR Methods; Figures 1 and S1F–S1H).

BreakDancer

We first used the bam2cfg.pl script (part of the BreakDancer v1.1.2 package (Chen et al., 2009) to generate a tab-delimited configuration file per family required to run BreakDancerMax. This configuration file specifies the locations of the BAM files, the desired detection parameters (the upper and lower insert size thresholds to detect SVs) and sample metadata (e.g., read group and sequencing platform); we used default detection parameters. We then ran BreakDancerMax to call SVs per chromosome within families. The resulting output files were combined for all chromosomes and samples and converted into a single VCF file using a custom script (see *SV post-detection processing* for details about genotyping). We filtered to exclude variants if the identified variant (i) was in a sequence contig, (ii) had a quality score < 80, (iii) had < 4 supporting reads, or (iv) had a length of < 71 base pairs (small indel).

LUMPY

We used SAMtools v1.1 (Li et al., 2009) to extract both the discordant paired-end reads and the split-read alignments per sample, generating two different sorted BAM files required to run LUMPY v0.2.11(Layer et al., 2014). We then ran lumpyexpress to call SVs within families. We merged the resulting VCF files per family (containing raw calls), into a single genotyped VCF file for all the samples in the cohort, using a custom script (see *SV post-detection processing* for details about genotyping). We filtered to exclude variants if the identified variant (i) was in a sequence contig or (ii) was a small insertion or inversions with a length of < 71 base pairs. No filter was applied for small duplications because the min length identified was 74 base pairs.

GenomeSTRiP

We obtained genotyped SV calls generated by the NYGC's in-house GenomeSTRiP v1.04 standard pipeline (Handsaker et al., 2011; Handsaker et al., 2015). This pipeline consists of three main modules: (i) SVPreprocess: a pre-processing module that was run per sample to generate genome-wide metadata required for next processes; (ii) SVDiscovery: a discovery module, that was run in three large batches to call deletions, producing a VCF file with raw calls detected per batch; and (iii) SVGenotyper: a module run to produce genotyped VCF files per sequencing batch. In total, we received three genotyped VCF files, for sequencing batch one (N = 956 samples), two (N = 538 samples), and three (N = 858 samples). We filtered out variants flagged as ''LowQual'' and merged the final set of SV calls for downstream analyses.

SMuFin

We adapted Somatic MUtation FINder (SMuFin) (Moncunill et al., 2014), a reference-free approach, for family-based structural variant detection by performing *de novo* alignment of child reads to the parental reads (Figure S1H), to provide high sensitivity and break point accuracy in the detection of SVs. Families were processed as independent trios and SMuFin was used to directly contrast sequencing reads between the parents and the offspring (Figure S1H). During the detection process, one parental genome is used as the reference genome to identify genetic variants in the children that were absent in that parent and then this process is repeated using the other parental genome as the reference genome. This produced one output file for each parent-offspring comparison run, containing the SVs detected per comparison. We then merged all the SV calls identified in phase-able individuals (i.e., individuals for which at least one biological parent was also sequenced) and classified them according to their inheritance patterns.

SV post-detection processing

We assumed heterozygosity for all SV calls, with two exceptions: (i) SVs identified in sex chromosomes from males, which were annotated as homozygous; and (ii) SVs identified by GenomeSTRiP, whose genotypes were defined by its SVGenotyper module. The inheritance type for all SVs identified in phase-able individuals was classified as: *de novo*, maternal, paternal, newly homozygous, newly hemizygous, unknown phase, missing, or uncertain – as defined above. For SVs, the missing classification was only applied to BreakDancer calls with a quality score of < 80 and/or < 4 reads supporting the variant call.

We focused on the analysis of high-confidence SVs, specifically deletions (DELs), duplications (DUPs), and inversions (INVs), by restricting to events identified by at least two detection algorithms and removing SVs that overlapped genomic regions of low complexity (i.e., centromeres, segmental duplications, regions of low mappability, and regions subject to somatic recombination in antibodies and T cell receptor genes) (Brandler et al., 2016) by more than 50%. We made two exceptions to the rule that at least two detection algorithms must detect an SV. The first exception was to exclude SVs detected by only LUMPY and BreakDancer because this subset of SVs had very low concordance with genotype array data (Table S5). The second exception was to include an SV event if it was called by at least two detection algorithms in one or more family members, but called by only one algorithm in another family member.

Even though WGS theoretically enables high-resolution prediction of breakpoints, the breakpoints called by the detection algorithms can vary due to technical differences between these methods and also between samples (e.g., coverage) despite the

fact that they are detecting the same underlying SV event. To adjust for this, SV calls made by different detection algorithms were considered to be the same SV event if they were: (i) called in the same individual, (ii) had a reciprocal overlap of at least 50%, and (iii) shared the same SV type (e.g., DEL) and inheritance pattern. A similar approach was subsequently applied to SVs within a family, where SV events are likely inherited and thus identical; the breakpoints of overlapping SVs (≥50% reciprocal overlap of the same SV type) identified in individuals within the same family were adjusted to the predicted minimum start and maximum end coordinates predicted (maximum size based on breakpoints) in family members with the SV call.

SVs were defined as rare if they had no more than 50% overlap in (a) regions commonly disrupted by SVs in our Curated Database of Genomic Variants (cDGV; allele frequency ≥ 0.001) and (b) regions commonly disrupted by the same SV type (allele frequency ≥ 0.01) in the HNP samples. We also classified SVs as rare if (c) they had a region of ≥ 500Kb that did not overlap with common SVs in cDGV (allele frequency ≥ 0.001) or HNP samples (allele frequency ≥ 0.01).

Finally, in order to facilitate prioritization for likely pathogenic variants, gene-based and region-based annotations were added to the final set of high-confidence SV calls by using custom scripts and the Bamotate annotation tool (Leppa et al., 2016).

Multi-algorithm consensus SV calls

The four algorithms chosen to call SVs use different detection strategies and are suitable for identifying different sizes and types of SVs with varying levels of sensitivity and specificity. Therefore, we ran a multi-algorithm comparison to identify high-quality SVs identified by at least two methods (as described above). We used BEDTools (Quinlan and Hall, 2010) to intersect SV calls detected by the different algorithms by performing an all-against-all comparison (Figure S1F; Table S5).

The start and end positions of identical SV events identified for an individual (≥50% reciprocal overlap of the same SV type and inheritance pattern) were reassigned based on the coordinates from the detection algorithm predicted to be more precise in calling breakpoints. By considering the strategy implemented to identify SVs (e.g., split-read methods can detect SVs at single base-pair resolution) for each detection algorithm, we defined the following rank for breakpoint precision accuracy: SMuFin (split-read and *de novo* assembly method) > LUMPY (split-read and read-pair method, with coordinates assigned within families) > GenomeSTRiP (split-read, read-pair and read-count method, with coordinates assigned within sequencing batch) > BreakDancer (read-pair detection method).

Array-based SV detection is a well-established method with high accuracy for certain SV classes, in particular large deletions (Miller et al., 2010). Thus, to confirm our ranking of algorithms by their SV breakpoint precision, we compared our WGS-based SV calls to SV calls obtained from Illumina genotyping array data (Leppa et al., 2016) on overlapping AGRE samples. Specifically, we identified a high confidence set of heterozygous deletions for which heterozygous deletions were also detected (≥50% reciprocal overlap) in the array data (n = 224 SVs). We then used GATK's VariantEval tool to generate het:hom metrics for SNVs identified within 224 heterozygous deletions. A heterozygous deletion with accurate break points would include only homozygous SNVs (het:hom ratio of zero). This analysis reavealed no significant differences between these methods (with all of them showing a median het:hom ratio of 0.01), but ranking of mean het:hom ratios was generally consistent with our ranking of algorithms by their SV breakpoint precision: SMuFin (0.028) < LUMPY (0.043) < BreakDancer (0.059) < GenomeSTRiP (0.067).

Joint LUMPY-BreakDancer SV call inspections

Copy Number Variants (CNVs) detected from genotyping array data can be visualized by plotting the B Allele Frequency and Log R Ratio values for array genotyped SNPs within the estimated CNV region and its flanking regions (25% of the length of the CNV on each side); we will refer to this as an "array visualization plot." Given the low concordance rate between LUMPY and BreakDancer SV calls with other methods (Table S5), we manually inspected array visualization plots generated by using available Illumina genotyping array data (Leppa et al., 2016) for regions with LUMPY-BreakDancer joint SV calls identified in the iHART WGS data.

We randomly selected LUMPY-BreakDancer detected SV events within bins containing events of different sizes/lengths (n = 218) and used a custom script to generate array visualization plots for each detected SV region. For each of the 218 SVs, an array visualization plot was generated for the carrier and all corresponding family members. Manual inspection of the array visualization plots was conducted (blinded with respect to the predicted carrier(s) of the LUMPY-BreakDancer SV call), and each SV was categorized as true or false. By treating the array-based true calls as the gold standard, we were able to estimate the validation rate for LUMPY-BreakDancer joint SV calls (Table S5).

Sensitivity to detect rare SVs

A set of rare SVs detected from Illumina genotyping array data (array-SVs) were available for 553 iHART fully phase-able samples (Leppa et al., 2016). We used BEDTools (Quinlan and Hall, 2010) to intersect our set of SV calls (WGS SV calls, DELs and DUPs) with rare SVs identified in genotyping array data (Leppa et al., 2016) in these 553 overlapping samples. We evaluated our sensitivity to detect array-SVs by considering events detected with ≥ 50% reciprocal overlap by both array and NGS in the same sample – both with and without LUMPY-BreakDancer joint SV calls (Table S5).

Defining rare inherited and private variants

We define rare inherited variants (SNVs and indels) as those with an allele frequency (AF) less than or equal to 0.1% in public databases (1000 g, ESP6500, ExACv3.0, cg46), internal controls, and iHART HNP samples and were restricted to those not missing in more than 25% of controls and not flagged as low-confidence by the Genome in a Bottle Consortium (GIAB; Zook et al., 2014). Rare SVs (DELs, DUPs, INVs) were defined as those with an AF < 0.001 in cDGV and an AF < 0.01 in iHART HNP samples.

We define private variants as variants that are observed in one and only one iHART/AGRE family (AF~0.05%) and are not missing in more than 25% of iHART HNPs. Additionally, private variants were (i) never observed in any control cohorts (AF = 0), (ii) not missing in more than 25% of the PSP control samples, and (iii) not flagged as low-confidence by the GIAB consortium. We only report analyses for iHART private variants in the 1,177 children with both biological parents sequenced (fully phase-able). For non-coding private inherited variants, variants present in gnomAD (version 2.0.2) were also removed.

Non-coding analyses

Definition of non-coding variants

We defined non-coding SNVs and indels as variants that do not occur within a coding transcript, as annotated by VEP. This includes 17 of the 35 VEP consequences: "mature miRNA variant," "5 prime UTR variant," "3 prime UTR variant," "non-coding transcript exon variant," "intron variant," "non-coding transcript variant," "upstream gene variant," "downstream gene variant," "TFBS ablation," "TFBS amplification," "TF binding site variant," "regulatory region ablation," "regulatory region amplification," "feature elongation," "regulatory region variant," "feature truncation," or "intergenic variant." If multiple annotations for consequence were present for a single variant, only the first most damaging consequence was considered in order to stringently filter for non-coding variants. Only variants that were not flagged as low-confidence by the GIAB consortium were considered. To increase our accuracy in assessing the allele frequency of these non-coding variants, we also annotated these variants with the Genome Aggregation Database (gnomAD) (version 2.0.2) allele frequencies identified from whole-genome sequencing of over 15K samples not enriched for ASD phenotypes. We defined promoters as 2Kb upstream and 1Kb downstream of the transcription start site (TSS) by referencing the longest transcript for each gene (ties in transcript length were resolved by selecting the lower Ensembl Transcript ID). The ASD-risk genes used for this analysis are the 69 genes with an FDR < 0.1 in the iHART TADA-mega analysis.

Samples included for non-coding analyses

iHART non-coding private variants were identified in the 1,177 children with both biological parents sequenced (fully phase-able) (N_{aff} = 960, N_{unaff} = 217). iHART non-coding RDNVs were considered after running ARC to identify high confidence variants and were restricted to those identified in the 716 non-ARC outlier samples (N_{aff} = 575, N_{unaff} = 141).

To increase our power for non-coding variants, we obtained data from 519 whole-genome sequenced Simons Simplex Collection (SSC) quads (mother, father, affected child, unaffected child). These data were also generated and processed to a per sample gVCF (GATK version 3.2-2) by NYGC. We then performed joint genotyping, annotation, and quality control using the same pipeline applied to the iHART genomes. After resolving 4 identity crises in these data by quality control, we removed one likely contaminated sample and two samples with unresolvable sex crises. This resulted in 516 quads and 3 trios from the SSC (N_{aff} = 517, N_{unaff} = 518). We identified an average of 89 raw RDNVs per child in this cohort. After applying ARC to these data, we obtain an average of 61.83 RDNVs per SSC child which is very similar to the genome-wide expectation and matches the average observed for iHART RDNVs after applying ARC (60.3 RDNVs per child in LCL-derived samples and 59.4 RDNVs per child in WB-derived samples). Given that the SSC cohort is comprised entirely of WB-derived samples, we identified zero ARC outliers (no samples with > 90% of their raw RDNVs removed by ARC). The resulting combined iHART + SSC whole-genome cohort includes 1,092 affected and 659 unaffected samples for RDNV analysis and 1,477 affected and 735 unaffected samples for the analysis of private inherited variants.

High-risk inherited variant analysis

To characterize potential high-risk inherited variants, we identified rare damaging variants that were transmitted to all affected individuals in a multiplex family, but not transmitted to unaffected children. High-risk inherited variants were further defined as those that disrupted a gene with a high probability of being loss-of-function (LoF) intolerant (pLI $\geq$ 0.9, n = 3,483 genes) (Lek et al., 2016). Such genes are also referred to as constrained genes because they are under evolutionary constraint – as evidenced by the lack of mutations in such genes in the general human population. Specifically, we considered rare PTVs (AF $\leq$ 0.001 in public databases and internal controls) or rare SVs (AF $\leq$ 0.001 in cDGV and AF $\leq$ 0.01 in HNPs) disrupting an exon or promoter, where the promoter was defined as being 2Kb upstream of the TSS. The families selected for the PTV analysis were restricted to a subset of 346 families with $\geq$ 2 genetically distinct (i.e., not a family with just a pair of affected MZ twins) fully phase-able affected children with a variable number of unaffected children. Given the small number of qualifying SVs in these ASD families, all families (n = 493) were considered.

We next used protein-protein interaction (PPI) analysis to assess whether the 98 genes harboring high-risk inherited variation showed evidence for biological convergence. To determine if these high-risk inherited variants formed a PPI network, we used the Disease Association Protein-Protein Link Evaluator (DAPPLE) (Rossin et al., 2011) and performed 1,000 permutations (within-degree node-label permutation). Given that PPI databases are incomplete and biased against typically less well-studied neuronal interactions (Parikshak et al., 2015), we also expanded the network to include indirect interactions among the seed genes.

When we combined both high-risk inherited variant classes (PTVs and SVs), we found that the protein products of the 98 genes harboring high-risk inherited variation formed a significant direct PPI network ($p < 0.008$, 1,000 permutations). The protein products of both of the high-risk inherited variant classes also formed a significant direct PPI network on their own ($p < 0.04$ for the 61 genes hit by qualifying PTVs and $p < 0.02$ for the 40 genes hit by qualifying SVs).

Gene set enrichment (STAR Methods) for the 98 genes harboring high-risk inherited variation identified a trend for enrichment for targets of RBFOX1 (Weyn-Vanhentenryck et al., 2014) ($p = 0.034$, uncorrected), which regulates neuronal alternative splicing and previously has been implicated in ASD (Martin et al., 2007; Sebat et al., 2007).

The PPI network formed by the 69 TADA ASD-risk genes and these 98 genes harboring high-risk inherited variants (n = 165 unique genes) was significant for all DAPPLE reported network properties (Rossin et al., 2011); this includes: the direct edges count (p = 0.036), the seed direct degrees mean (p = 0.046), the seed indirect degrees mean (p = 0.003), and the CI degrees mean (p = 0.005) (Figures 5A and S6B).

Simulations for high-risk inherited variants

We sought to establish how exceptional it was to observe 98 genes harboring high-risk inherited variation. To simplify the simulations, we focused on high-risk inherited PTVs (n = 57) identified in the subset of 323 families containing only fully phase-able children (excluding extended families). We also analyzed synonymous variants (SYN) with the same inheritance pattern as high-risk inherited variants (transmitted to all affected and no unaffected children), as a negative control, because this variant class is not expected to confer disease risk. First, we calculated the LCL-artifact rate for SNVs and indels (separately) for each parent in these 323 families. Rare SNVs and indels (AF $\leq$ 0.1%) on the autosomes, not falling in problematic regions (GIAB regions (Zook et al., 2014), problematic CNV regions (Brandler et al., 2016), or common CNV regions from cDGV), were categorized as being transmitted to at least one versus never transmitted to any of their offspring. A zero-inflated binomial model was then used to estimate the LCL-artifact rate per parent via maximum-likelihood. The parental LCL-artifact rate for SNVs and indels were highly correlated (Pearson correlation = 0.94); therefore, we used the combined SNV+indel parental LCL-artifact rate. The parental LCL-artifact rates were modest with a median of 0.05 (mean = 0.06).

To test for an excess of high-risk inherited PTVs in constrained genes, we performed simulations that permute the location of PTVs (or SYN) across genes and simulate LCL-artifact adjusted Mendelian inheritance. First, we extracted all qualifying variants in the parents (rare AF $\leq$ 0.1%, PTV (or SYN) – SNVs and indels – in non-GIAB regions). Second, we grouped genes into constraint score bins (spanning the full score range of 0-1) by either gnomAD pLI score or gnomAD o/e score. Third, we computed the per-bin PTV (or SYN) rates in an external cohort (either the SSC (Werling et al., 2018) or the AD cohort (Bennett et al., 2018)). These rates are the empirical ratio of PTVs in highly constrained genes (pLI $\geq$ 0.9) versus all genes (pLI-PTV)/(PTV) in each cohort: parents from this iHART cohort, parents from the SSC, or samples from the AD cohort. Finally, we counted the observed number of high-risk inherited variants within each constraint score bin, and compared these to 1,000 simulations of a null expectation. Each simulation randomly assigns each PTV to a constraint score bin according to the expected rates computed in one of the cohorts (iHART parents (iHART-matched), SSC parents (SSC-matched), or AD samples (AD-matched)), using a multinomial distribution. Each simulation subsequently simulates transmission to each child assuming a Mendelian transmission of 50% while adjusting for parental LCL artifact rates (for instance, a parent with a 5% LCL rate would have a 5% chance to not transmit a variant to any child, and a 95% to transmit the variant with Mendelian transmission).

For a null expectation based on AD-matched PTV rates, we found that the most constrained genes based on o/e (the lowest o/e bins; o/e (upper confidence interval) < 0.467) are significantly enriched for transmitted-to-all PTVs over the expectation (observed = 83, expected = 65, p = 0.022), and the same holds true for the most constrained genes based on pLI (the highest pLI bins; pLI > 0.889; observed = 46, expected = 32, p = 0.007) (Figure 2B). When matching to the SSC, we find the expectations and p values are, respectively, 80 (p = 0.402) and 39 (p = 0.172) (Figure 2B). While we observe both an excess of pLI-PTVs (class imbalance) and an excess of PTVs transmitted to all affected and no unaffected children (transmission disequilibrium) in the bins containing the constrained genes, the number of high-risk inherited variants (PTVs transmitted to all affected and no unaffected children in *only* constrained genes) were too few (n = 57 SNV/indel) to simultaneously test for transmission disequilibrium conditioned on constraint.

We also note that the simulation results were highly sensitive to the estimated parental LCL-artifact rates and the empirical ratio of PTVs in highly constrained genes (pLI $\geq$ 0.9) versus all genes (Figure 2B). The deviation of the synonymous variants from the expected odds ratio of 1 is likely due to slightly different LCL-artifact rates for synonymous variants (as opposed to PTVs).

Gene set enrichment

The purpose of gene set enrichment (GSE) analysis is to count the number of genes in common between two sets of genes and determine if there is greater overlap than expected by chance. We use a null model in which the probability that a gene is hit by mutation is proportional to the length of this gene, as previously described (Iossifov et al., 2014). In this model, we collapse all recurrent hits resulting in a gene being classified as hit (1) or not hit (0) in the sample of interest (e.g., ASD affected children). We then compare the genes targeted by at least one mutation in the sample (T) to a predefined gene set (*S*), and obtain the overlap (*O*) from the intersection of *T* and *S*. We estimate the probability $p(S)$ that an exonic mutation (and hence the gene) is contained within *S* by taking the ratio of the sum of the coding lengths of the genes of S and the sum of the coding lengths of all genes.

$$p(S) = \frac{\Sigma \text{ coding lengths of genes of S}}{\Sigma \text{ coding lengths of all genes}}$$

As described in Iossifov et al. (2014), we then perform a two-sided binomial test of $|O|$ outcomes in $|T|$ opportunities given the probability of success $p(S)$, where '||' denotes the number of gene members in a set.

For some analyses, only a portion of the genome was considered (e.g., only genes with a pLI $\geq$ 0.9), and thus all parameters (*T*, *S*, and $p(S)$) were adjusted to remove genes (and gene lengths) not being considered in the count of *T*. All gene sets (S), were first

converted to their HGNC symbol and then matched by HGNC symbol to the target genes (*T*) before intersecting to obtain *O*. In the analysis of high-risk inherited variants, the gene set enrichment analysis was adjusted to include only the 3,483 genes which have a pLI $\geq$ 0.9. In the TADA mega-analysis, the gene set enrichment analysis was adjusted to include only the 18,472 gencodeV19 TADA genes.

We selected 22 gene sets with known or hypothesized biological relevance in the study of ASD. This included four transcriptome co-expression studies: (1) one module downregulated (M12) and one module upregulated (M16) in ASD brain versus control brain (Voineagu et al., 2011), (2) three modules downregulated (M4, M10, M16) and three modules upregulated (M9, M19, M20) in ASD brain versus control brain (Parikshak et al., 2016), (3) three neurodevelopmental co-expression networks from multiple human brain regions across human development enriched for genes hit by a single *de novo* PTV in ASD patients from the Simons Simplex Collection (SSC) (3_5_PFC_MS, 4_6_PFC_MSC, and 8_10_MD_CBC) – after removing the nine high-confidence ASD (hcASD) genes on which these networks were seeded (Willsey et al., 2013), and (4) five neurodevelopmental co-expression modules – constructed agnostic to ASD-risk genes – enriched for ASD-risk genes/variants (M2, M3, M13, M16, and M17) (Parikshak et al., 2013). In addition to these 16 gene sets, we compiled a list of genes with $\geq$ 2 SSC probands harboring a *de novo* PTV (Iossifov et al., 2014); this gene set serves as a positive control. We also included FMRP targets (Darnell et al., 2011), CHD8 targets (Sugathan et al., 2014), RBFOX1 targets (Weyn-Vanhentenryck et al., 2014), and genes encoding proteins identified in the post synaptic density in human neocortex (Bayés et al., 2011). Finally, we used > 8,000 samples from various tissues (e.g., brain, heart, liver) in GTEx (Battle et al., 2017) data v6 (dbGap # phs000424.v6.p1) to identify genes enriched for expression in the brain versus other tissues. These genes had a 2-fold enrichment (FDR < 0.05) after regressing out RNA Integrity Number (RIN) and various sequencing covariates (principal component 1 and 2 of sequencing statistics provided by GTEx). Significance should only be considered for gene sets surviving multiple test correction (Bonferroni correction for the 22 gene sets tested or $p < 0.002$).

DLG2 association and haplotype prediction

The 2.5Kb deletion identified in the promoter region of *DLG2* is significantly associated with ASD when considering the three independent ASD carriers in the iHART cohort (3 of 484 unrelated, phase-able (at least one parent sequenced), affected children with SVs called) and the lack of any deletions intersecting this *DLG2* promoter region deletion among 212 unaffected children in this cohort (iHART) and 26,353 cDGV controls (curated DGV) (two-sided Fisher's Exact Test, $p = 5.7 \times 10^{-6}$, OR = Inf, 95% CI = 22.7- Inf). In other words, no deletions were found to overlap the *DLG2* promoter deletion in public databases nor in any of our controls (n = 26,565 controls). However, it is unclear if this SV is detectable by microarray. Since the majority of DGV SV detection was based on microarray, we restricted to only WGS control samples (212 unaffected children in this cohort and 2,677 cDGV controls), and found that this association is significant (two-sided Fisher's Exact Test, p = 0.003, OR = Inf, 95% CI = 2.47- Inf).

Given that all carriers of the recurrent, high-risk, inherited SV deletion disrupting the promoter of DLG2 (chr11:85339733-85342186) were of Hispanic or Latino origin, we wanted to eliminate the possibility that this was a rare population-specific event from a common ancestor. When restricting to only Hispanic or Latino (Ad Mixed American [AMR]) WGS control samples (98 unaffected children in this cohort and 351 cDGV controls), this association remains significant (two-sided Fisher's Exact Test, p = 0.006, OR = Inf, 95% CI = 1.92-Inf). To determine if this SV was always found on the same haplotype, we first extracted all high-confidence SNVs (genotype quality of $\geq$ 30 and $\leq$ 30% of samples with missing genotypes) in the region surrounding the SV (1Kb upstream and downstream the start and end positions of the SV, respectively). We then ran fastPHASE (Scheet and Stephens, 2006) to estimate the haplotype in this region for all the 2,308 WGS samples included in this study, as well as the corresponding haplotype frequencies (using –F option). Of the 40 possible estimated haplotypes, a different haplotype was found in each of the three families carrying the SV, with haplotype frequencies of 0.469, 0.024 and 0.001 (Table S1).

Artifact Removal by Classifier (ARC)

Artifact Removal by Classifier (ARC) is a random forest supervised model developed to distinguish true rare *de novo* variants from LCL-specific genetic aberrations or other types of artifacts such as sequencing and mapping errors (https://github.com/walllab/iHART-ARC). To train the model we used rare *de novo* variants identified in 76 pairs of fully phase-able monozygotic (MZ) twins with WGS data derived from LCL DNA. We performed GATK joint genotyping of variants in MZ twins together with all samples in the iHART cohort and identified the *de novo* variants as described above. We defined rare *de novo* variants as *de novo* variants with a population frequency of zero in the publicly available databases, UCLA internal controls, and HNP samples. In the training set, rare *de novo* variants identified in both MZ twins were labeled as true variants (positive class), whereas discordant calls were labeled as false variants (negative class). Our final training set consisted of 5,667 positive and 56,018 negative variants.

A random forest classifier with 1,000 decision trees was trained on these positive and negative examples. We used the RandomForestClassifier implementation from the Python scikit-learn package (version 0.18.1). Weights associated with classes were adjusted inversely proportional to the class frequencies by using sklearn 'balanced' class weight option to control for class imbalance (many more negative examples than positive). We performed hyperparameter optimization by grid search.

ARC features

Variants in both classes were annotated with 48 features; these features are related to intrinsic genomic properties (e.g., GC content and other properties implicated in *de novo* hotspots (Michaelson et al., 2012)), sample specific properties (e.g., genome-wide number of *de novo* SNVs), signatures of transformation of peripheral B lymphocytes by Epstein-Barr virus (e.g., number of *de novo* SNVs in

immunoglobulin genes), or variant properties (e.g., GATK variant metrics). We also annotated whether or not each variant fell into a region flagged as low-confidence (regions for which no high-confidence genotype calls were possible) by the GIAB Consortium (Zook et al., 2014); variants flagged as low-confidence (deemed "GIAB variants") were retained for calculating sample-level metrics but subsequently removed prior to running the classifier (5,373 positive and 53,622 negative variants remained for use in classifier). For the eleven features which occasionally had missing values, missing values were imputed and a feature "is.X.feature.na" was included to capture this imputation process as an independent feature. All non-missing GATK metrics were taken directly from the VCF, with the exception of ABhet (see ABhet adjustment details below). A complete list of features and the importance (relative importance of each random forest feature was obtained from the RFECV module from scikit-learn) of each feature used in the random forest classifier are shown in Figure 3A.

Evaluation of ARC performance

The performance of the model was first evaluated with the receiver operating characteristic (ROC) curve analysis using a ten-fold cross validation procedure. In the ten-fold cross validation, the entire training set was divided into ten folds such that the ratio of positive to negative examples was constant across folds. We achieved an AUC of > 0.98 (Figures S3A and S3B). The ROC and precision recall curves are shown in Figures S3C and S3D.

To assess the generalization error of our model, we additionally performed whole-genome sequencing (~30X) of matched whole blood (WB) and LCL samples from 17 fully phase-able individuals from the iHART cohort ("test set"). These samples were also jointly genotyped with all samples in the iHART cohort so as to preserve variant calling metrics between the training and test set. We followed the same procedure as in the training set to identify and extract rare *de novo* variants in our WB-LCL matched samples. We assumed that true *de novo* variants would be those identified in both the WB and LCL sample in a pair (deemed "concordant"). We further assumed that variants detected in only one sample of a pair (deemed "discordant"), would be due to LCL-specific aberrations (if called in LCL) or other sources of errors (if called in WB or LCL). In total, 1,512 concordant rare *de novo* variants (n = 1,291 after excluding GIAB variants) were called in these samples, which we used as positive examples in our test set. Furthermore, 2,560 discordant rare *de novo* variants (n = 1,898 after excluding GIAB variants) were called in only one sample of a pair (64% of discordant variants found only in LCL, 36% of discordant variants found only in WB) and were used as negative examples. We evaluated a model that was trained using the entire training set on this independent test set and achieved an AUC of 0.98 and an F1 score of 0.89.

To determine a cutoff point for the predicted ARC scores, below which a variant would be considered likely to be an LCL-specific genetic aberration or other type of artifact, we chose a conservative cutoff value. We selected a conservative ARC score threshold (0.4) that achieved a minimum precision and recall rate of 0.92 and 0.80, respectively, in the 10-fold cross validation training set (Figures S3C and S3D); and achieved a precision and recall rate of 0.98 and 0.84, respectively, in the test set (Figure S3H).

ABHet adjustment

ABHet is a variant-level annotation from GATK that aims to estimate if biallelic variants match expected allelic ratios. An ideal heterozygous variant will have a value of close to 0.5 and an ideal homozygous variant will have a value of close to 1.0. ABHet is calculated for a variant based on all samples in the VCF which are not homozygous reference at this site. The ABHet annotation is not currently provided by GATK for indels. Using the ABHet formula below, we manually calculated the ABHet value for all indels.

$$ABHet = \frac{\#\ \text{REF reads from heterozygous samples}}{\#\ \text{REF} + \text{ALT reads from heterozygous samples}}$$

Additionally, in the training set, we manually adjusted ABHet values by only including the proband and removing his/her twin(s) from the calculation. This corrects for bias introduced by applying the raw GATK metric calculated based on two samples to a single sample because we retain only the proband metrics (and exclude the MZ twin metrics) for shared *de novo* variants. This systematic bias is particularly apparent when comparing to the sample-level ADDP metric (formula below).

$$ADDP = \frac{\#\ \text{ALT reads in a sample at variant site}}{\#\ \text{REF} + \text{ALT reads in a sample at variant site}}$$

If a variant is present in only one sample in the VCF, then ABHet = = 1 – ADDP. In contrast, for shared *de novo* variants a variant is in two different samples (proband (x) and MZ twin(y)), and $ADDP_x$ is rarely equal to $ADDP_y$, and thus $ABHet_{xy}$! = 1 – $ADDP_x$.

Similarly, in the test set we manually adjusted the ABHet values by only including the LCL sample and removing its matched WB sample from the calculation.

Imputing missing values for ARC features

For eleven of the ARC features (Inbreeding coefficient, ABHet, ABHom, Overall non-diploid ratio (OND), Recombination rate, Base quality rank sum, Mapping quality rank sum, DNase hypersensitivity, Read position rank sum, Replication timing, Transcription in LCL), some variants had missing values. In general, we used the mean of all non-missing values to impute the missing values of a feature. However, for GATK's "OND" feature, missing values were imputed as zero. In order to account for missingness and capture this imputation process in the ARC model, a binary feature "is.X.feature.na" was included for all variants for each of these features, with the exception of the "OND" feature (as OND values were missing for the majority of variants).

For two ARC features, indels were occasionally annotated with multiple values – SimpleRepeats and EncodeCaltechRna SeqGm12878R2x75. For SimpleRepeats, if multiple values were listed, only the lowest value was retained. For EncodeCaltechRna SeqGm12878R2x75, only the max value was retained. We chose these features to be most conservative and least likely to bias the classifier. These exceptions are also captured by the "is.indel" feature.

ARC outlier samples

After applying ARC to all 1,377 children (partially or fully phase-able), we identified a subset of outlier samples for which > 90% of their raw DN variant calls had an ARC score of less than 0.4. These are samples for which > 90% of raw DN variant calls were excluded by ARC (partially phase-able n = 2; fully phase-able n = 346). These outlier samples were those with the largest number of raw DN variant calls prior to running ARC (biological sequencing source was LCL) and it's likely that the classifier was unable to confidently distinguish variants in these samples. Unless otherwise mentioned, all ARC outlier samples were excluded from downstream analyses involving *de novo* variants.

De novo mutation rate versus paternal age

We evaluated the correlation between DN variant rate in 574 fully phase-able iHART affected children (excluding MZ twins, ARC outliers, and one sample without paternal age information) and paternal age at the child's birth using a generalized quasi-Poisson linear model, assuming that the counts are distributed as an over-dispersed Poisson distribution (a generalized quasi-Poisson linear model):

$$R_C = T_C \times (A \times F_C + B)$$

Where R_C is the rate of DN events per child, F_C is the age of the father at the birth of the child and T_C is the percent of the child's genome covered at $\geq$ 10X and A and B are whole population parameters, estimated by maximizing the likelihood over all children (as previously described in Iossifov et al., 2014). We performed this analysis before and after ARC, considering only DN events not falling in GIAB low-confidence regions.

Given the well-known effect of paternal age on germline mutation, we tested for an effect of paternal age on the number of *de novo* mutations per affected ASD child and found a robust signal after running ARC ($p = 3.6 \times 10^{-13}$), but not prior to application of ARC (STAR Methods; Figure S4D). We observed an increase of 1.46 RDNVs per year of paternal age (95% CI = 1.37-1.55), matching previously published rates (Deciphering Developmental Disorders Study, 2017; Francioli et al., 2015; Goldmann et al., 2016; Michaelson et al., 2012).

Rates for rare *de novo* mutations

When calculating *de novo* mutation rates, we only considered the 1,177 children with both biological parents sequenced (fully phase-able). Rare *de novo* variants (absent in all controls) were restricted to those with an ARC score $\geq$ 0.4 that were not flagged as low-confidence by the GIAB consortium. We then excluded ARC outlier samples (n = 346). Consistent with what is shown in Figure S4B, there was no significant difference in the rate of rare *de novo* variants based on the biological sequencing source (WB versus LCL; after ARC and after excluding ARC outliers) when including all MZ twins. However, we observed that shared *de novo* (TRUE) variants from the LCL MZ twins have slightly inflated ARC scores (median number of *de novo* variants is 69), as compared to LCL non-MZ twin samples (median number of *de novo* variants is 57) (Figure S4A). This difference in *de novo* rates was significant when evaluated using Wilcoxon rank sum test ($p = 1.28 \times 10^{-12}$). The inflated ARC scores are likely due to the fact that these LCL MZ twins were used as the ARC training set; therefore, *de novo* variants from all MZ twin samples were excluded from all *de novo* rate calculations (n = 158, some of which are also ARC outliers n = 43). Therefore, all *de novo* mutation rate calculations were performed using 716 fully phase-able non-MZ twin and non-ARC outlier samples (N_{aff} = 575; N_{unaff} = 141).

We observed a mean genome-wide *de novo* mutation rate of 60.1 RDNVs per child (Figure S4B), which is consistent with previously reported genome-wide *de novo* mutation rates (mean = 64.4; range 54.8-81) (Besenbacher et al., 2016; Conrad et al., 2011; Kong et al., 2012; Michaelson et al., 2012; Turner et al., 2016; C. Yuen et al., 2017).

Power calculations for RDNVs

Given our observation that children from multiplex families and simplex families have comparable rates of rare *de novo* synonymous and missense variants in both affected and unaffected children but different rates for rare *de novo* PTVs (Table S2), we sought to determine if this represented a true difference in the underlying genetic architecture of multiplex ASD families by performing a Monte Carlo integration. This revealed that with the current iHART sample size (N_{aff} = 575, N_{unaff} = 141), we had only 51% power to detect an odds ratio greater than or equal to the odds ratio reported in simplex families (OR = 0.13/0.07 = 1.86) (Iossifov et al., 2014; Kosmicki et al., 2017) and that our power to reject the null hypothesis that affected and unaffected children have no difference in the rate of *de novo* PTVs was 70.8%. We estimate that once we expand our cohort by a factor of 2.5 (N_{aff} = 1,438, N_{unaff} = 353), we will have > 95% power to detect a rate difference in *de novo* PTVs if such a difference exists in multiplex ASD families.

Defining pathogenic *de novo* variants

We defined pathogenic *de novo* variants (Figure 3E) as missense or PTV variants passing ARC and found in one of the previously established 65 ASD-risk genes (Sanders et al., 2015). Despite finding no global excess of damaging RDNVs in ASD cases in the study,

we do identify PTVs and predicted deleterious missense (Mis3) RDNVs in previously established ASD-risk genes, including *CHD8*, *SHANK3*, and *PTEN* (Figure 3E; Table S3). As expected, such pathogenic RDNVs are only found in affected children in our cohort.

TADA mega-analysis

Samples and qualifying variants

We used the Transmitted And *De novo* Association (TADA) test (He et al., 2013) to combine evidence from rare *de novo* (DN) or transmitted (inherited) PTVs and *de novo* Mis3 variants identified in ASD cases. Within the 422 iHART families with at least one ASD case and both biological parents sequenced, there were 838 genetically non-identical (only one MZ twin retained) ASD cases available for the TADA analysis. These 838 affected samples, and their biological parents, were treated as independent trios for the TADA analysis. This approach means that siblings were treated as belonging to independent trios, an approach for which we also approximate the null distribution (see details on TADA simulations below). To further increase power for the identification of novel ASD-risk genes, we combined qualifying variants found in ASD cases from the current (iHART) cohort with the most recent TADA mega-analysis (Sanders et al., 2015), which included variants described in the Simons Simplex Collection (SSC) and the Autism Sequencing Consortium (ASC) cohorts, together with small *de novo* CNV deletions (SmallDel) identified in SSC and Autism Genome Project (AGP) probands (Table S3).

Qualifying variants in the iHART cohort included rare DN/transmitted PTV and rare DN Mis3 variants identified in the 838 affected samples, and not flagged as low-confidence by the GIAB consortium (Zook et al., 2014). Following the allele frequency threshold used in the previous TADA mega-analysis (Sanders et al., 2015), we required transmitted PTVs to have an AF $\leq$ 0.1% in public databases (1000 g, ESP6500, ExACv3.0, cg46), internal controls, and iHART HNP samples. DN variants identified in the iHART cohort were required to be absent in all public databases, internal controls, and HNP samples (AF = 0). High confidence DN variants were obtained by ARC for all non-MZ twin samples. DN variants shared by MZ twins (shared DN variants, used as TRUE examples in the ARC training set) were also included as qualifying variants without filtering on their ARC score. Additionally, for the 185 TADA samples identified as ARC outlier samples, we excluded DN variants in these samples and retained only their inherited PTVs as qualifying variants. We used the PolyPhen-2 (Adzhubei et al., 2010) v2.2.2r395 HDIV predictions from the Whole Human Exome Sequence Space (WHESS dataset) to annotate DN Mis3 variants in the iHART cohort. This method is highly concordant to the method (PolyPhen-2 web application) implemented for the ASC and SSC (Sanders et al., 2015), with our re-annotation resulting in identical Mis3 classifications for 99.8% of the reported DN Mis3 variants in the ASC and SSC cohorts. When multiple qualifying variants in a gene were found in the same sample, only the most damaging variant was retained.

We then tallied qualifying variants from the different cohorts into a gene by variant-type matrix for the TADA analysis, which contained variant counts for a total of 18,472 gencodeV19 genes with HGNC approved gene names (this excludes a subset of genes (193 out of 18,665) from the most recent TADA mega-analysis (Sanders et al., 2015) that could not be easily converted to a single non-redundant HGNC gencodeV19 gene). In particular, counts of DN PTV/Mis3 variants come from 4,689 ASD cases from ASC (De Rubeis et al., 2014), SSC (Iossifov et al., 2014), and iHART (this manuscript), while counts for the transmitted and non-transmitted PTVs are from 3,813 ASD cases and 7,609 controls from the ASC (De Rubeis et al., 2014) and iHART (this manuscript) (Table S3). Finally, counts of DN SmallDel were calculated in 4,687 ASD cases from the SSC (Sanders et al., 2015) and the AGP (Pinto et al., 2014; Table S3).

Critically, 424 AGRE samples (sample list obtained from B. Devlin, M. Daly, and C. Stevens, personal communication) were included as ''cases'' in the original ASC TADA analysis (De Rubeis et al., 2014) meaning that all qualifying PTVs identified in these cases were treated as transmitted PTVs because *de novo* status could not be determined. Given that iHART sequenced 119 of these samples (or the monozygotic twin of one of these samples) and their biological parents, we were able to recover the *de novo* status for variants identified in these samples (71 samples after excluding ARC outliers) by using the iHART data. Thus, we used iHART data to count qualifying DN PTV and Mis3 variants in these samples and allowed transmitted PTV counts to come from the original study (De Rubeis et al., 2014). To do this in a non-redundant way (without double-counting variants), we looked for all qualifying DN PTVs identified by iHART data in these samples in the ASC VCFs (downloaded from dbGAP (De Rubeis et al., 2014)) and subtracted a transmitted PTV count from the iHART mega-analysis TADA-ready table for each variant found in the ASC VCFs. In three instances, the transmitted PTV count from ASC cases was already zero for the gene harboring the corresponding variant and thus we left it at zero.

TADA parameters

The parameters used for performing the TADA analysis, matched those used in previous TADA mega-analyses (De Rubeis et al., 2014; He et al., 2013; Sanders et al., 2015); including the previously observed aggregate association signals used to estimate relative risk (RR, γ) for each variant class – DN PTV (γ = 20), DN SmallDel (γ = 15.3), DN Mis3 (γ = 4.7), and transmitted PTV (γ = 2.3) (use of these parameters facilitated replication of previous findings prior to adding the iHART cohort to perform a mega analysis). PTVs classified as uncertain or missing (as defined previously) in children were excluded. In addition to these RR parameters, we also assumed the fraction of ASD-risk genes (π) to be $\approx$0.05 (1,000 ASD-risk genes divided by a total of 18,472 genes), the PTV frequency parameters (required by TADA to integrate transmitted and non-transmitted PTV variant counts into the model) were ρ = 0.1 and ν = 200 and the gene mutation rates were taken directly from the most recent TADA mega-analysis (Sanders et al., 2015), with PTV and Mis3 gene mutation rates calculated by multiplying the exome mutation rates, originally estimated by Samocha et al. (Samocha et al., 2014), by the fractional constants of 0.074 and 0.32, respectively. This use of gene mutation rates as ground truth (rather than comparing to

control samples) facilitates the use of TADA in mega-analyses because differences in sample size and variant detection between studies impact the power of TADA, but are not a potential source of bias.

Novel gene discovery

We applied stringent parameters for declaring a gene as novel – genes had to have an FDR < 0.1 in our TADA mega-analysis and lack genome-wide statistical support in all previous studies (Sanders et al., 2015; De Rubeis et al., 2014) with statistical rigor. The *CACNA2D3* gene was significantly associated with ASD in the iHART mega-analysis, but not the previous TADA mega-analysis (Sanders et al., 2015); however it was previously reported (De Rubeis et al., 2014) and thus is not considered as a novel ASD-risk gene. In contrast, *MYO5A* was reported as a "putative ASD-risk gene" (C. Yuen et al., 2017), however the binomial test they use to obtain an FDR is not applied genome-wide (e.g., they first restrict to genes with $\geq$ 2 PTVs in genes with a pLI $\geq$ 0.9). Furthermore, they apply an FDR threshold of < 0.15 (the standard in the field is an FDR < 0.1) and they do not provide per gene FDR values. Therefore, we consider *MYO5A* a novel ASD-risk gene.

Removal of de novo *signal*

Given that our multiplex ASD familial cohort is expected to be depleted for *de novo* variation relative to simplex families, we also asked how our novel gene discovery would change if we ignored the contribution of *de novo* variants in the iHART cohort to the TADA mega-analysis (by assigning a relative risk of one to *de novo* variants in iHART children). Using this overly conservative approach, a total of 65 ASD-risk genes are identified at an FDR < 0.1, including six of the 16 novel genes identified in the iHART TADA mega analysis (*C16orf13*, *CCSER1*, *MLANA*, *PCM1*, *TMEM39B*, and *TSPAN4*) and five additional genes (*ASXL3*, *CDH13*, *NR3C2*, *SCN7A*, *STARD9*) Table S3.

Replication of previous TADA-mega analysis

Comparison of the iHART TADA-mega analysis to the previously published findings (Sanders et al., 2015) identified 16 newly-significant (FDR < 0.1) ASD-risk genes plus *CACNA2D3,* which was previously reported as an ASD-risk gene (De Rubeis et al., 2014; Table 1; Figure S5D). We failed to replicate 13 of the genes previously published with an FDR < 0.1 (Sanders et al., 2015; Figure S5C). The q-values for these 13 genes were borderline significant in iHART (Figure S5C), and their simulation p values were greater (min p value = 0.01, max p value = 0.06; Figure S5E) than those of the 69 ASD-risk genes we identified in the TADA mega-analysis with high confidence, which include the 16 newly significant genes (min p value = 0.001, max p value = 0.006) (Figures 4B, S5D, and S5F). While some of the genes that failed to replicate in our study may reach genome-wide significance again as sample sizes grow, at this stage our data do not support them.

TADA simulations

The distribution of the TADA statistic (under the null) is known for independent trios (He et al., 2013), but not for multiplex families. Therefore, we estimated the distribution of the null TADA statistic by simulating Mendelian transmission and *de novo* mutation across the family structures used in our TADA-mega analysis. This simulation was based on the observed qualifying variant counts and family structures from our TADA-mega analysis datasets, which included: (1) iHART multiplex families, (2) ASC and SSC trios and ASC case-control samples, and (3) small deletions from Sanders et al. (Sanders et al., 2015; Table S3). Simulations under the null model (1.1 million-simulations) were conducted prior to running TADA with the same parameters used for our TADA-mega analysis (see "TADA mega-analysis").

The occurrence of rare *de novo* variants (RDNVs) was simulated by randomly shuffling genes carrying the observed qualifying RDNVs across the genome of each sample by redrawing in proportion to the gene-specific mutation rates (derived from Samocha et al. (Samocha et al., 2014)). For example, if an affected sample harbored 8 RDNVs, these RDNVs would be placed in 8 genes in simulation 1, independently in 8 genes in simulation 2, and so on, where the probability of a gene containing an RDNV is proportional to its gene mutation rate. This method was applied to simulate RDNVs in affected children from iHART multiplex families and affected children from ASC and SSC trios.

The occurrence of transmitted (inherited) and non-transmitted variants was simulated by (A) randomly shuffling genes carrying the observed qualifying variants in the parents of a given family, by redrawing in proportion to the gene-specific mutation rates and (B) randomizing the Mendelian inheritance of such variants across all children (affected and unaffected) in the family. Randomization of the Mendelian inheritance simply means that for each simulation a variant can be transmitted to each child, regardless of affected status, with a 50% probability. For example, in Family001, if mom harbored 10 qualifying PTV variants and dad harbored 10 qualifying PTV variants; then in each simulation each of these 20 variants would be randomly placed in a gene according to its gene-specific mutation rate and is either transmitted or not transmitted to each of the children in the family. This method was applied to simulate transmitted and non-transmitted PTVs in the cohorts listed in Table S3.

Finally, we simulated small deletions disrupting 2-7 genes at a time (Sanders et al., 2015). For each observed small deletion containing N_{genes}, we selected a contiguous set of N_{genes} by redrawing in proportion to the multi-gene mutation rates. Multi-gene mutation rates were calculated by summing single-gene mutation rates of adjacent genes using sliding windows of K genes across the genome. For example, if a small deletion disrupted 5 genes in an affected sample, then for each simulation a contiguous set of 5 genes would be randomly selected for this sample with a probability proportional to the 5-gene-sliding-window multi-gene mutation rates.

The resulting set of simulation-based Bayes factors from TADA were multiplied together. A single p value for each gene was generated, reflecting how unlikely it is to have observed the Bayes factor obtained in our TADA-mega analysis given the 1.1 million simulation-based Bayes factors observed for this gene (Figures S5A and S5B).

We used the simulation p values to identify genes reaching genome-wide significance after applying a stringent Bonferroni correction for the total number of genes included in the TADA analysis (0.05/18,472 = $2.7x10^{-06}$). We restricted this to genes obtaining an FDR < 0.1 by TADA and a simulation p value of less than or equal to $2.7x10^{-06}$ (Table S3). If we remove the requirement for a TADA-mega analysis FDR < 0.1, then a 25th gene, *DNAH10*, also reaches genome-wide significance implicating that variants in this gene show over transmission to affected children in our multiplex children.

Genes with large inherited PTV contribution

Given our signal for rare inherited variants, we sought to highlight genes for which a large contribution of the TADA ASD-risk association signal is derived from inherited PTVs. Conservatively, we considered only variants where the inheritance was known (*de novo* versus inherited). Therefore, we adjusted the total number of TADA-qualifying variants to ignore PTVs from cases because some of the TADA-mega analysis qualifying variants originate from case-control studies (not iHART) where inheritance is unknown. We applied two methods to identify genes with a large contribution from inherited PTVs. Method 1: The total number of qualifying variants (N) in each TADA gene was defined as $N_{DN.PTV} + N_{DN.SmallDel} + N_{DN.Mis3} + N_{Inherited.PTV}$; and if $N_{Inherited.PTV}/N \geq 70\%$, then this gene was considered to have a higher proportion of inherited risk variants. Method 2: Alternatively, we identified genes for which the main driver of the TADA association signal was from inherited PTVs. We defined this class of genes as those where the Bayes Factor from inherited PTVs was greater than the Bayes Factor from all other *de novo* variant classes ($BF_{inheritedPTV} > BF_{dnPTV}$ & $BF_{inheritedPTV} > BF_{dnSmallDel}$ & $BF_{inheritedPTV} > BF_{dnMis3}$). For *PCM1*, the Bayes Factor contribution from inherited PTVs was greater than the Bayes Factor from any class of *de novo* variants, indicating that the association signal for *PCM1* is mainly driven by inherited PTVs.

Single cell RNA-seq

Gene cell type enrichment scores were obtained from an unpublished single cell RNA sequencing (scRNA-seq) dataset of GW17-18 human fetal cortex, a human fetal forebrain scRNA-seq dataset from Nowakowski et al. (Nowakowski et al., 2017), and adult brain scRNA-seq dataset from Lake et al. (Lake et al., 2018; Figures S6C and S6D). Cell type enrichment lists were grouped into major cell classes (glutamatergic, GABAergic, glial and other support cells). Broadly expressed genes were determined by enrichment in neuronal and glial or other support cell types, or above a mean expression threshold across all cells in the dataset but without cell type specific enrichment. Enrichment log2 odds ratios were calculated using a general linear model (binomial distribution).

Identifying candidate ASD genes with NetSig

In order to identify genes whose encoded proteins directly interact with potential ASD-risk genes more than expected by chance, we ran NetSig (Horn et al., 2018). NetSig requires two input files: (1) a set of genes and their associated q-values (or p values) and (2) a PPI network. We input the q-values obtained in the iHART TADA mega-analysis and known protein-protein interactions from InWeb v3 (Lage et al., 2007) after converting to HGNC and restricting to genes included in the iHART TADA mega-analysis (12,015 genes); this resulted in a subset of 302,991 known PPIs. Given that iHART SVs were not included in the TADA analysis (Table S3), and therefore do not contribute to the input q-values in this analysis, we explored enrichment for NetSig significant genes using the direct and indirect network seeded by high-risk inherited PTVs (Figure 2C).

Zebrafish experiments

Generation of zebrafish nr3c2 mutant

The zebrafish *nr3c2* mutant was generated using CRISPR/Cas9 as described (Hwang et al., 2013) with sgRNA target sequence 5′-GGTGTGTGGTACGAGAGCGG-3′. The mutant contains a 5 bp deletion (open reading frame nucleotides 2120-2124, 5′-CCGCT-3′) that shifts the translational reading frame after amino acid 707 and results in a premature stop codon after amino acid 738, compared to 970 amino acids for the WT protein. The predicted mutant protein lacks the ligand binding domain, and thus should be non-functional. Mutant animals were genotyped using the primers 5′-CTTCCCTGCAGAGCTCAAAG-3′ and 5′-ATAGCCAGCGAACAC CACTT-3′, which produce a 164 or 159 bp band for the WT or mutant allele, respectively. *nr3c2* heterozygous mutants were outcrossed to the parental TLAB strain for three generations before use in experiments. For each behavioral experiment, *nr3c2* +/− animals were in-crossed, generating *nr3c2* −/−, −/+ and +/+ sibling progeny. Experiments were performed blind to genotype, and animals were genotyped using PCR after each experiment. Multiple sequence alignments were performed using Megalign Pro (DNASTAR Lasergene).

Pharmacology

MK-801 (M107, Sigma Aldrich) was dissolved in dimethyl sulfoxide (DMSO, 4948-02, Macron Chemicals) as a 100 mM stock solution. Immediately before each experiment, this stock solution was diluted in system water for a final concentration of 20 μM. WT TLAB fish were exposed to either 20 μM MK-801 in 0.02% DMSO or 0.02% DMSO vehicle control for 1 hour prior to behavioral testing. For ethanol experiments, WT TLAB fish were exposed to ethanol (V1016, Koptec) diluted in system water at a final concentration of 0.5% for 1 hour prior to behavioral testing. After each drug treatment, fish were rinsed in fresh system water 3 times before behavioral testing.

Social preference assay

Beginning at 2 weeks of age, and becoming robust at 3 weeks of age, zebrafish show what has been described as social behavior by exhibiting a strong preference to remain in a compartment where they can view conspecifics compared to a compartment where they

cannot (Dreosti et al., 2015). This behavior is not simply a result of attraction to a novel or moving object, as it is only elicited by conspecifics of similar size and behavioral patterns (Dreosti et al., 2015; Larsch and Baier, 2018). Based on these observations, we developed a modified version of a previously-described social preference assay (Dreosti et al., 2015). Zebrafish were raised on a 14:10 hour light:dark cycle and were fed rotifers (*Brachionus plicatilis*) twice per day until reaching 2 weeks of age. Fish were then fed brine shrimp (*Artemia salina*) until 3-4 weeks of age, at which point their behavior was assayed. The behavioral assay was performed using a flat-bottom 12-well plate containing round wells made of clear plastic (CC7672-7512, CytoOne) and custom-built removable opaque dividers. Single "test" animals, whose behaviors were analyzed, were placed in each of the 4 middle wells of the plate, and a WT conspecific of similar age and size was placed in a well either above or below each middle well. Wells were filled with fresh system water and the plate was placed in a custom-modified, Zebrabox (Viewpoint Life Sciences) that was illuminated with infrared and white LEDs. The 12-well plate was housed in a chamber filled with recirculating water to maintain a constant temperature of 28.5°C. Locomotor activity was monitored using an automated videotracking system (Viewpoint Life Sciences) with a Dinion one-third inch monochrome camera (Dragonfly 2, Point Grey) fitted with a fixed-angle megapixel lens (M5018-MP, Computar) and infrared filter. The tracking mode was used to record the location of each test animal, with the following empirically determined settings: low detection threshold = 130; x min size = 3; inactivity = 5. Animals were given a 5-minute habituation period before the start of data acquisition. During a 10-minute baseline period, opaque dividers were inserted between each well to prevent the animals from seeing each other. The dividers separating each row of wells (but not the dividers separating each column of wells) were then removed, allowing each test animal to view one well containing a conspecific and one empty well. The fish were given another 5-minute habituation period, followed by a 10-minute post-baseline period. For data acquisition, wells containing test fish were divided into two 0.5 cm × 2.2 cm zones, one closest to the well containing a conspecific and one closest to the empty well (indicated as blue and orange boxes in Figure 6A, respectively). The amount of time spent by a test fish in each zone during the baseline and post-baseline periods was recorded.

Social preference of test fish was quantified by calculating the social preference index (SPI) = (time spent in zone near the conspecific – time spent in zone near the empty well)/time spent in both zones. Thus, SPI = 1 indicates a fish that spends 100% of its time near a conspecific, SPI = −1 indicates a fish that spends 100% of its time near the empty well, and SPI = 0 indicates a fish that spends equal amounts of time near the conspecific and near the empty well. Data analysis and statistical tests were performed using Prism (GraphPad).

To validate the social preference assay, we treated zebrafish with either MK-801, an NMDA receptor antagonist that disrupts rodent (Moy et al., 2013) and zebrafish (Zimmermann et al., 2016) social behaviors, or DMSO vehicle control, for one hour prior to performing the behavioral assay. Animals treated with DMSO on average showed no spatial preference during the baseline period and a strong preference for conspecifics during the post-baseline period (Figure S7C). This behavior was only observed in animals 3 weeks of age or older (data not shown), as previously reported (Dreosti et al., 2015). In contrast, while animals treated with 20 μM MK-801 also on average showed no spatial preference during the baseline period, social preference for conspecifics during the post-baseline period was abolished (Figure S7D). To further validate the assay, we treated zebrafish with ethanol, which has also been shown to reduce preference for conspecifics in 3-week old zebrafish (Dreosti et al., 2015). Similarly, we found that treatment with 0.5% ethanol for 1 hour prior to behavioral testing significantly reduced social preference (Figure S7G). Furthermore, both MK-801 and ethanol treatment significantly suppressed the increase in SPI during the post-baseline period compared to the baseline period (Figures S7E and S7H), indicating reduced social preference. Taken together, these results reproduce observations obtained using a similar assay (Dreosti et al., 2015) and suggest that our assay can identify social interaction defects in zebrafish.

Zebrafish size was quantified by measuring body length from the tip of the mouth through the midline of the body to the end of the tail fin in single frames of video recordings of the social preference assay using ImageJ (Schneider et al., 2012). The social behavioral deficit observed in *nr3c2* −/− animals (Figures 6B and 6C) is unlikely to be due to developmental delay because there was no significant difference in the size of *nr3c2* −/−, +/− and +/+ siblings when the assay was performed (Figure S7I).

Sleep/wake assay

Sleep/wake analysis was performed as previously described (Prober et al., 2006). Zebrafish were raised on a 14:10 hour light:dark cycle until 4-days post-fertilization, when individual animals were placed into each well of a 96-well plate (7701-1651, Whatman) containing 650 μL of E3 embryo medium (5 mM NaCl, 0.17 mM KCl, 0.33 mM $CaCl_2$, 0.33 mM $MgSO_4$, pH 7.4). Plates were sealed with an optical adhesive film (4311971, Applied Biosystems) to prevent evaporation. The sealing process introduces air bubbles in some wells, which are discarded from analysis. Animals were blindly assigned a position in the plate and were genotyped by PCR after the behavioral experiment was complete. Locomotor activity was monitored using an automated videotracking system (Viewpoint Life Sciences) with a Dinion one-third inch monochrome camera (Dragonfly 2, Point Grey) fitted with a fixed-angle megapixel lens (M5018-MP, Computar) and infrared filter. The movement of each larva was recorded at 15 Hz using the quantization mode with 1-minute time bins. The 96-well plate and camera were housed inside a custom-modified, Zebrabox (Viewpoint Life Sciences) that was continuously illuminated with infrared LEDs, and illuminated with white LEDs from 9 a.m. to 11 p.m. The 96-well plate was housed in a chamber filled with recirculating water to maintain a constant temperature of 28.5°C. The parameters used for detection were: detection threshold, 15; burst, 29; freeze, 3, which were determined empirically. A movement was defined as a pixel displacement between adjacent video frames preceded and followed by a period of inactivity of at least 67 ms (the limit of temporal resolution). Any one-minute period with no movement was defined as one minute of sleep because this is associated with a significant increase in arousal threshold (Prober et al., 2006). A sleep bout was defined as a continuous string of sleep minutes. Sleep

latency was defined as the length of time from lights off at night to the start of the first sleep bout. Data were processed using custom PERL and MATLAB (The Mathworks, Inc.) scripts. Statistical tests were performed using Prism (GraphPad).

QUANTIFICATION AND STATISTICAL ANALYSIS

Unless otherwise noted, statistical calculations were done using R (3.5.1). DAPPLE metrics results for evaluating the significance of PPI networks were all done using 1,000 permutations (within DAPPLE parameter) and P values < 0.05 were considered significant. For gene set enrichment analyses, significance should only be considered for gene sets surviving multiple test correction (Bonferroni correction for the 22 gene sets tested or p < 0.002). NetSig genes were considered significant if they obtained a P value < 0.05. Unless otherwise specified, enrichment tests (e.g., enrichment of NetSig genes within high-risk inherited PPI networks) was performed by Fisher exact test; we considered P values < 0.05 as significant and also report the odds ratio (OR) with its associated 95% confidence interval.

All statistics for Artifact Removal by Classifier (ARC) are described within the Method Details and corresponding figures. The samples included in the training and test set are shown in Table S1. We also re-emphasize that we selected a conservative threshold of ARC score $\geq$ 0.4 to consider only RDNVs with extremely high confidence.

Determining rate differences between groups

Unless otherwise specified, rates comparisons between phenotypic groups (affected versus unaffected) were calculated by taking the number of variants per child and performing a quasi-Poisson linear regression and resulting P values < 0.05 were considered significant. This method enabled us to adjust for both biological sequencing source (WB versus LCL) and biological sex (male versus female). Biological sex was not used as a covariate for hemizygous variants because only male children are considered. Unless otherwise noted, rates are displayed as the mean number of variants with error bars representing the standard error. Here we reiterate the sample sizes for each of the rate tests performed: (i) rare inherited coding variants (N_{aff} = 960, N_{unaff} = 217), (ii) coding RDNVs (N_{aff} = 575, N_{unaff} = 141), (iii) iHART non-coding RDNVs (N_{aff} = 575, N_{unaff} = 141), (iv) iHART non-coding inherited variants (N_{aff} = 960, N_{unaff} = 217), (v) iHART+SSC non-coding RDNVs (N_{aff} = 1092, N_{unaff} = 659), (vi) iHART+SSC non-coding inherited variants (N_{aff} = 1477, N_{unaff} = 735).

TADA and TADA simulations

The sample sizes for the TADA-mega analysis are provided in Table S3. Benjamini-Hochberg correction was performed for TADA results and q-values (False Discovery Rate (FDR)) < 0.1 were considered significantly associated with ASD. When we apply the field standard FDR < 0.1, we identify 69 genome-wide significant genes. The TADA simulations were performed using the same sample sizes (and family structures) as used in the TADA-mega analysis. For the TADA simulations, only genes with a P value < $2.7\text{x}10^{-06}$ were considered as reaching genome-wide significance because these genes pass the stringent Bonferroni correction for the total number of genes included in the TADA analysis (0.05/18,472 = $2.7\text{x}10^{-06}$).

Zebrafish statistics

The Shapiro-Wilk normality test was used to determine whether data in each experiment was normally distributed. Most datasets were normally distributed and were analyzed as mean ± standard error of the mean using parametric statistical tests, except where noted that data was analyzed as median ± 95% confidence interval using non-parametric statistical tests. The specific test used to assess statistical significance in each experiment is described in each Figure Legend. Statistical tests were performed using Prism (GraphPad). Data were considered to be statistically significant if p < 0.05.

DATA AND CODE AVAILABILITY

The whole-genome sequencing data generated during this study are available from the Hartwell Foundation's Autism Research and Technology Initiative (iHART) following request and approval of the data use agreement available at http://www.ihart.org. Access to the whole-genome sequencing data generated in this study will be subject to approval by Autism Speaks and AGRE. Details about the format of the data, access options, and access instructions are included at http://www.ihart.org.

We also freely provide the code for ARC (Artifact Removal by Classifier), our random forest supervised model developed to distinguish true rare *de novo* variants from LCL-specific genetic aberrations or other types of artifacts such as sequencing and mapping errors, together with a full tutorial at https://github.com/walllab/iHART-ARC.

Interactive genotype/phenotype search engine

To facilitate sharing of iHART data with the broader autism research community and patients, we implemented a set of online data access methods to preview and search genetic variants and phenotypic traits (http://www.ihart.org/home).

Zebrafish data

The zebrafish datasets generated and analyzed in this study, and the code used to generate the data, are available upon request.

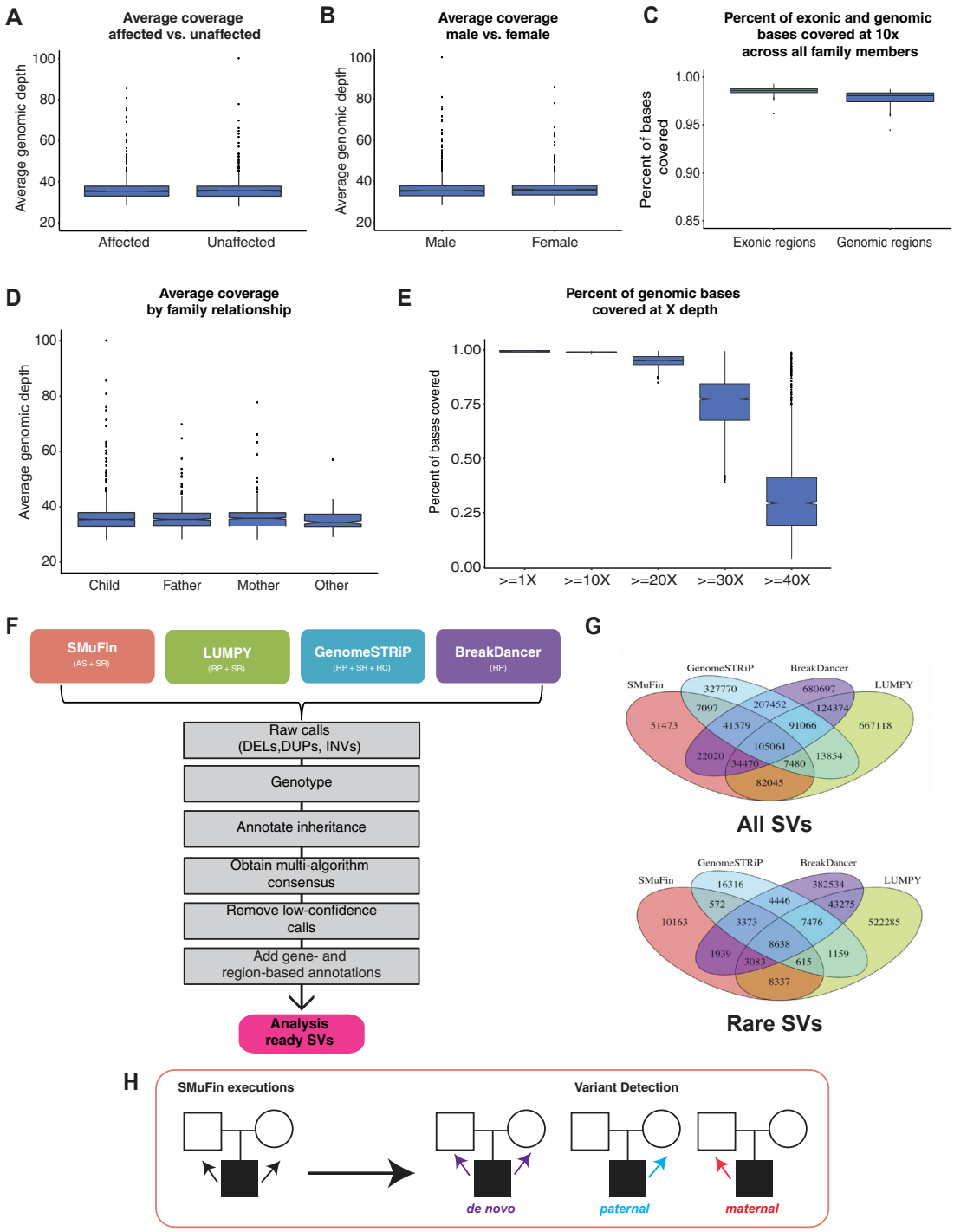

Figure S1. WGS Coverage Statistics for 2,308 iHART/AGRE Samples and the High-Resolution Detection of Large SVs, Related to Figure 1

There were no significant differences in the average fold coverage per sample across the cohort and no differences in the categories of (A) ASD affectation status, (B) sex, or (D) family member type – where family member type was simplified to include Mother, Father, Child (proband, sibling, MZ or DZ twin) and Other (e.g., cousin). (C) The percent of exonic and genomic bases covered at ≥ 10x in all family members for each of the 422 fully-phaseable iHART families. Exonic regions were defined as those annotated as protein-coding exons in Gencode V19 (> 75Mb). Genomic regions were defined as all non-N bases in the reference genome (> 2.8Gb). (E) The percentage of genomic bases covered at greater than or equal to 1X, 10X, 20X, 30X, and 40X bases for the 2,308 iHART samples with WGS data. On average, 98.97 ± 0.37 % of bases were covered at a depth of ≥ 10X. (F) An overview of our custom multi-algorithm consensus SV pipeline for high-resolution detection of large structural variants (SVs) from whole-genome sequence data. The four boxes at the top list the four main algorithms used to call SVs, and the parenthetical describes the detection strategy(s) used by each algorithm: AS, *de novo* assembly method; SR, split-read method; RP, read-pair method;

(legend continued on next page)

RC, read-count method. (G) Venn diagrams of structural variants detected by four different algorithms for all and rare (AF < 0.001 in cDGV and AF < 0.01 in iHART HNP samples) SVs (DELs, DUPs and INVs) detected in 1,377 phase-able WGS samples by SMuFin, LUMPY, GenomeSTRiP and BreakDancer, after excluding events with ≥ 50% overlap with genomic low-complexity regions (Brandler et al., 2016). Additional per-algorithm filters were also applied prior to the generation of this Venn diagram as described in STAR Methods. (H) A schematic overview of the SMuFin detection pipeline. Families are processed as independent trios, where the sequence reads from a child are aligned to the mother's genome and then the father's genome, treating the parental genome as the reference genome in both comparisons. Each comparison, or SMuFin execution, results in variants identified in the child by that parent-offspring comparison. All three members of the trio are considered for assigning the corresponding inheritance of variants identified in the child. A variant detected when comparing to both mom and dad is *de novo,* while a variant detected only when comparing to mom is paternally inherited and a variant detected only when comparing to dad is maternally inherited.

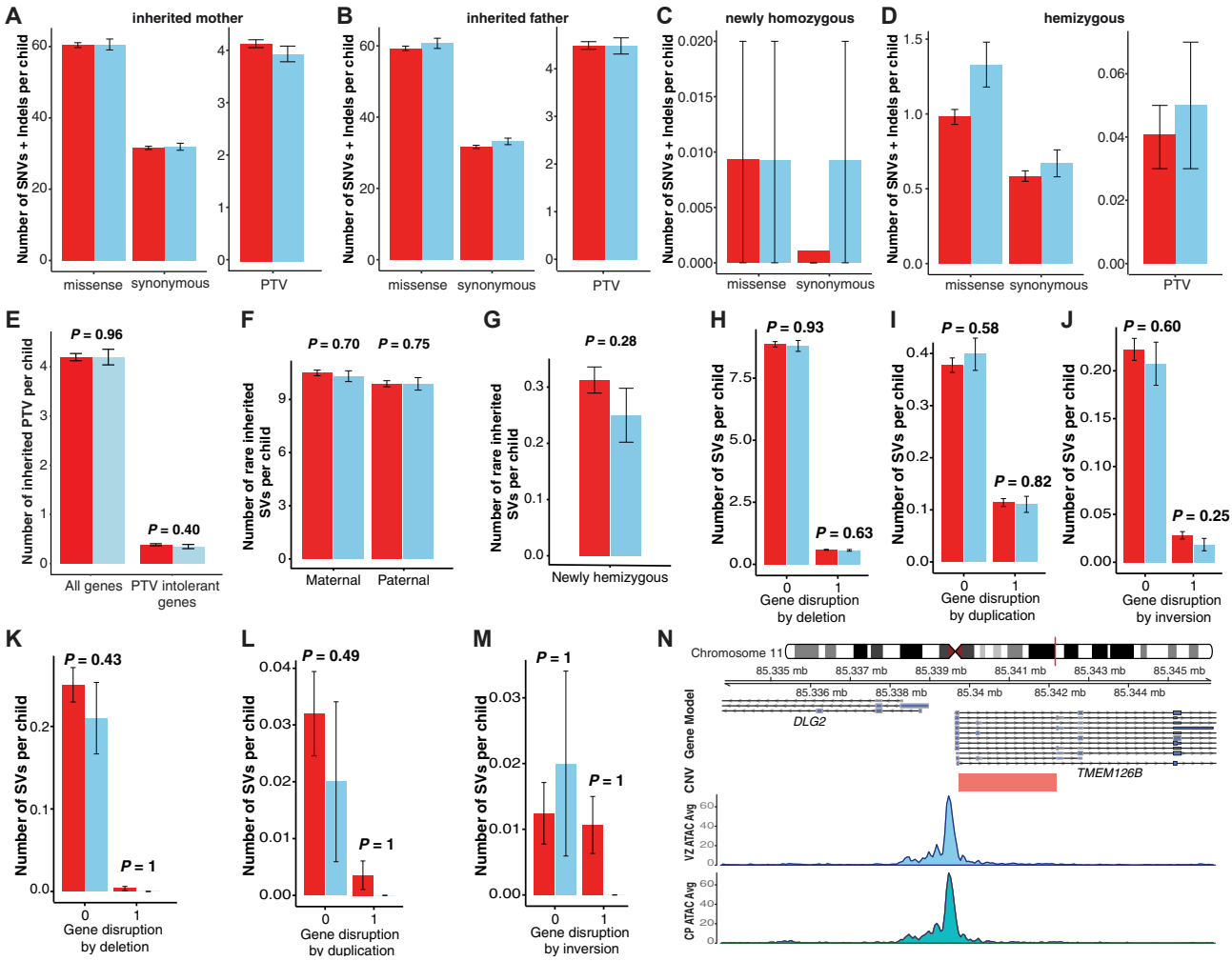

Figure S2. Additional Details for Rare Inherited PTVs and SVs, Related to Figure 2

(A-D) Rare inherited coding variants by consequence and inheritance. The rate of rare inherited coding variants per fully phase-able child is displayed for 960 affected (red) and 217 unaffected (blue) children by both variant consequence and inheritance, this includes newly hemizygous variants in 563 affected (red) and 100 unaffected (blue) male children. The graph for newly homozygous PTVs (C) was excluded because none were identified in affected or unaffected children. Mean ± SE rates are shown. (E) The rate of private inherited PTVs in 960 affected (red) and 217 unaffected (blue) children iHART children for all genes versus PTV intolerant genes. We found no excess of inherited private PTVs in mutation intolerant genes (pLI $\geq$ 0.9) (Lek et al., 2016) in affected subjects (p = 0.40, quasi-Poisson linear regression). Mean ± SE rates are shown. (F) The rate of rare inherited SVs per fully phase-able child is displayed for 960 affected (red) and 217 unaffected (blue) children by inheritance type. Mean ± SE rates are shown. (G) The rate of rare inherited SVs per fully phase-able child is displayed for newly hemizygous variants in 563 affected (red) and 100 unaffected (blue) male children. (H-M) The rate of rare inherited SVs per fully phase-able child identified in 960 affected (red) and 217 unaffected (blue) children by inheritance type; this includes newly hemizygous variants in 563 affected (red) and 100 unaffected (blue) male children. Mean ± SE rates are shown. Maternally and paternally inherited SVs by affectation status and gene disruption for deletions (H), duplications (I), and inversions (J). Newly hemizygous SVs by affectation status and gene disruption for deletions (K), duplications (L), and inversions (M). (N) The DLG2 promoter-disrupting 2.5Kb deletion (chr11: 85339733 – 85342186), displayed as an orange rectangle, detected in three independent iHART families. This 2.5Kb deletion is transmitted to all affected members of two different iHART families. This deletion falls in a recently-defined, functional, non-coding regulatory region in developing human brain (chr11:85338026-85340560) (de la Torre-Ubieta et al., 2018); below the deletion we show the average ATAC-seq peak read depth from the cortical plate (CP) and ventricular zone (VZ) of developing human brain samples (n = 3).

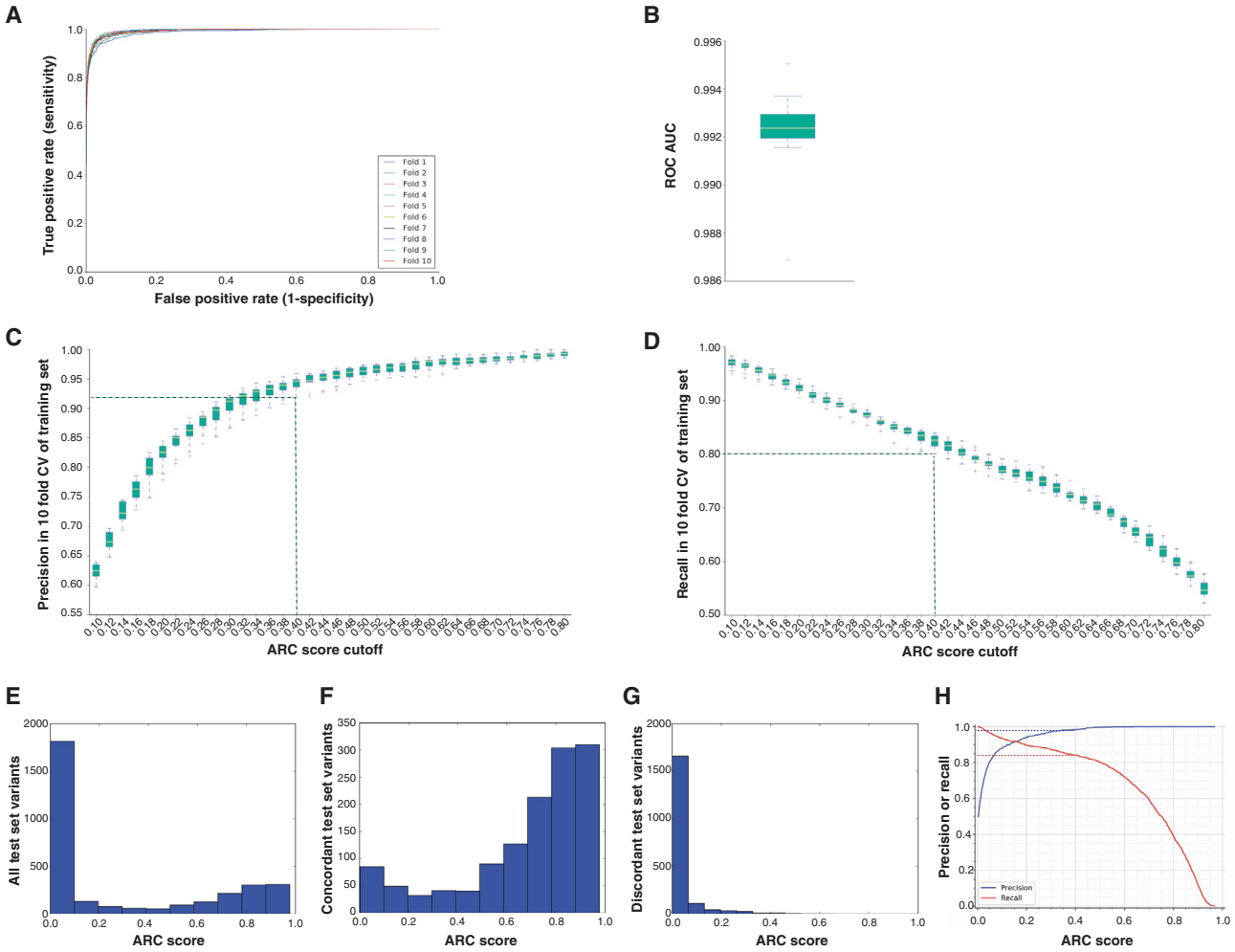

Figure S3. ARC Performance in the Training and Test Sets, Related to Figure 3

The 10-fold cross validation (CV) for the ARC training set (A-D). (A) Receiver Operating Characteristic (ROC) curves for the true positive rate (Sensitivity) is plotted as a function of the false positive rate; (B) Area Under the ROC Curve (ROC AUC) statistics (median = 0.992) for each of the 10-folds; (C) Precision rates versus predicted score cutoffs – the dashed line at the selected score (0.4) highlights that the minimum precision across all 10-folds is > 0.9; (D) Recall rates versus predicted score cutoffs – the dashed line at the selected score (0.4) highlights that the minimum precision across all 10-folds is ~0.8. ARC performance in the test set (E-H). (E) Distribution of all test set variants by ARC score; (F) Distribution of all TRUE test set variants by ARC score – the majority of concordant variants have an ARC score of $\geq$ 0.4; (G) Distribution of all FALSE test set variants by ARC score – almost all discordant variants have an ARC score of < 0.4; (H) The precision and recall rates versus predicted ARC score cutoff in the test set – the dashed line at the selected score (0.4) highlights that the precision is > 0.95 and the recall is > 0.85.

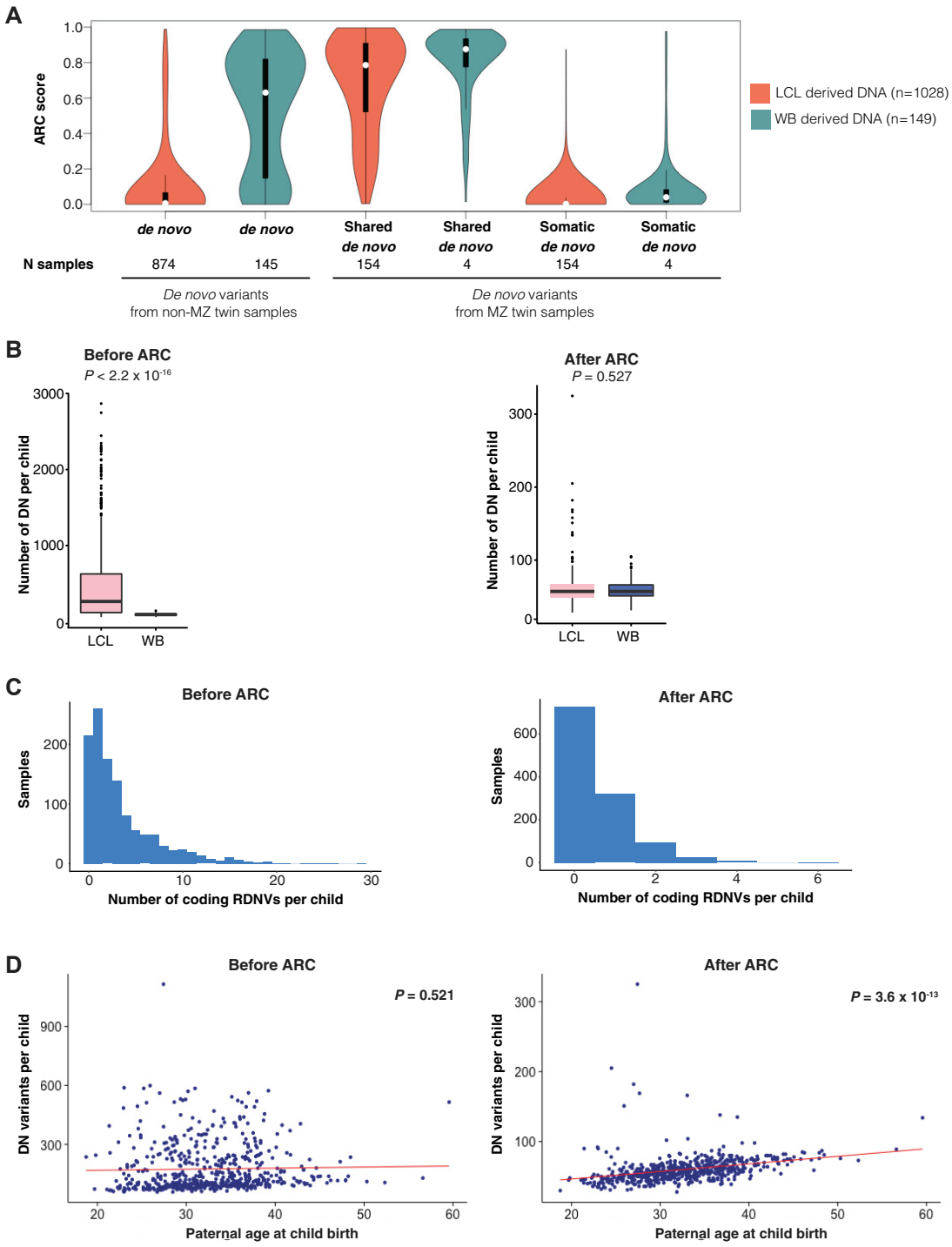

Figure S4. RDNVs Identified in iHART Samples before and after ARC, Related to Figure 3

(A) The ARC score distribution for raw *de novo* variants identified in 1,177 fully phase-able samples – displayed as non-MZ twin samples versus MZ twin samples. Samples for which DNA was derived from LCL or WB are shown in red and green, respectively. All LCL MZ twins were included in the ARC training set and all WB MZ twins were included in the ARC test set. (B) The number of rare *de novo* variants identified in LCL (pink) and WB (blue) fully phase-able (non-MZ twin) samples before ARC (N = 1,019 samples) and the number of rare *de novo* variants identified in LCL (pink) and WB (blue) fully phase-able (non-MZ twin) samples after ARC (variants with an ARC score < 0.4 are filtered out) and after excluding ARC outlier samples (samples with > 90% DNs removed by ARC) (N = 716). After ARC, there is no significant difference in the rate of rare *de novo* variants based on the biological sequencing source (LCL_{mean} = 60.3 and WB_{mean} = 59.4; LCL_{median} = 57 and WB_{median} = 57). The difference in DN rates between the biological sequencing source (LCL versus WB) was evaluated using Wilcoxon rank sum test. (C) The

(legend continued on next page)

number of rare *de novo* coding variants identified per fully phase-able sample displayed as histograms. The coding RDNVs before ARC are from 1,177 fully phase-able samples and after ARC (variants with an ARC score < 0.4 are filtered out) and after excluding ARC outlier samples (samples with > 90% DNs removed by ARC) (n = 831 samples). (D) The correlation between the rate of rare *de novo* variants and paternal age before and after ARC. This analysis considers 574 fully phase-able ASD children (excluding MZ twins and ARC outliers) for which paternal age was known. The red line is the linear regression line. The graph on the left shows the raw number of rare *de novo* variants (SNVs and indels) per child by paternal age at the time of the participant's birth in years. The graph on the right shows the number of rare *de novo* variants (SNVs and indels) per child after running ARC by paternal age at the time of the participant's birth in years.

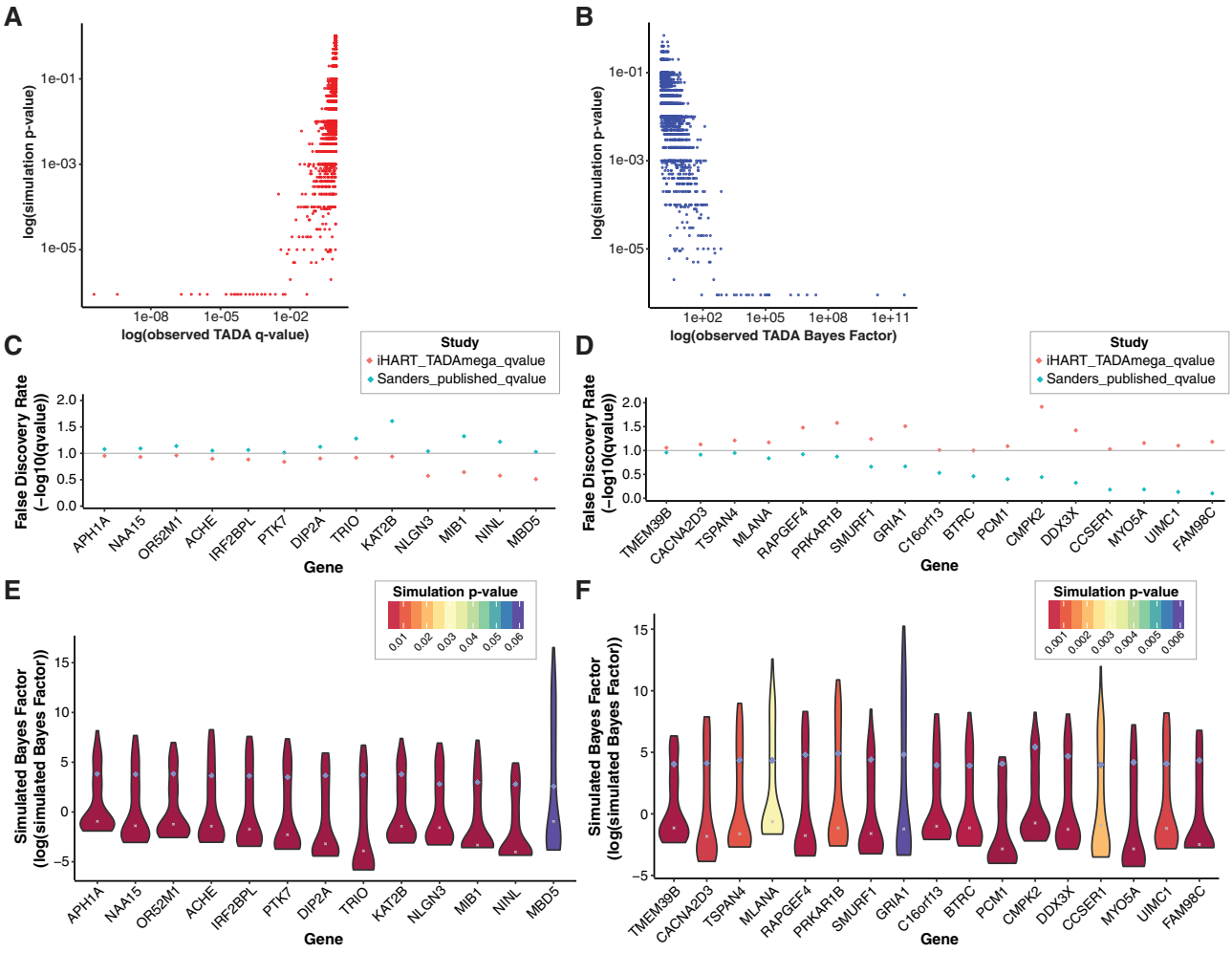

Figure S5. TADA Mega-analysis Simulation Results, Related to Figure 4

(A) For each of the 18,472 TADA genes, the observed FDR in the iHART TADA-mega analysis is plotted against the simulated p value. Genes with the smallest FDRs also have small simulated p values, as expected. (B) The observed Bayes Factor (BF), for genes with a BF > 1, in the iHART TADA-mega analysis is plotted against the simulated p value. Genes with the largest BF also have small simulated p values, as expected. (C-F) The TADA-mega analysis results from the previous study versus current iHART study. Genes are sorted by increasing difference in the FDR (q-value) obtained in Sanders et al. (2015) versus the current iHART TADA-mega analysis. In panels (C) and (D) the per-gene TADA FDR is displayed as the -log10(q-value) (higher dots have a lower FDR) obtained in Sanders et al. (2015) (green) and the current iHART study (red) and the horizontal line marks the FDR = 0.1 threshold; for (C) the 13 genes with an FDR < 0.1 in Sanders et al. (2015) that failed replication in iHART (FDR > 0.1), and (D) the 16 newly significant genes identified in the iHART mega analysis with an FDR < 0.1. Note that the *CACNA2D3* gene is significantly associated with ASD in the iHART mega-analysis, but not the previous TADA mega-analysis. However, it was previously reported in De Rubeis et al. (2014) and thus we do not consider it a new risk gene. Below this, in panels (E) and (F), are the per-gene violin plots of Bayes Factors (displayed as log(simulated Bayes Factor)) obtained for each of the 1.1 million TADA simulations. The gray "x" marks the median simulated Bayes Factor, the blue dot indicates the observed Bayes Factor in the iHART TADA mega analysis, and the violin plots are filled according to their simulation p value; for (E) the 13 genes with an FDR < 0.1 in Sanders et al. (2015) that failed replication in iHART (FDR > 0.1) (max p value = 0.06) and (F) the 16 newly significant genes (plus *CACNA2D3*) identified in the iHART mega analysis with an FDR < 0.1 (max p value = 0.006).

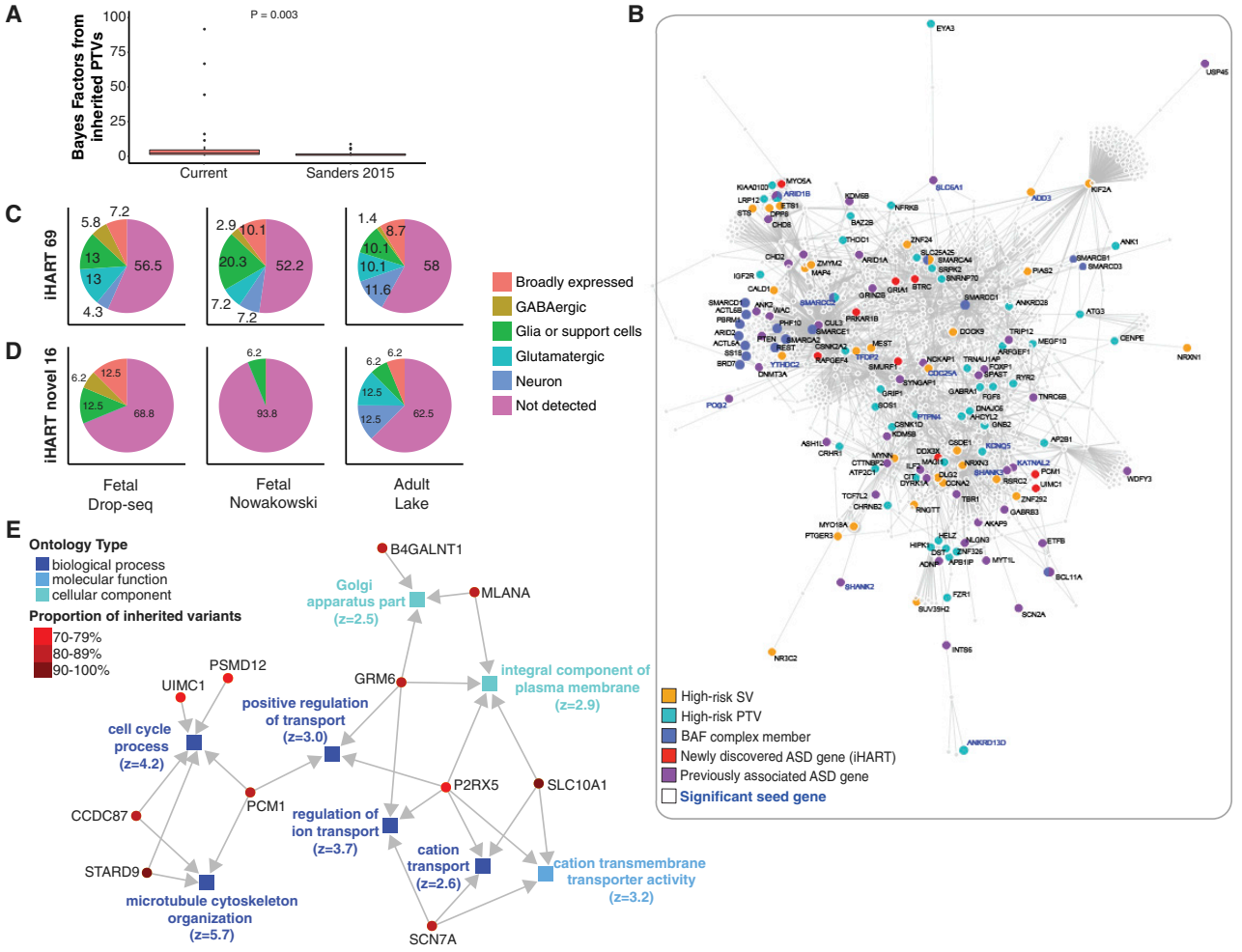

Figure S6. Biological Insights from Known and Novel ASD Risk Genes Identified in the TADA Mega Analysis, Related to Figure 4

(A) A boxplot for the inherited PTV Bayes Factors observed for the 35 genes with an FDR < 0.2 in the current iHART TADA mega analysis that had an FDR > 0.2 in the et al., 2015 TADA mega analysis (Sanders et al., 2015) (Kruskal–Wallis test, p = 0.003). (B) The indirect PPI network formed by the 69 ASD-risk genes and the 98 genes harboring high-risk inherited variants (n = 165 unique genes). The resulting indirect PPI was significant for two connectivity metrics – seed indirect degrees mean p = 0.003, and CI degrees mean p = 0.005. Proteins encoded by a gene with a high-risk inherited PTVs are shown in teal and SVs are shown in gold. Proteins encoded by a previously established ASD-risk gene (Sanders et al., 2015) are shown in purple, newly identified ASD-risk gene (iHART TADA mega analysis) are shown in red, those belonging to the BAF complex are shown in blue, and any protein falling in more than one category is colored with all categorical colors that apply (e.g., *ARID1B*). The gene label for significant seed genes are bold and blue. (C-D) Enrichment of iHART ASD-risk genes in single-cell RNA seq (scRNA-seq) cell type expression signatures. Genes enriched in major cell type classes were obtained from human fetal brain datasets and an adult brain dataset, and the percentage of iHART ASD-risk genes in each cell type class is shown. (C) iHART 69 ASD-risk genes in fetal cell classes (left and center) and adult cell classes (right). (D) iHART 16 novel ASD-risk genes in fetal cell classes (left and center) and adult cell classes (right). Significant $\log_2$ odds ratios of neuronal cell type enrichment: Fetal drop-seq glutamatergic, 3; GABAergic 4.7; neuron 4.8. Fetal (Nowakowski et al., 2017) glutamatergic, 1.6; GABAergic 2.4; neuron 5.4. Adult (Lake et al., 2018) Glutamatergic, 2.9; GABAergic 0.65; Neuron 3.4. The Broad expression class was defined as expression in neuronal cell types and glial cell types and Neuron class was defined as expression in glutamatergic and GABAergic cell types. The numbers inside each pie chart indicate the percentage of iHART ASD-risk genes in that cell type. (E) The interaction network for the gene ontology over-represented terms, and associated genes, for the genes enriched in inherited variation (TADA FDR < 0.2, proportion of inherited variants ≥ 70%). We focused on the 23 genes with an FDR < 0.2 for which the majority (≥70%) of their qualifying risk variants were inherited PTVs. The z-score is displayed together with each color-coded ontology term (squares) and the genes are color coded by the proportion of qualifying TADA variants that were inherited PTVs (circles).

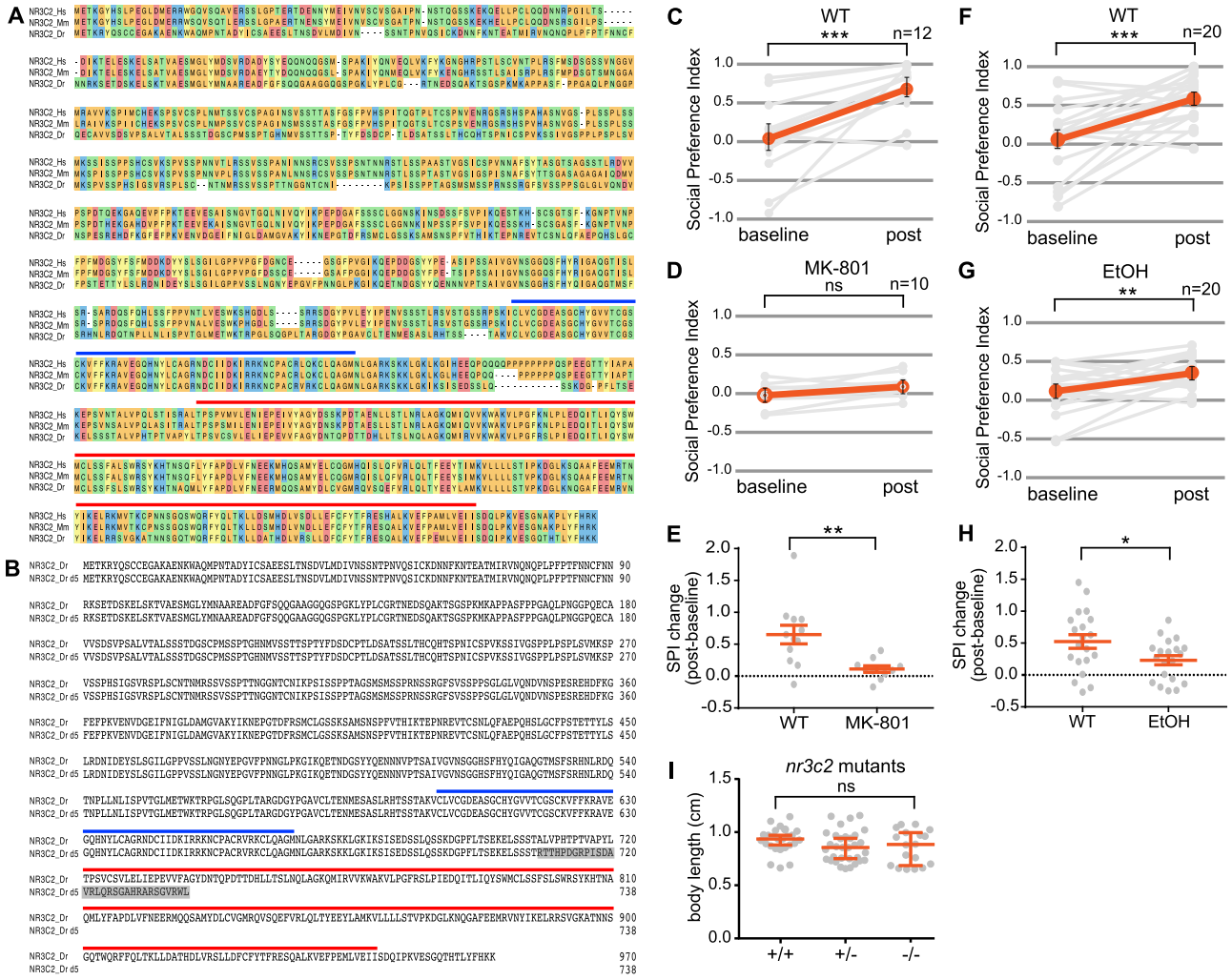

Figure S7. NR3C2 Protein Sequence Alignment, Zebrafish Mutant Sequence, and Validation of the Social Preference Assay, Related to Figure 6

(A) Multiple sequence alignment for human (Hs), mouse (Mm) and zebrafish (Dr) NR3C2 proteins. Amino acids are colored according to their chemical properties to highlight identical and similar residues. (B) Alignment of WT and mutant zebrafish NR3C2 proteins. Gray shading indicates altered amino acid sequence in the mutant. Blue and red lines indicate DNA binding domain and ligand binding domain, respectively. (C-I) Validation of the social preference assay. (C,D) WT zebrafish treated with DMSO vehicle control showed a significantly higher SPI during the post-baseline period compared to the baseline period, but WT zebrafish treated with 20 μM MK-801 did not. (E) The increase in SPI in the presence of a conspecific was significantly smaller for zebrafish treated with MK-801 compared to controls. (F,G) Both untreated WT zebrafish and WT zebrafish treated with 0.5% ethanol showed a significantly higher SPI during the post-baseline period compared to the baseline period, although the SPI increase was smaller for ethanol-treated animals. (H) The increase in SPI in the presence of a conspecific was significantly smaller for zebrafish treated with 0.5% ethanol compared to controls. (I) There was no significant difference in the body length of *nr3c2* +/+, +/− and −/− siblings for the data presented in Figures 6B and 6C. Grey data points and lines represent individual animals. Red lines indicate mean ± SEM (C-H) or median ± 95% confidence interval (I). *p < 0.05; **p < 0.01; ***p < 0.001, ns = not significant by paired t test (C,D,F,G), unpaired t test (E,H), or Kruskal-Wallis test with Dunn's multiple comparison test (I).